

# **Role of $\beta$ -Catenin Signaling for the Growth and Selective Poisoning of *Ctnnb1*-Mutated Mouse Liver Tumors**

## **Dissertation**

der Mathematisch-Naturwissenschaftlichen Fakultät  
der Eberhard-Karls-Universität Tübingen  
zur Erlangung des Grades eines  
Doktors der Naturwissenschaften  
(Dr. rer. nat.)

vorgelegt von

**Yasmin Singh**

aus Ulm

Tübingen

**2013**

Tag der mündlichen Qualifikation:

16.10.2013

Dekan:

Prof. Dr. Wolfgang Rosenstiel

1. Berichterstatter:

Prof. Dr. Michael Schwarz

2. Berichterstatter:

Prof. Dr. Klaus Schulze-Osthoff

The presented doctoral thesis was carried out at the Institute of Experimental and Clinical Pharmacology and Toxicology, Department of Toxicology, at the University of Tuebingen from March 2009 to July 2013 under the supervision of Prof. Dr. Michael Schwarz.

## **Acknowledgment**

At first, I want to thank Prof. Dr. Michael Schwarz for giving me the opportunity to do my thesis in his group, for the interesting topic and for his support and great supervision. I also thank Dr. Münzel for being one of my examiners in the doctoral examination.

I want to thank all my colleagues for the great time and the pleasant working atmosphere during the last years. My special thanks go to Dr. Albert Braeuning for his help with all sorts of problems. I thank Elke Zabinsky, Johanna Mahr and Silvia Vetter for the really great technical assistance and Annette von Bank for managing all administrative issues.

Also I want to thank the Deutsche Forschungsgemeinschaft (SFB773) for the financial support.

The most important acknowledgment to the end: my biggest hug and thanks go to all my friends and of course to my family for their support in any way.

**Data presented in this work have been published:**

Braeuning A, **Singh Y**, Rignall B, Buchmann A, Hammad S, Othman A, von Recklinghausen I, Godoy P, Hoehme S, Drasdo D, Hengstler JG, Schwarz M (2010) Phenotype and growth behavior of residual  $\beta$ -catenin-positive hepatocytes in livers of  $\beta$ -catenin-deficient mice. *Histochem Cell Biol* 134:469-481

**Singh Y**, Braeuning A, Schmid A, Pichler BJ, Schwarz M (2013) Selective poisoning of *Ctnnb1*-mutated hepatoma cells in mouse liver tumors by a single application of acetaminophen. *Arch Toxicol* (in press)

Ganzenberg K, **Singh Y**, Braeuning A (2013) The time point of  $\beta$ -catenin knockout in hepatocytes determines their response to xenobiotic activation of the constitutive androstane receptor. *Toxicology* 308:113-121

**Singh Y**, Braeuning A, Port J, Schwarz M Genetic ablation of  $\beta$ -catenin inhibits the proliferative phenotype of mouse liver adenomas. (manuscript in preparation)

**Parts of this work have been presented:**

Baden-Württemberg ToxNet Meeting 2010, Freiburg: „Effect of  $\beta$ -Catenin Signaling on Etoposide-induced Apoptosis” (poster presentation)

DGPT Jahrestagung 2012, Dresden: „Gezielte Vergiftung von  $\beta$ -Catenin (*Ctnnb1*)-mutierten Mauslebertumoren durch einmalige Behandlung mit Acetaminophen“ (oral presentation)

Baden-Württemberg ToxNet Meeting 2012, Karlsruhe: „Selective Poisoning of *Ctnnb1*-Mutated Hepatoma Cells in Mouse Liver Tumors by a Single Application of Acetaminophen” (poster presentation)

## Abbreviations

<b>AAP</b>	acetaminophen
<b>AB</b>	alamar blue
<b>AEC</b>	3-amino-9-ethylcarbazole
<b>AFC</b>	7-amino-3-trifluoromethylcoumarine
<b>ALT</b>	alanine aminotransferase
<b>AP</b>	alkaline phosphatase
<b>APC</b>	adenomatous polyposis coli
<b>AST</b>	aspartate aminotransferase
<b>ATP</b>	adenosine triphosphate
<b><math>\beta</math>-Gal</b>	$\beta$ -galactosidase
<b>B-raf</b>	V-raf murine sarcoma viral oncogene homolog B1
<b>BrdU</b>	5-bromodeoxyuridine
<b>BSA</b>	bovine serum albumin
<b>CK1<math>\alpha</math></b>	casein kinase 1 $\alpha$
<b>CMV</b>	cytomegaly virus
<b>c-myc</b>	v-myc myelocytomatosis viral oncogene homolog
<b>Cre</b>	Cre recombinase
<b>CTNNB1/ Ctnnb1</b>	gene encoding $\beta$ -catenin in humans/ mice
<b>Cx</b>	connexin
<b>CYP</b>	cytochrome P450 enzyme
<b>DEN</b>	N-nitrosodiethylamine
<b>DMEM</b>	Dulbecco's Modified Eagle Medium
<b>DMSO</b>	dimethyl sulfoxide
<b>DNA</b>	deoxyribonucleic acid
<b>DTT</b>	dithiothreitol
<b>Dvl</b>	dishevelled
<b>EDTA</b>	ethylenediaminetetraacetic acid
<b>EtOH</b>	ethanol
<b>FCS</b>	fetal calf serum
<b>FZ</b>	frizzled
<b>GJIC</b>	gap-junctional intercellular communication
<b>G6Pase</b>	glucose-6-phosphatase
<b>GS</b>	glutamine synthetase
<b>GSH</b>	glutathione
<b>GSK3<math>\beta</math></b>	glycogen synthase kinase 3 $\beta$
<b>GST</b>	glutathione-S-transferase
<b>Ha-ras</b>	Harvey rat sarcoma viral oncogene homolog
<b>HB</b>	hepatoblastoma
<b>HCC</b>	hepatocellular carcinoma
<b>HE</b>	hematoxylin/ eosin
<b>HEPES</b>	4-(2-hydroxyethyl)-1-piperazineethanesulfonic acid
<b>HIF1<math>\alpha</math></b>	hypoxia-inducible factor 1 $\alpha$
<b>HNF4<math>\alpha</math></b>	hepatocyte nuclear factor 4 $\alpha$
<b>HGF</b>	hepatocyte growth factor
<b>HRP</b>	horseradish peroxidase

<b>IκB</b>	inhibitor of nuclear factor κB
<b>IGF</b>	insulin-like growth factor
<b>IgG</b>	immunoglobulin G
<b>IHC</b>	immunohistochemistry
<b>KO</b>	knockout
<b>LB</b>	lysogeny broth
<b>LEF</b>	lymphoid enhancer factor
<b>LRP5/ 6</b>	low density lipoprotein receptor-related protein
<b>MAPK</b>	mitogen-activated protein kinase
<b>MRI</b>	magnetic resonance imaging
<b>NAPQI</b>	N-acetyl- <i>p</i> -benzoquinone-imine
<b>NFκB</b>	nuclear factor κB
<b>NTP</b>	nucleoside triphosphate
<b>p53</b>	protein 53
<b>PB</b>	phenobarbital
<b>PBS</b>	phosphate buffered saline
<b>PCR</b>	polymerase chain reaction
<b>PI3K</b>	phosphoinositide 3-kinase
<b>POD</b>	peroxidase
<b>P/ S</b>	penicillin/ streptomycin
<b>Rb</b>	retinoblastoma
<b>RNA</b>	ribonucleic acid
<b>SD</b>	standard deviation
<b>SDS</b>	sodium dodecyl sulfate
<b>STF</b>	SuperTopflash
<b>SULT</b>	sulfotransferase
<b>Tam</b>	tamoxifen
<b>TCF</b>	T-cell factor
<b>TEMED</b>	tetramethylethylenediamine
<b>Tris</b>	tris(hydroxymethyl)aminomethane
<b>TTR</b>	transthyretin
<b>TUNEL</b>	terminal deoxynucleotidyl transferase-mediated dUTP nick end labeling
<b>UGT</b>	uridine glucuronosyl transferase
<b>VEGFR</b>	vascular endothelial growth factor receptor
<b>Wnt</b>	wingless-type MMTV integration site family
<b>WT</b>	wild type
<b>X-Gal</b>	5-bromo-4-chloro-3-indolyl-β-D-galactopyranoside

# Table of Contents

<b>1. INTRODUCTION</b> .....	<b>1</b>
1.1. LIVER PHYSIOLOGY .....	1
1.2. DRUG METABOLISM IN THE LIVER .....	3
1.3. THE WNT/ $\beta$ -CATENIN SIGNALING PATHWAY .....	4
1.4. CARCINOGENESIS .....	6
1.4.1. The Role of $\beta$ -Catenin in Tumorigenesis .....	8
1.5. HEPATOCELLULAR MALIGNANCIES.....	8
1.5.1. Chemically Induced Hepatocarcinogenesis in Mice.....	10
1.6. AIMS AND OBJECTIVES .....	11
<b>2. MATERIALS</b> .....	<b>12</b>
2.1. LABORATORY EQUIPMENT .....	12
2.2. EXPENDABLE ITEMS .....	13
2.3. CHEMICALS AND BIOCHEMICALS.....	15
2.4. BUFFERS AND SOLUTIONS .....	18
2.4.1. Cell Culture .....	18
2.4.2. Cell Treatment .....	19
2.4.3. Plasmid Preparation .....	20
2.4.4. Reporter Gene Analysis.....	20
2.4.5. Cell Viability Assays.....	21
2.4.6. Determination of Apoptosis.....	21
2.4.7. Gel Electrophoresis .....	22
2.4.8. Immunohistochemistry.....	24
2.5. PRIMERS.....	26
2.5.1. Genotyping .....	26
2.5.2. Sequencing.....	27
2.6. siRNA .....	27
2.7. ANTIBODIES FOR IHC.....	27
2.8. VECTORS.....	28
2.9. CELL LINES .....	29
2.10. MOUSE STRAINS .....	29
2.11. SOFTWARE .....	29
<b>3. METHODS</b> .....	<b>30</b>

3.1.	CELL CULTURE .....	30
3.1.1.	General Remarks .....	30
3.1.2.	Medium Change and Passaging of Cells .....	30
3.1.3.	Thawing and Freezing of Cells.....	31
3.1.4.	Treatment of Cells.....	31
3.2.	PLASMID PREPARATION .....	32
3.2.1.	Plasmid Progeny and Isolation.....	32
3.2.2.	DNA Quantification.....	32
3.3.	ELECTROPHORESIS .....	33
3.3.1.	Agarose Gel Electrophoresis.....	33
3.3.2.	Polyacrylamide Gel Electrophoresis.....	33
3.4.	TRANSFECTION .....	33
3.5.	REPORTER GENE ANALYSIS.....	34
3.6.	CELL VIABILITY ASSAYS.....	34
3.7.	DETERMINATION OF APOPTOSIS .....	34
3.7.1.	Protein Isolation .....	34
3.7.2.	Caspase 3/ 7 Activity Measurement.....	35
3.7.3.	Bradford Protein Quantification .....	35
3.7.4.	Hoechst Staining.....	35
3.8.	ANIMAL EXPERIMENTS .....	36
3.8.1.	General Remarks .....	36
3.8.2.	Organ Harvesting .....	36
3.8.3.	Tumor Analysis .....	36
3.8.4.	Mutation Analysis .....	37
3.9.	ANIMAL EXPERIMENT I: ABLATION OF $\beta$ -CATENIN IN CTNNB1-MUTATED MOUSE LIVER TUMORS .....	38
3.9.1.	Animal Breeding.....	38
3.9.2.	Genotyping.....	38
3.9.3.	Induction of Ctnnb1-Mutated Mouse Liver Tumors .....	39
3.9.4.	Tamoxifen-Induced KO of Ctnnb1 in Livers of Transgenic Mice .....	40
3.10.	ANIMAL EXPERIMENT II: POISONING OF CTNNB1-MUTATED MOUSE LIVER TUMORS BY AAP .....	40
3.10.1.	AAP Dose Finding Study.....	40
3.10.2.	Induction of Ctnnb1-Mutated Mouse Liver Tumors .....	41
3.10.3.	Treatment of Tumor-Bearing Mice with a Single Dose of AAP.....	41



3.10.4. Magnetic Resonance Imaging .....	43
3.11. IMMUNOHISTOCHEMISTRY.....	43
3.11.1. Frozen Liver Slices .....	43
3.11.2. Carnoy Fixation.....	43
3.11.3. Formalin Fixation .....	43
3.11.4. Preparation of Paraffin Sections .....	44
3.11.5. G6Pase Staining.....	44
3.11.6. HE Staining.....	44
3.11.7. GS/ CYP/ E-Cadherin/ $\beta$ -Catenin/ BrdU Staining .....	44
3.11.8. GS/ BrdU and GS/ Cx32 Double Staining.....	45
3.11.9. GS/ HNF4 $\alpha$ Double Staining.....	45
3.11.10. Masson-Goldner Trichrome Staining.....	45
3.11.11. TUNEL Assay.....	46
3.11.12. $\beta$ -Catenin Staining of Cells.....	46
3.12. STATISTICS .....	46
<b>4. RESULTS .....</b>	<b>47</b>
4.1. ABLATION OF $\beta$ -CATENIN IN CTNNB1-MUTATED MOUSE LIVER TUMORS .....	47
4.1.1. Analysis of Tumor Genotype after KO of Ctnnb1 .....	48
4.1.2. Analysis of Tumor Phenotype after KO of Ctnnb1 .....	49
4.1.3. Importance of $\beta$ -Catenin for the Proliferation of Ctnnb1-Mutated Tumor Cells.....	52
4.1.4. The Role of $\beta$ -Catenin in Cx32-Mediated Cell-Cell Communication .....	55
4.1.5. Effect of $\beta$ -Catenin Ablation on Cell Death in Tumors from Ctnnb1 KO Mice.....	58
4.2. ROLE OF ACTIVATED $\beta$ -CATENIN IN ETOPOSIDE-INDUCED APOPTOSIS IN MOUSE HEPATOMA CELLS .....	60
4.3. SELECTIVE POISONING OF CTNNB1-MUTATED MOUSE LIVER TUMORS BY AAP ...	66
4.3.1. Phenotype of Generated Mouse Liver Tumors .....	67
4.3.2. Hepatotoxicity of AAP in Normal Liver Tissue .....	68
4.3.3. Acute Effects of AAP Treatment on GS-Positive Tumors .....	70
4.3.4. Resistance of GS-Positive Tumor Cell Populations.....	73
4.3.5. Effects of AAP Treatment on GS-Negative Tumors.....	75
4.3.6. Regeneration Processes and Long-Term Effects .....	76
4.3.7. Monitoring of Tumor Burden by MRI.....	81
<b>5. DISCUSSION .....</b>	<b>84</b>
5.1. ABLATION OF $\beta$ -CATENIN IN CTNNB1-MUTATED MOUSE LIVER TUMORS .....	84

5.2. ROLE OF $\beta$ -CATENIN IN ETOPOSIDE-INDUCED APOPTOSIS IN MOUSE HEPATOMA CELLS.....	89
5.3. SELECTIVE POISONING OF CTNNB1-MUTATED MOUSE LIVER TUMORS BY AAP ...	92
<b>6. SUMMARY.....</b>	<b>98</b>
<b>7. ZUSAMMENFASSUNG.....</b>	<b>100</b>
<b>8. LITERATURE.....</b>	<b>102</b>
<b>9. CURRICULUM VITAE .....</b>	<b>111</b>

## 1. Introduction

### 1.1. Liver Physiology

The human liver is the largest internal organ with an average weight of ~1,500 grams. It consists of four lobes of unequal size and shape and plays a major role in metabolism and detoxification, but also in other physiological processes. These include the synthesis of bile and of certain plasma proteins, the storage of glycogen, the processing of hemoglobin and the production, degradation and activation of certain hormones (Jungermann and Katz, 1989).

Two afferent vessels supply the liver with blood: the portal vein carrying nutrient-rich blood and the hepatic artery transporting oxygen-rich blood. Branches of both veins enter the sinusoids, special blood vessels with fenestrated endothelium that allow the nutrients to pass through and to enter the liver cells. The blood then exits the liver via the central veins and empties into the *vena cava inferior*. The liver is occupied by non-parenchymal cells comprising endothelial cells, Kupffer cells, Ito cells, and pit cells; and parenchymal cells, also referred to as hepatocytes (Jungermann, 1995). In the liver lobules, the functional units of the liver, hepatocytes are arranged in a roughly hexagonal shape surrounding the central vein. Branches of the hepatic artery, portal vein and bile duct located at the corners of each lobule form the so-called portal triad (Jungermann and Katz, 1989). Bile ducts transport the bile from the liver into the small intestine or to the gallbladder for storage.

The localization of hepatocytes along the blood stream affects their metabolic function and divides the liver lobules into three different zones: the periportal region (zone 1) near the portal veins, the midzonal region (zone 2) and the perivenous or pericentral zone (zone 3) surrounding the central veins (Rappaport *et al.*, 1954;

## Introduction

Gebhardt, 1992). This model of metabolic zonation proposes that processes including the oxidative energy metabolism, gluconeogenesis, and urea synthesis are predominantly active in periportal hepatocytes, whereas hepatocytes close to the central veins are more involved in glycolysis, glutamine synthesis, and xenobiotic metabolism (Jungermann and Sasse, 1978; Jungermann and Katz, 1982; Gebhardt and Mecke, 1983; Figure 1).

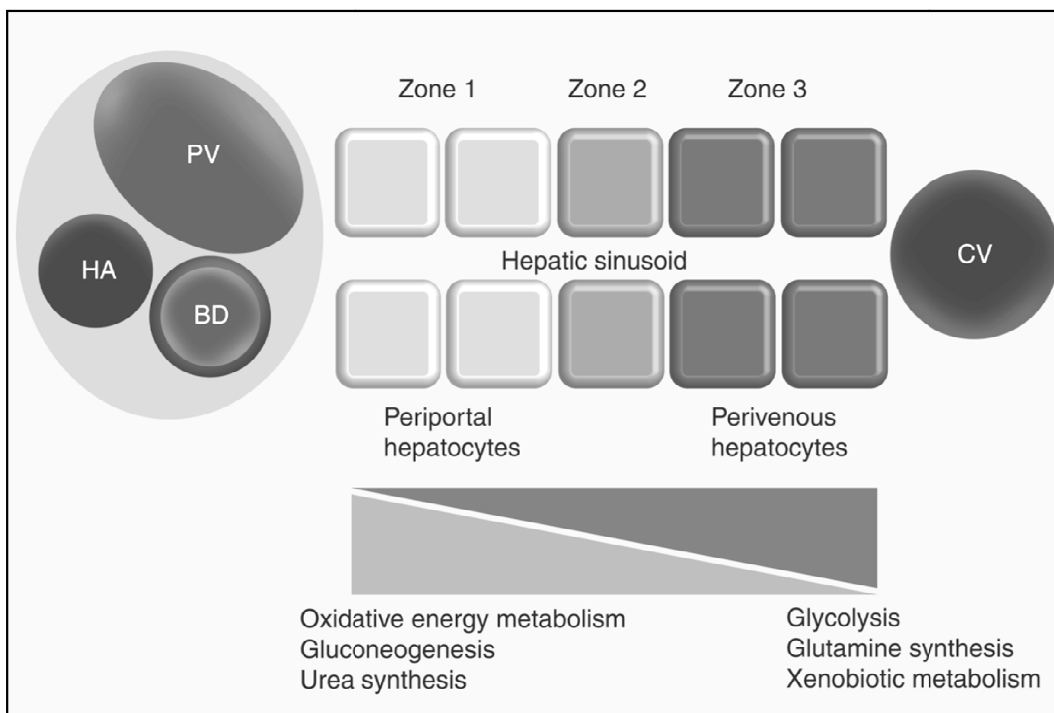


**Figure 1: Metabolic zonation in the liver.** Three zones are defined: a periportal zone (zone 1), a midzonal region (zone 2) and a perivenous or pericentral zone (zone 3). Abbreviations: PV, portal vein; HA, hepatic artery; BD, bile duct; CV, central vein. Taken from (Behari, 2010).

Several studies showed that  $\beta$ -catenin plays a crucial role in liver zonation, positively controlling the mRNA and protein expression of perivenous hepatocytes (Hailfinger *et al.*, 2006; Benhamouche *et al.*, 2006; Sekine *et al.*, 2006). A comparable expression pattern is found in murine hepatomas mutated in *Ctnnb1*, encoding  $\beta$ -catenin. On the other hand, periportal gene expression correlates with that of liver tumors mutated in

## Introduction

*Ha-ras*, leading to aberrant activation of the mitogen-activated protein kinase (MAPK) pathway (Stahl *et al.*, 2005; Braeuning *et al.*, 2007a).

### 1.2. Drug Metabolism in the Liver

The liver is the center of drug metabolism. Liver enzymes catalyze the conversion of lipophilic xenobiotics into hydrophilic products that can be excreted. The metabolism is divided into three phases: functionalization, conjugation, and excretion. In the so-called phase I, substrates are modified by introducing polar, reactive groups. Cytochrome P450 (CYP) enzymes belong to the group of phase I enzymes that catalyze the oxidation of substances. The most common reaction is a monooxygenase reaction thereby introducing one oxygen atom into the substrate. Phase II drug metabolizing enzymes comprise mainly transferases which mediate the conjugation of substrates with hydrophilic compounds. The excretion of the conjugates is accomplished by membrane transporters during the phase III (Marquardt and Schäfer, 2003).

Acetaminophen (AAP), also known as paracetamol, is widely used as a painkiller. In the liver, it undergoes distinct metabolic reactions via phase I and II enzymes (Figure 2). The majority (~90%) of AAP is directly conjugated with sulfate or glucuronic acid, leading to renal excretion (Cummings *et al.*, 1967). Only a minor fraction (5-10%) is converted into the toxic intermediate N-acetyl-*p*-benzoquinone-imine (NAPQI) (Miner and Kissinger, 1979). This reaction is mainly catalyzed by the phase I enzyme CYP2E1 (Raucy *et al.*, 1989; Dahlin *et al.*, 1984). Due to the overlapping substrate specificities, other CYP enzymes, e.g. 1A2, 3A4, and 2D6, also catalyze this reaction, but to a lesser extent (Raucy *et al.*, 1989; Dong *et al.*, 2000; Thummel *et al.*, 1993). NAPQI is further conjugated with glutathione (GSH) via glutathione-S-

## Introduction

transferases (GST) and excreted. High doses of AAP lead to depletion of GSH and accumulation of NAPQI. Subsequent hepatocellular death results from covalent protein binding and increased oxidative stress (Mitchell *et al.*, 1973; Hinson *et al.*, 2010). CYP enzymes are primarily expressed in hepatocytes located in the pericentral liver regions (Jungermann and Katz, 1982; Gebhardt, 1992). Thus, AAP-induced toxicity first occurs in the centrilobular hepatic regions (Dixon *et al.*, 1971).

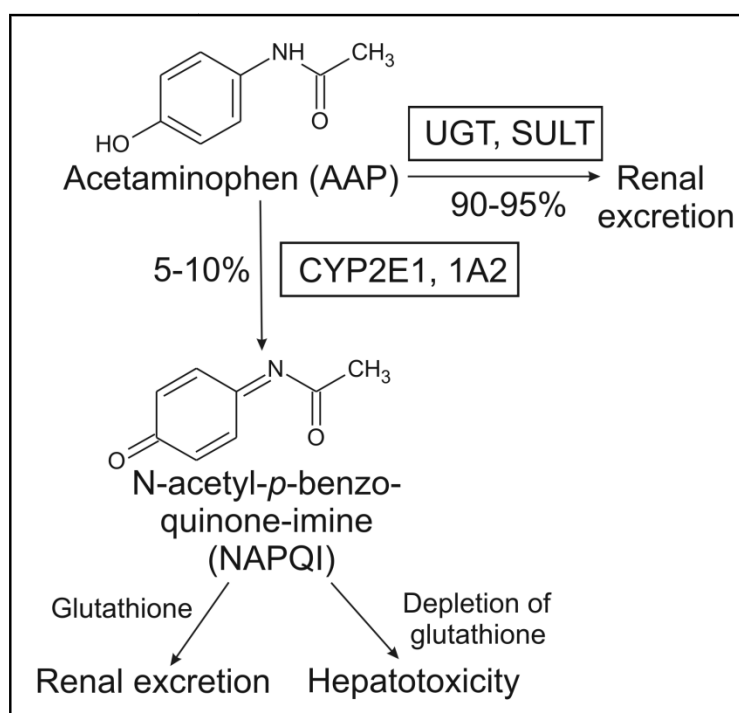


**Figure 2: Mechanism of CYP-induced hepatotoxicity of acetaminophen.** Abbreviations: AAP, acetaminophen; UGT, UDP-glucuronosyl transferase; SULT, sulfotransferase; CYP, cytochrome P450. Modified from (Singh *et al.*, 2013).

### 1.3. The Wnt/ $\beta$ -Catenin Signaling Pathway

The name Wnt is a composition of the *Drosophila Wingless (Wg)* gene and its homolog, the mouse mammary oncogene *Integration-1 (Int-1)* (Sharma *et al.*, 1976; Nusse and Varmus, 1982). Wnt-dependent signaling comprises three pathways, among them the evolutionary conserved Wnt/  $\beta$ -catenin pathway (or canonical Wnt pathway). It controls important cell processes during embryonic development and

## Introduction

tissue homeostasis (Logan and Nusse, 2004). De-regulation of the Wnt/  $\beta$ -catenin pathway can lead to birth defects and various diseases, including cancer (Polakis, 2000; Logan and Nusse, 2004). The canonical Wnt signaling pathway is activated by Wnt ligands, secreted lipid-modified glycoproteins, which regulate the amount of the transcriptional co-activator  $\beta$ -catenin (MacDonald *et al.*, 2009). In the absence of Wnt molecules, cytoplasmic  $\beta$ -catenin is degraded by a protein complex consisting of the adenomatous polyposis coli (APC) protein, glycogen synthase kinase 3 $\beta$  (GSK3 $\beta$ ), Axin, and casein kinase 1 $\alpha$  (CK1 $\alpha$ ). Phosphorylation of  $\beta$ -catenin at the amino terminal region is catalyzed by CK1 $\alpha$  and GSK3 $\beta$  and precedes ligase-mediated ubiquitination followed by proteasomal degradation. When Wnt ligands bind to the seven-transmembrane receptor frizzled (Fz)/ low density lipoprotein receptor-related protein 5 or 6 (LRP5/ 6) complex, the Wnt/  $\beta$ -catenin signaling pathway is activated. Dishevelled (Dvl) recruitment and LRP5/ 6 phosphorylation, together with translocation of the Axin complex to the Fz receptor, prevent  $\beta$ -catenin phosphorylation. Stabilized  $\beta$ -catenin accumulates, wanders into the nucleus and forms a complex with DNA-bound T-cell factor (TCF)/ lymphoid enhancer factor (LEF) transcription factors. This activates the transcription of target genes (Klaus and Birchmeier, 2008). An overview of the canonical Wnt signaling pathway is given in Figure 3.

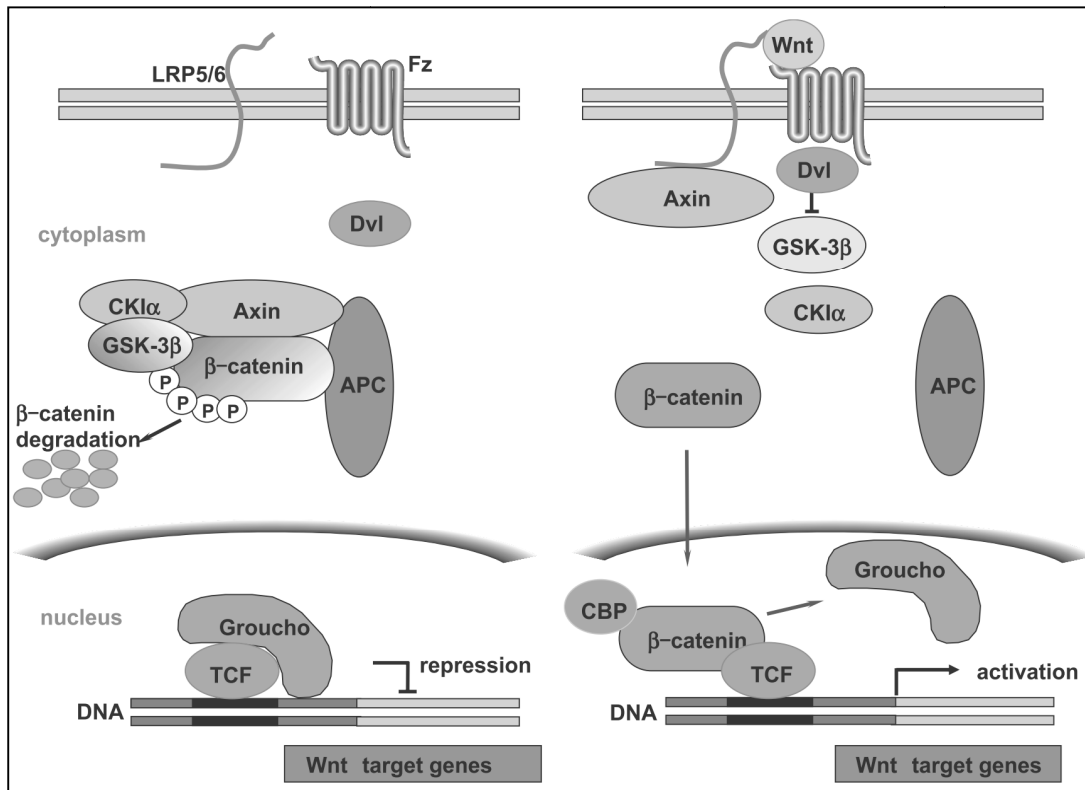


**Figure 3: Overview of the inactive (left) and active (right) Wnt/ β-catenin signaling pathway.**

Abbreviations: LRP5/ 6, low density lipoprotein receptor-related protein 5/ 6; Fz, frizzled; Dvl, dishevelled; CKIα, casein kinase 1α; GSK-3β, glycogen synthase kinase 3β; APC, adenomatous polyposis coli; CBP, CREB-binding protein; TCF, T-cell factor. Taken from (Takahashi-Yanaga and Sasaguri, 2007).

### 1.4. Carcinogenesis

According to the WHO, cancer is the second leading cause of death worldwide. The term carcinogenesis describes the transformation of normal cells into malignant tumor cells. The process of carcinogenesis includes three distinct stages: initiation, promotion, and progression (Foulds, 1954; Weinstein *et al.*, 1984; Figure 4). The first step towards tumor formation is DNA damage, caused spontaneously or by exogenous compounds. At this stage, different scenarios are possible: the damage may be repaired, apoptosis can be induced or the manifestation of a mutation, an irreversible genetic change, follows. There are two types of critical genes that are



## Introduction

primarily affected by these mutations: proto-oncogenes and tumor suppressor genes (Barrett and Wiseman, 1987). Proto-oncogenes play a role in normal cell growth and differentiation. Prominent examples include *C-MYC*, *CTNNB1*, *B-RAF*, or the *RAS* genes. Mutations may lead to activated oncogenes resulting in increased cell proliferation (Croce, 2008). Negative regulators of cell growth are referred to as tumor suppressors. Inactivating mutations in tumor suppressor genes, e.g. in *TP53*, *RB*, or *APC*, cause a loss of their function thereby driving tumorigenesis (Weinberg, 1991; Levine, 1993). In contrast, tumor promoters do not directly interact with the DNA but contribute to the clonal expansion of initiated cells by stimulation of cell proliferation or inhibition of apoptosis. This process is reversible and requires the presence of the promoting agent for a longer time period (Slaga, 1983). The transformation of a benign into a malignant tumor is referred to as tumor progression. This final step is characterized by increasing genetic instability, metastasizing, invasion, and tumor growth independent of external stimuli (Nowell, 1986).

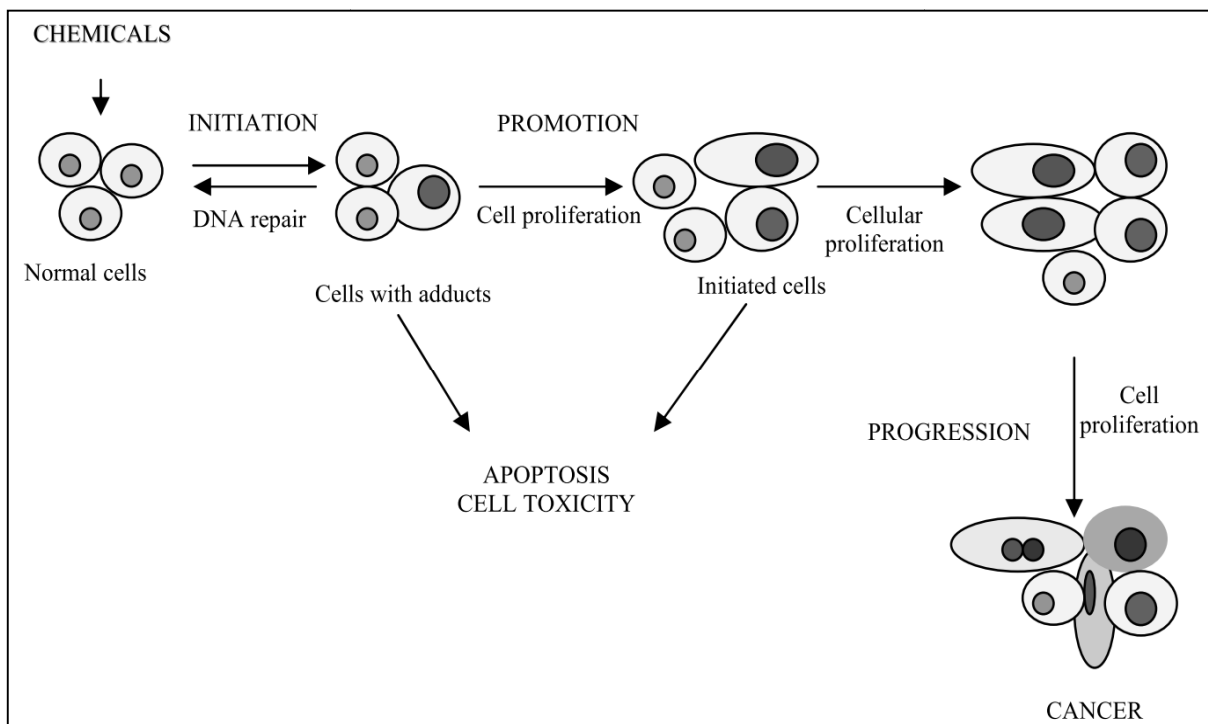


**Figure 4: Multi-stage model of carcinogenesis.** Taken from (Oliveira *et al.*, 2007).

#### **1.4.1. The Role of $\beta$ -Catenin in Tumorigenesis**

The *CTNNB1* gene is considered a proto-oncogene, as activating mutations in *CTNNB1* are associated with many cancers. Respective mutations are predominantly located in either codons 33, 41, or 45 of exon 3, thereby affecting the phosphorylation sites of  $\beta$ -catenin and preventing its degradation (Polakis, 1999; Morin, 1999). Recent studies suggest that the Wnt/  $\beta$ -catenin signaling pathway confers tumor cells with a selective growth advantage by increasing cell proliferation and inhibiting apoptosis (Cadoret *et al.*, 2001; Colnot *et al.*, 2004; Orford *et al.*, 1999; Shang *et al.*, 2004). Enhanced cell proliferation could be a consequence of target gene expression involved in cell cycle progression (He *et al.*, 1998; Shtutman *et al.*, 1999). Several *in vivo* experiments also demonstrated the important role of  $\beta$ -catenin in the regulation of cell proliferation in the liver (Cadoret *et al.*, 2001; Colnot *et al.*, 2004; Stein *et al.*, 2011). Additionally,  $\beta$ -catenin is involved in the prevention of apoptosis *in vitro* (Zhang *et al.*, 2001; Shang *et al.*, 2004; Gaujoux *et al.*, 2013) and its inhibition rendered cancer cells sensitive to apoptosis induced by different anticancer drugs (Saifo *et al.*, 2010; Chen *et al.*, 2001; Ellerkamp *et al.*, 2013). Moreover, the survival of murine skin tumor cells depends on the presence of  $\beta$ -catenin: using a transgenic mouse model, knockout of *Ctnnb1* in skin tumors harboring an activated Wnt/  $\beta$ -catenin signaling pathway resulted in complete tumor regression (Malanchi *et al.*, 2008).

#### **1.5. Hepatocellular Malignancies**

The most frequent form of liver cancer is hepatocellular carcinoma (HCC). The geographic variability in HCC incidences is mainly caused by the occurrence of chronic hepatitis B and C infections in developing countries. Other risk factors include

## Introduction

alcohol and tobacco abuse as well as aflatoxin B1 exposure (Bosch *et al.*, 2004). Due to its very poor prognosis, HCC is one of the most common causes of death from cancer (Parkin *et al.*, 2002). Besides vaccination against hepatitis being the most important measure for preventing liver cancer, the only curative treatment options are orthotopic liver transplantation, surgical resection, and local destruction (Taieb *et al.*, 2006). Common therapeutic strategies are often complicated by the occurrence of drug resistance (Thomas and Zhu, 2005; Shen *et al.*, 1991; Warmann *et al.*, 2002). Clinical studies with conventional chemotherapeutic agents including 5-fluorouracil, cisplatin, etoposide, and irinotecan were disappointing (Taieb *et al.*, 2006; Yoshino *et al.*, 1989). Thus, over recent years, research has focused on the development of new treatment approaches interfering with specific pathways often de-regulated in liver cancer. These include the MAPK, PI3K (phosphatidylinositide 3-kinase), VEGFR (vascular endothelial growth factor receptor), IGF (insulin-like growth factor), HGF (hepatocyte growth factor) and the Wnt/  $\beta$ -catenin signaling pathway (Whittaker *et al.*, 2010). Since ~20% of HCCs harbor activating mutations in *CTNNB1* (Giles *et al.*, 2003), extensive research also focuses on the role of the Wnt/  $\beta$ -catenin signaling pathway in liver cancer and efforts are also being made to target this pathway.

Hepatoblastoma (HB) is a rare malignant liver tumor mainly occurring in infants and children (Darbari *et al.*, 2003). Common therapy includes primarily surgery and furthermore liver transplantation and chemotherapy (von Schweinitz, 2012; Reynolds *et al.*, 1992). Cisplatin alone or in combination with other cytostatics is an effective treatment approach (von Schweinitz, 2012; Pritchard *et al.*, 2000; Reynolds *et al.*, 1992). Although the overall survival rate of HB patients is more than 90%, alternative options for high-risk or recurrent HBs are needed due to occurring treatment

## Introduction

resistance (von Schweinitz *et al.*, 1997). Activating mutations in *CTNNB1* are also very common in HBs (50-90%) (Lopez-Terrada *et al.*, 2009; Koch *et al.*, 1999).

### 1.5.1. Chemically Induced Hepatocarcinogenesis in Mice

Certain mouse strains frequently develop spontaneous liver tumors and are also highly susceptible to chemically induced carcinogenesis making them a useful model to study the mechanisms of hepatocarcinogenesis (Leenders *et al.*, 2008; Maronpot *et al.*, 1995). Previous works showed that liver tumors induced in male C3H/He mice predominantly harbor mutations either in *Ha-ras*, *B-raf*, or *Ctnnb1*, depending on the treatment regimen. Mutations in the *Ha-ras* or *B-raf* gene are very often observed when two weeks old mice are given a single intraperitoneal injection of the liver carcinogen N-nitrosodiethylamine (DEN) (Bauer-Hofmann *et al.*, 1992; Jaworski *et al.*, 2005). In contrast, about 80% of generated liver tumors harbor activating mutations in *Ctnnb1* after mice are applied DEN at the age of six weeks followed by chronic treatment with the tumor promoter phenobarbital (PB) (Aydinlik *et al.*, 2001). Furthermore, *Ctnnb1*-mutated liver tumors in mice display high expression of glutamine synthetase (GS), a marker for hepatic  $\beta$ -catenin activation (Loeppen *et al.*, 2002; Cadoret *et al.*, 2002). Respective tumors also express certain enzymes involved in xenobiotic metabolism, including CYP2E1 and 1A2 (Loeppen *et al.*, 2005). In contrast, those enzymes are almost entirely absent from tumors mutated in the *Ha-ras* gene (Hailfinger *et al.*, 2006).

## 1.6. Aims and Objectives

Aberrant activation of the Wnt/  $\beta$ -catenin signaling pathway is often observed in liver tumors. Despite extensive research, the exact role of  $\beta$ -catenin in hepatocarcinogenesis is still unclear. In murine skin tumors with increased Wnt/  $\beta$ -catenin signaling, knockout of *Ctnnb1* led to complete tumor regression within several weeks (Malanchi *et al.*, 2008). Based on this observation, an *in vivo* study in transgenic mice was performed to investigate if ablation of  $\beta$ -catenin led to similar effects in *Ctnnb1*-mutated liver tumors. Furthermore, the ability of  $\beta$ -catenin to prevent apoptosis was analyzed using mouse hepatoma cell lines. *Ctnnb1*-mutated liver tumors in mice were found to exhibit high expression of certain xenobiotic enzymes, including CYP2E1 and 1A2 (Loeppen *et al.*, 2005). Therefore, the second animal experiment aimed to take advantage of this characteristic metabolic profile. The impact of a single high dose AAP treatment on *Ctnnb1*-mutated, CYP-positive liver tumors was assessed with respect to its potential relevance for tumor therapy.

## 2. Materials

### 2.1. Laboratory Equipment

<b>Appliance</b>	<b>Manufacturer</b>	<b>Product name</b>
autoclave	Webeco, Bad Schwartau	Autoklav C
balances	Sartorius, Göttingen	Analytic
	Sartorius, Göttingen	Basic
	Sartorius, Göttingen	CP922
	Mettler, Giessen	Laborwaage K7
	Mettler, Giessen	Laborwaage P1200
burner	WLD-TEC, Göttingen	Gasprofi 1 micro
camera	Zeiss, Göttingen	AxioCam MRc
CCD camera	Raytest, Straubenhardt	CSC chemoluminescence detection module
centrifuges	Eppendorf, Wesseling	Centrifuge 5410
	Eppendorf, Wesseling	Centrifuge 5417 R
	Heraeus, Hanau	Sepatech Biofuge 13
	Heraeus, Hanau	Sepatech Megafuge 1.0 R
	Hettich, Tuttlingen	Micro Rapid/ K
chemistry analyzer	IDEXX Laboratories, Ludwigsburg	VetTest 8008
cryostat microtome	Reichert-Jung, Wetzlar	Frigocut 2800
digital camera	Nikon, Düsseldorf	Coolpix 950
drying oven	Heraeus, Hanau	
electrophoresis chamber	Gibco BRL, Karlsruhe	H 6
heat sterilizer	Heraeus, Hanau	VTR 5022
incubator	Heraeus, Hanau	BB 220 CU
laminar flow	BDK, Sonnenbühl	Sterilbank UVF 6.12 S
light microscope	Leitz, Wetzlar	Labovert FS
	Zeiss, Göttingen	Imager.M1
magnetic stirrer	Janke & Kunkel, Staufen	IKA-Combimag RCT
	Janke & Kunkel, Staufen	IKA-Mag RH
	Bachofer, Reutlingen	MR 80
microwave	Bosch, Stuttgart	Bosch 600 W
multiwell plate reader	Perkin Elmer, Waltham, USA	1420 Multilabel Counter Victor <sup>3</sup> V
PCR cabinet	Safetech Limited, Hongkong, China	Cleansphere CA100

## Materials

PCR machine	Biometra, Göttingen Perkin Elmer, Waltham, USA	UNO-Thermoblock GeneAmp PCR System 2400
peristaltic pump	KNF Neuberger, Freiburg	Miniport
pH-meter	WTW, Weilheim	pH 522
power supply	Desaga, Wiesloch Pharmacia, Uppsala, Sweden	Desatronic 3x500/ 100 LKB EPS 500/ 400
respiratory masks	Sigma, Taufkirchen	Consort EV243
shaker	Roth, Karlsruhe Braun, Melsungen Heidolph, Kelheim	FFA2P3 RD Certomat HK Titramax 1000
spectrophotometer	Peqlab, Erlangen	NanoDrop ND-1000
thermoblock	Eppendorf, Hamburg Eppendorf, Hamburg	5436 5320
ultrasound device	Bandelin, Berlin	Sonorex Super RK 102 P
UV lamp	Biometra, Göttingen	TI 1
vortex mixer	Bender & Hobein, Bruchsal Heidolph, Schwabach Heidolph, Schwabach	Vortex Genie 2  Reax top Reax 2000
water bath	GF, Burgwedel	1083
water preparation plant	Millipore, Schwalbach	Milli Q Plus

## 2.2. Expendable Items

Item	Source	Product name
0.2 ml reaction tubes	Peqlab, Erlangen	
0.6 ml reaction tubes	Biozym, Oldendorf	
1.3 ml Li-Heparin tubes	Sarstedt, Nümbrecht	
1.5 ml reaction tubes	Eppendorf, Hamburg Greiner Bio-One, Frickenhausen Sarstedt, Nümbrecht	
1.8 ml cryo tubes	Nunc, Wiesbaden	Cryo Tube Vials
2 ml reaction tubes	Eppendorf, Hamburg Sarstedt, Nümbrecht	
5 ml polystyrene tubes	BD, Heidelberg	Falcon 2058
15 ml tubes	BD, Heidelberg	Falcon 2096

## Materials

50 ml tubes	BD, Heidelberg	Falcon 2070
cages	Techniplast, Neumarkt	Macrolon Typ 2
cannula (0.9x40 mm)	BD, Heidelberg	Microlance 3
cannula (0.5x16 mm)	BD, Heidelberg	Microlance 3
cell culture dishes	BD, Heidelberg	Falcon 3003
cell culture plates	BD, Heidelberg	Falcon 3224
	BD, Heidelberg	Falcon 3226
	BD, Heidelberg	Falcon 3075
cell scraper	Corning, Inc., NY, USA	Costar Cell Lifter
counting chamber	n.n.	Fuchs-Rosenthal chamber
cover slips	Langenbrinck, Emmendingen	Deckgläser 24x32 mm
	Menzel, Braunschweig	Deckgläser Ø 30 mm
dako pen	Dako, Glostrup, Denmark	Pen no. S 2002
gel loader tips	Peqlab, Erlangen	MultiFlex
glass pipettes	Brand, Wertheim	
glass ware	Schott, Mainz	
gloves	Ansell, Munich	Micro Touch Hygrip
microscope slides	Langenbrinck, Emmendingen	
multi-channel pipette	Brand, Wertheim	Transferpipette-12
	ABIMED, Langenfeld	Discovery
nitrile gloves	Kimberly-Clark, Dallas, USA	Safeskin Purple Nitrile
parafilm	Pechiney, Chicago, USA	PM-996
pasteur pipettes	WU Mainz, Mainz	
pipettes and tips	Biozym, Oldendorf	
	Eppendorf, Hamburg	
	Gilson, Limburg	
pipettors	Brand, Wertheim	Accu-jet pro
procedure mask	Kimberly-Clark, Dallas, USA	The Lite One
Q-tips	NeoLab, Heidelberg	
scalpel	Braun, Melsungen	
sterile filter	Millipore, Eschborn	Steritop 0.22 µm
syringes	Braun, Melsungen	Injekt 1 ml
	Braun, Melsungen	Injekt 10 ml
	BD, Heidelberg	Plastipak
syringe filter 0.45 µm	Sartorius, Göttingen	Minisart



## 2.3. Chemicals and Biochemicals

<b>Reagent</b>	<b>Manufacturer</b>
Ac-DEVD-AFC	Biomol, Hamburg
acetaminophen	Sigma, Taufkirchen
acetic acid (100%)	Merck, Darmstadt
acrylamide (30%)	Roth, Karlsruhe
AFC	Biomol, Hamburg
agarose	Peqlab, Erlangen
3-amino-9-ethylcarbazole	Sigma, Taufkirchen
ammonium peroxodisulfate	Merck, Darmstadt
ammonium sulfide solution	Merck, Darmstadt
ampicillin (sodium salt)	Sigma, Taufkirchen
ampuwa (sterile water)	Fresenius-Kabi, Bad Homburg
ATP	PJK GmbH, Kleinblittersdorf
bacto tryptone	Applichem, Darmstadt
bacto yeast extract	Applichem, Darmstadt
benzonase	Sigma, Taufkirchen
boric acid	Roth, Karlsruhe
bortezomib	LC Laboratories, Woburn, USA
Bradford protein assay	Bio-Rad, Munich
5-bromodeoxyuridine	Applichem, Darmstadt
bromophenol blue	Merck, Darmstadt
BSA	Serva, Heidelberg
BSA solution (20 mg/ ml)	Fermentas, St. Leon-Rot
calf intestinal alkaline phosphatase	Invitrogen, Karlsruhe
chloral hydrate	Riedel-de Haen, Seelze
chloroform	Merck, Darmstadt
citric acid	Applichem, Darmstadt
coelenterazine	PJK GmbH, Kleinblittersdorf
coenzyme A	PJK GmbH, Kleinblittersdorf
corn oil	Mazola, Unilever, Hamburg
dimethylformamide	Merck, Darmstadt
dithiothreitol	Sigma, Taufkirchen
D-luciferine	PJK GmbH, Kleinblittersdorf
DMEM/ F-12	Gibco/ BRL, Karlsruhe
DMSO	Applichem, Darmstadt
DNA ladder 1 kb	Fermentas, St. Leon-Rot
dNTP mix (2 mM)	Fermentas, St. Leon-Rot
doxycycline	Sigma, Taufkirchen

## Materials

EDTA	Merck, Darmstadt
Entellan	Merck, Darmstadt
Eosin G	Merck, Darmstadt
ethanol	Merck, Darmstadt
ethidium bromide	Serva, Heidelberg
etoposide	Sigma, Taufkirchen
Fast Red substrate	Kem-En-Tec, Copenhagen, Denmark
FCS	Gibco/ BRL, Eggenstein
ficoll type 400	Sigma, Taufkirchen
geneticin sulfate G418	Biochrom, Berlin
glucose-6-phosphate	Sigma, Taufkirchen
glutaraldehyde	Serva, Heidelberg
HCl	Merck, Darmstadt
hematoxylin	Roth, Karlsruhe
hepes (acid)	Roth, Karlsruhe
HiPerFect	Qiagen, Hilden
H <sub>2</sub> O <sub>2</sub> (30%)	Applichem, Darmstadt
Hoechst 33258	Invitrogen, Karlsruhe
hygromycin B	InvivoGen, San Diego, USA
<i>In Situ</i> Cell Death Detection Kit, POD	Roche, Mannheim
isopropanol	Merck, Darmstadt
Kaiser's glycerol gelatine	Merck, Darmstadt
KAl(SO <sub>4</sub> ) <sub>2</sub> x 12 H <sub>2</sub> O	Merck, Darmstadt
KCl	Merck, Darmstadt
K <sub>3</sub> [Fe <sup>(III)</sup> (CN) <sub>6</sub> ]	Merck, Darmstadt
K <sub>4</sub> [Fe <sup>(II)</sup> (CN) <sub>6</sub> ]	Merck, Darmstadt
KH <sub>2</sub> PO <sub>4</sub>	Merck, Darmstadt
K <sub>2</sub> HPO <sub>4</sub> x 3 H <sub>2</sub> O	Merck, Darmstadt
lead nitrate	Serva, Heidelberg
LiCl	Roth, Karlsruhe
Lipofectamine 2000	Invitrogen, Karlsruhe
maleic acid	Merck, Darmstadt
Masson-Goldner trichrome staining kit	Roth, Karlsruhe
methanol	Merck, Darmstadt
MG-132	Enzo Life Sciences Inc. Farmingdale, USA
MgCl <sub>2</sub> (25 mM)	Fermentas, St. Leon-Rot
MgCl <sub>2</sub> x 6 H <sub>2</sub> O	Merck, Darmstadt
MgSO <sub>4</sub> x 7 H <sub>2</sub> O	Merck, Darmstadt
NaCl	Merck, Darmstadt

## Materials

NaHCO <sub>3</sub>	Merck, Darmstadt
Na <sub>2</sub> HPO <sub>4</sub> x 2 H <sub>2</sub> O	Merck, Darmstadt
NaIO <sub>3</sub>	Merck, Darmstadt
NaN <sub>3</sub>	Merck, Darmstadt
NaOH	Merck, Darmstadt
N-nitrosodiethylamine	Sigma, Taufkirchen
NP-40	Sigma, Taufkirchen
Opti-MEM	Gibco/ BRL, Eggenstein
orange G dye	Merck, Darmstadt
paraformaldehyde	Sigma, Taufkirchen
Passive Lysis Buffer	Promega, Mannheim
pBR322 DNA-MspI digest	NEB, Ipswich, USA
penicillin/ streptomycin	Biochrom, Berlin
phenobarbital-containing diet	Ssniff, Soest
proteinase K	Boehringer, Mannheim
QIAfilter Plasmid Midi Kit	Qiagen, Hilden
resazurin	Sigma, Taufkirchen
SDS	Serva, Heidelberg
sodium acetate	Merck, Darmstadt
sodium citrate	Merck, Darmstadt
streptavidin (AP-conjugated)	Spa, Milan, Italy
sucrose	Merck, Darmstadt
swine serum (normal)	Dako, Glostrup, Denmark
tamoxifen	Sigma, Taufkirchen
10x Taq buffer	Fermentas, St. Leon-Rot
Taq polymerase (native, 5 U/ μl)	Fermentas, St. Leon-Rot
Taq polymerase (recombinant, 1 U/ μl)	Fermentas, St. Leon-Rot
TEMED	Roth, Karlsruhe
tricine	Applichem, Darmstadt
tris (base)	Sigma, Taufkirchen
triton X-100	Serva, Heidelberg
trypsin/ EDTA solution	Biochrom, Berlin
tween-20	Sigma, Taufkirchen
X-Gal substrate	Peqlab, Erlangen
xylene	VWR International GmbH, Darmstadt
xylene cyanol	Sigma, Taufkirchen

## 2.4. Buffers and Solutions

### 2.4.1. Cell Culture

#### DMEM/ F-12

Reagent	Volume/ Weight
DMEM/ F-12 medium	6 g
NaHCO <sub>3</sub>	1.22 g
H <sub>2</sub> O <sub>dest</sub>	ad 450 ml

- adjust to pH 7.2 with HCl (conc), filtrate sterile (pore size 0.22 µm), store at 4 °C
- before use, add 10% (v/ v) FCS (heat-inactivated at 56 °C for 30 min), 1% (v/ v) penicillin (10,000 U/ ml)/ streptomycin (10 mg/ ml) solution, store at 4 °C
- for cultivation of stably transfected cells, add 0.5% (v/ v) geneticine (20 mg/ ml) and 0.1% (v/ v) hygromycin B (100 mg/ ml) (for preparation of solutions see following sections)

#### 100 mM hepes buffer

Reagent	Volume/ Weight
hepes (acid)	11.92 g
H <sub>2</sub> O <sub>dest</sub>	ad 500 ml

- adjust to pH 7.4 with NaOH

#### 20 mg/ ml geneticin solution

Reagent	Volume/ Weight
geneticin sulfate (activity 701 µg/ mg)	1.43 g
100 mM hepes buffer pH 7.4	50 ml

- filtrate sterile (pore size 0.45 µm), store at -20 °C

#### 100 mg/ ml hygromycin B

Reagent	Volume/ Weight
hygromycin B (activity 990 µg/ mg)	2.02 g
100 mM hepes buffer pH 7.4	20 ml

- filtrate sterile (pore size 0.45 µm), store at -20 °C

#### 10x PBS

Reagent	Volume/ Weight
NaCl	80 g
KCl	2 g
KH <sub>2</sub> PO <sub>4</sub>	2 g
Na <sub>2</sub> HPO <sub>4</sub> x 2 H <sub>2</sub> O	14.35 g
H <sub>2</sub> O <sub>dest</sub>	ad 1,000 ml

- autoclave (30 min)

## Materials

### 2.4.2. Cell Treatment

#### **Doxycycline**

Reagent	Volume/ Weight	Stock conc	Final conc
doxycycline	10 mg	1 mg/ ml	0.1-10 µg/ ml
H <sub>2</sub> O <sub>dest</sub>	10 ml		

- filtrate sterile (pore size 0.45 µm), prepare 1 ml aliquots and store at -20 °C protected from light

#### **LiCl**

Reagent	Volume/ Weight	Stock conc	Final conc
LiCl	424 mg	1 M	15 mM
H <sub>2</sub> O <sub>dest</sub>	10 ml		

- filtrate sterile (pore size 0.45 µm), store at 4 °C

#### **NaCl**

Reagent	Volume/ Weight	Stock conc	Final conc
NaCl	584 mg	1 M	15 mM
H <sub>2</sub> O <sub>dest</sub>	10 ml		

- filtrate sterile (pore size 0.45 µm), store at 4 °C

#### **Etoposide**

Reagent	Stock conc	Final conc
etoposide in DMSO	50 mM	10 µM

- store at room temperature protected from light

#### **Bortezomib**

Reagent	Stock conc	Final conc
bortezomib in DMSO	10 µM	5-100 nM

- store at -20 °C

#### **MG-132**

Reagent	Stock conc	Final conc
MG-132 in DMSO	1 mM	1 µM

- store at -20 °C

## Materials

### 2.4.3. Plasmid Preparation

#### LB medium

Reagent	Volume/ Weight
NaCl	10 g
bacto tryptone	10 g
bacto yeast extract	5 g
H <sub>2</sub> O <sub>dest</sub>	ad 1,000 ml

- adjust to pH 7 with NaOH, autoclave (30 min), store at room temperature
- add 0.1% (v/ v) ampicillin (100 mg/ ml) shortly before use

### 2.4.4. Reporter Gene Analysis

#### DTT

Reagent	Volume/ Weight	Stock conc	Final conc
DTT	1.545 g	1 M	33.3 mM
H <sub>2</sub> O <sub>dest</sub>	10 ml		

- filtrate sterile (pore size 0.45 µm) and store at -70 °C

#### Firefly luciferase buffer

Reagent	Volume/ Weight
ATP	292 mg
Coenzyme A	207 mg
tricine	3.58 g
MgSO <sub>4</sub> x 7 H <sub>2</sub> O	1.32 g
200 mM EDTA	500 µl
D-luciferin	132 mg
H <sub>2</sub> O <sub>dest</sub>	ad 1,000 ml

- adjust to pH 8 and cool on ice before adding D-luciferin, filtrate sterile (pore size 0.22 µm), prepare 10 ml aliquots and store at -70 °C protected from light
- add DTT (1 M) prior to use

#### 1000x coelenterazine

Reagent	Volume/ Weight
coelenterazine	0.605 mg
methanol	1 ml

- prepare 50 µl aliquots and store at -70 °C protected from light

## Materials

### 1 M $K_xPO_4$ pH 5.1

Reagent	Volume/ Weight
$K_2HPO_4 \times 3 H_2O$	22.82 g
$KH_2PO_4$	34.02 g
$H_2O_{dest}$	350 ml

### Renilla luciferase buffer

Reagent	Volume/ Weight
200 mM $Na_2EDTA$	11 ml
1 M $K_xPO_4$ pH 5.1	220 ml
BSA	0.44 g
NaCl	64.3 g
$NaN_3$	84.5 mg
$H_2O_{dest}$	ad 1,000 ml

- adjust to pH 5, filtrate sterile (pore size 0.22  $\mu m$ ), prepare 10 ml aliquots and store at -20 °C

- add coelenterazine prior to use

## 2.4.5. Cell Viability Assays

### 10x Alamar Blue solution

Reagent	Volume/ Weight
resazurin	10 mg
$H_2O_{dest}$	10 ml

- filtrate sterile (pore size 0.45  $\mu m$ ) and store at 4 °C

## 2.4.6. Determination of Apoptosis

### Lysis buffer

Reagent	Volume/ Weight
1 M tris pH 8	5 ml
NaCl	0.7 g
0.5 M EDTA pH 8	1 ml
NP-40	0.5 ml
$H_2O_{dest}$	ad 100 ml

- store at 4 °C

- add 0.5% 1 M DTT (see 2.4.4) prior to use

## Materials

### AFC solution

Reagent	Volume/ Weight	Stock conc	Final conc
AFC	0.1 mg	0.1 mg/ ml	1 µg/ ml
DMSO	1 ml		

- store at -20 °C protected from light
- solution is diluted in lysis buffer prior to use

### Ac-DEVD-AFC solution

Reagent	Volume/ Weight	Stock conc	Final conc
Ac-DEVD-AFC	5 mg	10 mM	50 µM
DMSO	686 µl		

- store at -20 °C
- solution is diluted in lysis buffer prior to use

### BSA standard curve

Reagent	Volume/ Weight	Stock conc	Final conc
BSA	5 mg	5 mg/ ml	0-500 µg/ ml
H <sub>2</sub> O <sub>dest</sub>	1 ml		

- store at -20 °C

### Paraformaldehyde solution (3% w/ v)

Reagent	Volume/ Weight
paraformaldehyde	3 g
PBS	100 ml

- pre-heat PBS to 200 °C
- prepare freshly

### Hoechst 33258 solution

Reagent	Volume/ Weight
Hoechst 33258	1 mg
PBS	1 ml

- store at -20 °C protected from light
- solution is diluted 1:100 in PBS prior to use

## 2.4.7. Gel Electrophoresis

### Agarose Gel Electrophoresis

#### 50x TAE buffer

Reagent	Volume/ Weight
tris (base)	242 g
0.5 M EDTA pH 8	100 ml
glacial acetic acid	57.1 ml
H <sub>2</sub> O <sub>dest</sub>	ad 1,000 ml



## Materials

### 6x loading buffer

Reagent	Volume/ Weight
saccharose	50 g
SDS	1 g
orange G dye	0.5 g
H <sub>2</sub> O <sub>dest</sub>	ad 100 ml

### DNA ladder 1 kb

Reagent	Volume
DNA ladder 1 kb (1 µg/ µl)	1 µl
6x loading buffer	1 µl
H <sub>2</sub> O <sub>dest</sub>	ad 7 µl

- store at -20 °C

## Acrylamide Gel Electrophoresis

### 5x TBE buffer pH 8

Reagent	Volume/ Weight
tris (base)	54 g
boric acid	27.5 g
0.5 M EDTA pH 8	20 ml
H <sub>2</sub> O <sub>dest</sub>	ad 1,000 ml

### 10x loading buffer

Reagent	Volume/ Weight
bromophenol blue	25 mg
xylene cyanol	25 mg
ficoll type 400	1.5 g
0.5 M EDTA pH 8	1 ml
H <sub>2</sub> O <sub>dest</sub>	ad 10 ml

- store at 4 °C

### pBR322 DNA-Mspl digest

Reagent	Volume
pBR322 DNA-Mspl digest (1 µg/ µl)	10 µl
loading buffer	10 µl
H <sub>2</sub> O <sub>dest</sub>	ad 50 µl

## Materials

### 10% acrylamide gel

Reagent	Volume/ Weight
H <sub>2</sub> O <sub>dest</sub>	16.6 ml
5x TBE buffer	7.2 ml
acrylamide (30%)	12 ml
ammonium persulfate (10% w/ v)	200 µl
TEMED	20 µl

### Ethidium bromide solution

Reagent	Volume/ Weight	Stock conc	Final conc
ethidium bromide	10 mg	10 mg/ ml	0.5 µg/ ml
H <sub>2</sub> O <sub>dest</sub>	1 ml		

- store at 4 °C

## 2.4.8. Immunohistochemistry

### Carnoy's fixative

Reagent	Volume
ethanol	60 ml
chloroform	30 ml
glacial acetic acid	10 ml

- prepare shortly before use

### 10x 0.1 M citrate buffer pH 6

Reagent	Volume/ Weight
citric acid (sodium salt)	29.41 g
H <sub>2</sub> O <sub>dest</sub>	1,000 ml

### TB buffer pH 8.7

Reagent	Volume/ Weight
tris (base)	6 g
MgCl <sub>2</sub> x 6 H <sub>2</sub> O	406 mg
H <sub>2</sub> O <sub>dest</sub>	ad 1,000 ml

### TBS/ T pH 7.4

Reagent	Volume/ Weight
tris (base)	6 g
NaCl	5.8 g
tween-20	1 ml
H <sub>2</sub> O <sub>dest</sub>	ad 1,000 ml

## Materials

### PBS/ S

Reagent	Volume/ Weight
1x PBS	100 ml
BSA	1 g
NaCl	2.03 g

### PBS/ T

Reagent	Volume
1x PBS	100 ml
tween-20	0.2 ml

### Acetate buffer

Reagent	Volume/ Weight
sodium acetate	6.48 g
glacial acetic acid	1.21 ml
H <sub>2</sub> O <sub>dest</sub>	ad 1,000 ml

### AEC staining buffer

Reagent	Volume/ Weight
acetate buffer	14 ml
dimethylformamide	1 ml
3-amino-9-ethylcarbazole	4 mg
H <sub>2</sub> O <sub>2</sub> (30%)	15 µl

- dissolve 3-amino-9-ethylcarbazole in dimethylformamide before adding acetate buffer

- add H<sub>2</sub>O<sub>2</sub> shortly before use

### Mayer's Hemalum

Reagent	Volume/ Weight
hematoxylin	1 g
NaIO <sub>3</sub>	0.2 g
KAl(SO <sub>4</sub> ) <sub>2</sub> x 12 H <sub>2</sub> O	50 g
chloral hydrate	50 g
citric acid	1 g
H <sub>2</sub> O <sub>dest</sub>	ad 1,000 ml

- dissolve first 3 components in H<sub>2</sub>O<sub>dest</sub>, then add chloral hydrate and citric acid

### 0.2 M tris/ maleate buffer

Reagent	Volume/ Weight
tris (base)	24.2 g
maleic acid	23.2 g
H <sub>2</sub> O <sub>dest</sub>	ad 1,000 ml

## Materials

### G6Pase incubation buffer

Reagent	Volume/ Weight
tris/ maleate buffer	100 ml
H <sub>2</sub> O <sub>dest</sub>	133 ml
2% w/ v lead nitrate solution	25 ml
glucose-6-phosphate	250 mg

- add lead nitrate solution dropwise
- add glucose-6-phosphate shortly before use

### X-Gal staining solution

Reagent	Volume/ Weight	Stock conc	Final conc
X-Gal	100 mg	100 mg/ ml	1 mg/ ml
DMF	1 ml		

- store at -20 °C

### X-Gal staining buffer

Reagent	Volume/ Weight
K <sub>4</sub> [Fe <sup>(III)</sup> (CN) <sub>6</sub> ]	210 mg
K <sub>3</sub> [Fe <sup>(III)</sup> (CN) <sub>6</sub> ]	160 mg
MgCl <sub>2</sub> x 6 H <sub>2</sub> O	40.6 mg
NP-40	20 µl
SDS	10 mg
PBS	ad 100 ml

- add 1% X-Gal staining solution prior to use

## 2.5. Primers

### 2.5.1. Genotyping

Gene	Cre
Primer pair	up.int.cre/ int.cre.rev
Forward primer (5'-3')	TCCATGAGTGAACGAACCTGGTCCG
Reverse primer (5'-3')	TTTGCCTGCATTACCGGTTCGATGC
Product size (bp)	400

Gene	<i>Ctnnb1</i> <sup>loxP/loxP</sup>
Primer pair	662/ 803n
Forward primer (5'-3')	ACTGCCTTTGTTCTCTTCCCTTCTG
Reverse primer (5'-3')	CAGCCAAGGAGAGCAGGTGAGG
Product size (bp)	loxP: 180; WT: 140

## Materials

### 2.5.2. Sequencing

<b>Gene</b>	<b><i>Ctnnb1</i></b>
Primer pair	S1/ S2
Forward primer (5'-3')	ACTCTGTTTTTACAGCTGACCT
Reverse primer (5'-3')	CAAGAGCAAGTAGCTGGTAAA
Product size (bp)	248

### 2.6. siRNA

<b>Name</b>	<b>si<i>Ctnnb1</i> (Mm_Ctnnb_2_HP)</b>
Sense (5'-3')	r(GAUAGAAAUGGUCCGAUUA)dTdT
Antisense (5'-3')	r(UAAUCGGACCAUUUCUAUC)dTdG

<b>Name</b>	<b>siscrambled (Allstars AF 488)</b>
Sense (5'-3')	r(UUCUCCGAACGUGUCACGU)dTdT
Antisense (5'-3')	r(ACGUGACAGGUUCGGAGAA)dTdT

### 2.7. Antibodies for IHC

#### Primary antibodies:

<b>Antigen</b>	<b>Species</b>	<b>Dilution</b>	<b>Cat-No.</b>	<b>Manufacturer</b>
<b>BrdU</b>	mouse, monoclonal	1:100	M0744	Dako, Glostrup, Denmark
<b><math>\beta</math>-catenin</b>	rabbit, polyclonal	1:50	9587	Cell Signaling, Danvers, USA
<b>Active <math>\beta</math>-catenin</b>	rabbit, polyclonal	1:400	8814S	Cell Signaling, Danvers, USA
<b>Connexin 32</b>	rabbit, polyclonal	1:250	34-5700	Invitrogen/ Zymed, Darmstadt
<b>CYP1A2</b>	rabbit, polyclonal	1:1,000	-	Gift of Dr. R. Wolf, University of Dundee, UK
<b>CYP2E1</b>	rabbit, polyclonal	1:500	MFO-100	Stressgen, Victoria, Canada
<b>E-cadherin</b>	rabbit, monoclonal	1:50	3195	Cell Signaling,

## Materials

				Danvers, USA
<b>GS</b>	rabbit, polyclonal	1:1,000	G2781	Sigma, Taufkirchen
<b>HNF4<math>\alpha</math></b>	mouse, monoclonal	1:100	PP-H1415-00	R&D Systems, Wiesbaden

### Secondary antibodies/ conjugates:

Antigen	Species	Dilution	Cat-No.	Manufacturer
<b>Mouse IgG</b> HRP-conjugated	goat polyclonal	1:20	A-2554	Sigma, Taufkirchen
<b>Rabbit IgG</b> HRP-conjugated	swine polyclonal	1:100	P0217	Dako, Glostrup, Denmark
<b>Mouse IgG</b> Biotin-conjugated	goat polyclonal	1:200	FR14-61	Spa, Milan, Italy
<b>Rabbit IgG</b> Biotin-conjugated	goat polyclonal	1:200	111-065-003	Dianova, Hamburg
<b>Rabbit IgG</b> $\beta$ -Gal-conjugated	goat polyclonal	1:50	A132GN	American Qualex, St. Clemente, USA
<b>Biotin</b> AP-Streptavidin conjugate		1:200	016-050-084	Dianova, Hamburg
<b>Rabbit IgG</b> Cy3-conjugated	goat polyclonal	1:100	111-165-144	Dianova, Hamburg

## 2.8. Vectors

**pRL-CMV:** Expression of the renilla luciferase under the control of the constitutively active cytomegaly virus promoter.

**Resistance:** Ampicillin

**Manufacturer:** Promega, Mannheim

**pTALuc/ STF:** Expression of the Firefly luciferase reporter under the control of 7x TCF/ LEF binding sites.

**Resistance:** Ampicillin

**Manufacturer of vector backbone:** Clontech, Mountain View, USA

## 2.9. Cell Lines

Name	Cell type	Mutation status	Reference
70.4	mouse hepatoma, strain C3H/ He	<i>Ctnnb1</i> wt/ wt	Kress <i>et al.</i> , 1992
70.4 Mo clone 50	stably transfected subclone of 70.4	<i>Ctnnb1</i> wt/ wt	Diploma thesis Moritz Horn, Tuebingen Zeller <i>et al.</i> , 2012
70.4 STF clone 15	stably transfected subclone of 70.4	<i>Ctnnb1</i> wt/ wt	Braeuning <i>et al.</i> , 2007b

## 2.10. Mouse Strains

Strain	Source	Reference
C3H/ He, male	Charles River, Sulzfeld	
<i>Ctnnb1</i> <sup>loxP/loxP</sup>	J. Huelsken, Swiss Institute for Experimental Cancer Research, Lausanne, Switzerland	Huelsken <i>et al.</i> , 2001
<i>Apc</i> <sup>loxP/loxP</sup> , TTR-Cre-Tam	S. Colnot, Institut Cochin, Paris, France	Colnot <i>et al.</i> , 2004

## 2.11. Software

Product name	Manufacturer
Adobe Photoshop	Adobe Systems Incorporated, San Jose, USA
Axiovision Rel. 4.5	Zeiss, Oberkochen
Chromas Lite	Technelysium, Brisbane, Australia
CorelDRAW Graphics Suite 12	Corel Corporation, Ottawa, Canada
CSC Camera Controller 1.11	Raytest GmbH, Straubenhardt
EndNote X2	EndNote, Carlsbad, USA
Microsoft Office 2007	Microsoft Corporation, Redmond, USA
NanoDrop ND-1000 V3.2.1	PerkinElmer, Waltham, USA
OriginPro 8G	OriginLab Corporation, Northampton, USA
Victor Workout 1.5	PerkinElmer, Waltham, USA
Windows Vista	Microsoft Corporation, Redmond, USA

### **3. Methods**

#### **3.1. Cell Culture**

##### **3.1.1. General Remarks**

Working steps with cell cultures have to be conducted under sterile conditions to prevent contaminations with microorganisms. Therefore all work is performed under a lamina flow with temporary UV light. All stable equipment is autoclaved while heat-sensitive solutions, e.g. cell culture medium, are sterile filtrated prior to use. Additionally, work materials are disinfected with 70% ethanol before putting them under the bench.

Solutions required for cell culture are pre-heated to 37 °C and cells are cultured in an incubator at 37 °C and 5% CO<sub>2</sub>. All mouse hepatoma cell lines used in this work are routinely cultured in DMEM/ F-12 medium supplemented with 10% FCS and 1% P/ S.

##### **3.1.2. Medium Change and Passaging of Cells**

Medium has to be changed every second day. Therefore it is sucked off with a pasteur pipette and fresh medium is carefully added to the cell layer.

When cells reach a confluence of about 80-100%, they are detached from the dish using a trypsin/ EDTA solution. The reaction is stopped by addition of cell culture medium. Singularization of cells is achieved by pipetting the suspension up and down several times. The desired aliquot of the cell suspension is seeded on a new dish and filled up with fresh medium. To reach a defined cell number per volume, cells have to be counted using a Fuchs-Rosenthal chamber before plating.



## Methods

### 3.1.3. Thawing and Freezing of Cells

Frozen cells are thawed at room temperature and quickly after thawing transferred into a Falcon tube already containing 10 ml of warmed up culture medium. After centrifugation (800 rpm, 5 min, 4 °C), the supernatant is sucked off and the cell pellet is resuspended in 10 ml fresh medium. The first medium change should be conducted after 24 hours to remove unattached, dead cells.

For storage, the confluent cells are trypsinized and centrifuged (1,000 rpm, 5 min, 4 °C). The cell pellet is resuspended in 10 ml cooled culture medium containing 10% (v/v) DMSO. Aliquots of 1 ml are transferred into cryo vials and incubated on ice for one hour. Afterwards, vials are frozen at -70 °C overnight and then stored in liquid nitrogen.

### 3.1.4. Treatment of Cells

The cell culture medium is sucked off and fresh medium containing the drug in the final concentration is added to the cells. Cells are treated for 24 h prior to luciferase or caspase measurements, or to stainings. Concentrations of used compounds are listed in section 2.4.2. Mechanism of action is shown in Table 1.

Reagent	Mechanism of action
LiCl	GSK3 $\beta$ inhibitor
Doxycycline	Activation of Tet System
Etoposide	Topoisomerase II inhibitor
Bortezomib	Proteasome inhibitor
MG-132	Proteasome inhibitor

**Table 1: Mechanism of action of different drugs used to treat mouse hepatoma cells**

## Methods

### 3.2. Plasmid Preparation

#### 3.2.1. Plasmid Progeny and Isolation

Bacteria carrying the desired plasmid DNA can be easily propagated using frozen glycerol stocks. After thawing, a small amount of bacteria is transferred into 200 ml LB medium containing a plasmid-specific selection antibiotic and shaken overnight at 37 °C.

The QIAfilter Plasmid Midi Kit (Qiagen) is used for plasmid isolation according to the manufacturer's instructions. The protocol is based on a modified alkaline lysis procedure, followed by plasmid DNA binding to an anion-exchange resin. After several washing steps proteins, RNA, and impurities are removed and eluted DNA is dissolved in H<sub>2</sub>O<sub>dest</sub>. An aliquot of plasmid DNA is loaded on a 1% w/ v agarose gel to check for successful isolation (see section 3.3.1).

#### 3.2.2. DNA Quantification

Concentration and purity of DNA and RNA can be measured using a Nanodrop photometer. The optical density is detected at 260 nm and the DNA concentration is determined via the following equation:

$$C_{(DNA)} (\mu\text{g/ ml}) = F_{\text{emp}} * E_{260 \text{ nm}} * DF$$

$F_{\text{emp}}$  = empiric factor (DNA = 50, RNA = 40)

$E_{260 \text{ nm}}$  = extinction at 260 nm

DF = dilution factor

The ratio  $E_{260 \text{ nm}} / E_{280 \text{ nm}}$  indicates the level of purity of the DNA solution. Solutions with a value of 1.8-2.0 are considered to be pure and can be used for further experiments.

### **3.3. Electrophoresis**

#### **3.3.1. Agarose Gel Electrophoresis**

Agarose is dissolved in 1x TAE buffer by boiling in the microwave. After cooling down to 50 °C, ethidium bromide (0.03% v/ v) is added and the solution is filled into a gel rack. DNA samples are mixed with 6x loading buffer and applied to the gel together with an appropriate DNA size marker. The gel is run at 75-90 V for 30-60 min and photographed under UV light.

#### **3.3.2. Polyacrylamide Gel Electrophoresis**

An acrylamide gel is prepared using solutions given in section 2.4.7. After polymerization, the gel is put into a gel rack filled with 1x TBE buffer. PCR samples are mixed with loading buffer and, together with a DNA marker, applied to the gel. The gel run takes about 75 min at 300 V. Afterwards, the gel is dyed in ethidium bromide solution (0.5 µg/ ml) for 10 min and DNA fragments are visualized under UV light.

### **3.4. Transfection**

Plasmids carrying reporter genes are introduced into cells via lipofection-based transient transfection. Lipofectamine 2000 is used according to the manufacturer's instructions. Cells are seeded in 500 µl antibiotic-free medium on 24-well plates for 24 h to reach a confluence of 60% at the time of transfection. Each well is transfected with 0.8 µg DNA and 1.6 µg Lipofectamine dissolved in transfection solution prior to cell treatment described in section 3.1.4. For transfection of siRNA, cells are seeded on 6-well plates and each well is transfected with 20 nM siRNA and 12 µl HiPerFect dissolved in transfection solution prior to cell treatment described in section 3.1.4.

## Methods

Stably transfected cells used in further experiments have persistently introduced the linearized plasmid vector into their DNA.

### **3.5. Reporter Gene Analysis**

Expression of the Firefly luciferase gene is under the control of pathway-specific enhancer elements cloned into the SuperTopflash (STF) reporter vector. The pRL-CMV vector is co-transfected as internal standard as it contains the Renilla luciferase gene under the control of a constitutive active promoter. After lysis of cells, the activities of both luciferase enzymes are detected via measurement of generated luminescence.

### **3.6. Cell Viability Assays**

The Alamar Blue Assay (AB) is based on the reduction of resazurin (7-Hydroxy-3*H*-phenoxazin-3-one 10-oxide) to a fluorescent dye. This reaction only takes place in metabolic active cells and the colored product can be measured photometrically. The AB solution is added to the cells two hours before cell lysis and used as a reference for Firefly luciferase measurements in stably transfected cells.

### **3.7. Determination of Apoptosis**

#### **3.7.1. Protein Isolation**

The culture medium is taken from each well and centrifuged (2,300 g, 5 min). The cell pellet is resuspended in lysis buffer, complemented with DTT (0.5% v/ v). The obtained suspension is re-added to the corresponding well and incubated for 15 min at 37 °C. Remaining attached cells are scraped off and the suspension is transferred into an Eppendorf cup. After vigorous vortexing, a centrifugation step follows

## Methods

(21,000 g, 10 min, 4 °C). The supernatant is collected in pre-chilled cups and an aliquot is taken for protein determination. Samples are stored at -70 °C.

### **3.7.2. Caspase 3/ 7 Activity Measurement**

The activity of 3/ 7 effector caspases is detected by cleavage of the DEVD-AFC peptide sequence to the fluorescent dye AFC. After adding the DEVD-AFC mix to the protein lysates, the fluorescence is monitored every 10 min for 1 h at 37 °C. Caspase activity can be calculated with the help of an AFC calibration curve.

### **3.7.3. Bradford Protein Quantification**

The Bradford assay is used to determine the protein concentration by use of Coomassie Brilliant Blue dye that binds to proteins and can be measured photometrically. A BSA standard curve allows the quantification of protein samples.

### **3.7.4. Hoechst Staining**

The fluorescent dye Hoechst 33258 intercalates with DNA and is used to detect apoptotic cell nuclei. After washing with PBS, cells are fixed with 3% w/ v paraformaldehyde on ice for 10 min followed by washing with PBS and H<sub>2</sub>O<sub>dest</sub>. The cells are stained by adding 10 µg/ ml Hoechst 33258 solution and incubated for 20 min in the dark. After washing, the cells are coated with glycerol gelatine and mounted under cover slips. The stained cells can be visualized under the fluorescence microscope.

## **3.8. Animal Experiments**

### **3.8.1. General Remarks**

All animals were kept on a 12 h dark/ light cycle and had access to food and tap water *ad libitum*. Mice were housed singly or in pairs in macrolon cages and received humane care and protocols complied with institutional guidelines. For organ harvesting, mice were sacrificed between 9 and 11 a.m. to avoid circadian influences.

### **3.8.2. Organ Harvesting**

To monitor hepatocyte proliferation, 5-bromodeoxyuridine (BrdU) was added to the drinking water (1 mg/ ml, freshly prepared every day) and given to the animals for 3 consecutive days prior to sacrifice. Mice were then killed in a chamber filled with 95% CO<sub>2</sub>/ 5% O<sub>2</sub> followed by neck-stretching. The abdomen was cut open and the liver was bled by opening the *vena cava inferior*. After isolation and washing in cold PBS, the liver was weighed and photographed. Liver lobes were isolated and shock-frozen on dry ice before storage at -70 °C or were fixed in Carnoy's solution or in 4% paraformaldehyde for later paraffin embedment.

### **3.8.3. Tumor Analysis**

Images of stained liver sections were acquired using an Axio Imager light microscope with Axiovision Rel. 4.5 software. Areas of liver and tumor sections were determined by using a Wacom Cintiq 21UX pen display.

## Methods

### 3.8.4. Mutation Analysis

Liver sections were mounted on dialysis tubes and stained for either GS or glucose-6-phosphatase (G6Pase) to differentiate tumors from normal liver tissue. Tumor areas were punched out with a sharpened cannula and digested with proteinase K for 1 h at 50 °C before heat-inactivation at 95 °C for 20 min (Table 2).

Reagent	Volume (µl)
H <sub>2</sub> O sterile	32
10x PCR buffer (+ MgCl <sub>2</sub> )	5
Proteinase K (10 mg/ ml)	2
<b>Total volume</b>	<b>39</b>

**Table 2: Proteinase K digestion for mutation analysis**

Obtained DNA was amplified by PCR to screen for mutations in exon 3 of the *Ctnnb1* gene (Table 3, for further details see (Huelsenken *et al.*, 2001)). Primers are listed in section 2.5.2.

Reagent	Volume (µl)
dNTPs (2 mM)	5
Forward primer (10 µM)	2.5
Reverse primer (10 µM)	2.5
BSA (20 mg/ ml)	1
Taq polymerase (2 U/ µl)	1
Genomic DNA	39
<b>Total volume</b>	<b>51</b>
<b>PCR program ("8")</b>	
Denaturation	95 °C, 60 sec
Annealing	58 °C, 60 sec
Elongation	72 °C, 60 sec
Cycles	40

**Table 3: *Ctnnb1* PCR**

## Methods

Aliquots of PCR products were loaded on a polyacrylamide gel to check for successful PCR. Sequencing of amplified samples was performed at the 4base lab GmbH in Reutlingen using the same primer pairs as for PCR.

### **3.9. Animal Experiment I: Ablation of $\beta$ -Catenin in *Ctnnb1*-Mutated Mouse Liver Tumors**

#### **3.9.1. Animal Breeding**

A transgenic mouse line with a conditional hepatocyte-specific knockout in the *Ctnnb1* gene was generated. Therefore *Ctnnb1*<sup>loxP/loxP</sup> mice homozygous for a modified *Ctnnb1* gene carrying loxP sites flanking the exons 3 and 6 (Huelsenken *et al.*, 2001) were interbred with TTR-Cre-Tam mice expressing the Cre recombinase under control of a hepatocyte-specific transthyretin (TTR) promoter inducible by tamoxifen (Tannour-Louet *et al.*, 2002). Two groups of generated *Ctnnb1*<sup>loxP/loxP</sup>, TTR-Cre-Tam mice were used for the subsequent animal experiment: mice heterozygous for *Cre* (“*Ctnnb1* knockout (KO) mice”) and respective control mice, negative for the *Cre* allele (“*Ctnnb1* wild type (WT) mice”).

#### **3.9.2. Genotyping**

Animals were sedated in an isolated chamber filled with isoflurane. A small piece of ear was cut out and obtained tissue material was digested with proteinase K at 56 °C for at least 3 h followed by heat-inactivation at 95 °C (listed in Table 4).



## Methods

Reagent	Volume (µl)
H <sub>2</sub> O sterile	72
10x PCR buffer (- MgCl <sub>2</sub> )	8
Proteinase K (20 mg/ ml)	2
<b>Total volume</b>	<b>82</b>

**Table 4: Proteinase K digestion for genotyping**

After a short centrifugation step (13,000 rpm, 5 min), the DNA-containing supernatant was taken. Genotyping for *Ctnnb1*<sup>loxP/loxP</sup> and *Cre* was performed by PCR (Table 5).

Primers are listed in 2.5.1.

Reagent	Volume (µl)	
	<i>Ctnnb1</i> <sup>loxP/loxP</sup>	<i>Cre</i>
H <sub>2</sub> O sterile	26	17
10x Taq buffer (- MgCl <sub>2</sub> )	5	5
MgCl <sub>2</sub> (25 mM)	3	4
dNTPs (2 mM)	5	10
Forward primer (10 µM)	2.5	4
Reverse primer (10 µM)	2.5	4
Taq polymerase (1 U/ µl)	1	1
Genomic DNA	5	5
<b>Total volume</b>	<b>50</b>	<b>50</b>
PCR program		
	“.7”	“0”
Denaturation	95 °C, 60 sec	95 °C, 60 sec
Annealing	60 °C, 60 sec	68 °C, 60 sec
Elongation	72 °C, 60 sec	72 °C, 60 sec
Cycles	35	35

**Table 5: PCR for *Ctnnb1*<sup>loxP/loxP</sup> and *Cre***

### 3.9.3. Induction of *Ctnnb1*-Mutated Mouse Liver Tumors

Generation of liver tumors in transgenic mice was conducted as previously described (Moennikes *et al.*, 2000). Therefore 6 weeks old male C3H/ He mice (36 *Ctnnb1* KO and 16 *Ctnnb1* WT mice) were injected a single intraperitoneal dose of DEN (90 µg/ g body weight) followed by a treatment-free period of 3 weeks. Animals were

## Methods

then fed a diet containing PB (0.05%) for 25 weeks followed by a PB-free diet for at least 3 weeks.

### 3.9.4. Tamoxifen-Induced KO of *Ctnnb1* in Livers from Transgenic Mice

Tamoxifen was dissolved in ethanol (67 mg/ ml) and further diluted in corn oil (10 mg/ ml) (Ganzenberg *et al.*, 2013). A total of 1.5 mg tamoxifen was applied intraperitoneally for 5 consecutive days. Sacrifice was between 1 to 7 weeks after the last tamoxifen treatment (Figure 5).



**Figure 5: Treatment regimen of animal experiment I.** Transgenic male *Ctnnb1*<sup>loxP/loxP</sup>, TTR-Cre-Tam mice were given a single intraperitoneal injection of 90 µg/ g body weight N-nitrosodiethylamine (DEN) followed by treatment with 0.05% phenobarbital (PB) for 25 weeks. After 1 week on a PB-free diet, 1.5 mg tamoxifen was applied intraperitoneally to the animals for 5 consecutive days. Animals were sacrificed at the age of 37 to 43 weeks. Group sizes: n = 36 *Ctnnb1* knockout (KO) mice; n = 16 *Ctnnb1* wild type (WT) mice.

## 3.10. Animal Experiment II: Poisoning of *Ctnnb1*-Mutated Mouse Liver Tumors by AAP

### 3.10.1. AAP Dose Finding Study

This experiment was conducted prior to the main study described in section 3.10.3. Male C3H/ He mice were injected different AAP doses and killed 1 to 7 days after treatment (Table 6).

## Methods

AAP (mg/ kg body weight)	Number of mice
200	3
300	3
400	3

**Table 6: AAP doses and number of treated mice.** Male C3H/ He mice were injected a single intraperitoneal dose of AAP, varying from 200 to 400 mg/ kg body weight and killed at different time points after treatment.

Blood samples of mice were taken from the *vena cava inferior* quickly after sacrifice. All following steps were conducted at the laboratory of Dr. F. Iglauer (University of Tuebingen). Samples were centrifuged (6,000 rpm, 5 min) in heparin collection tubes to obtain blood serum. Activities of the liver enzymes alanine aminotransferase (ALT) and aspartate aminotransferase (AST) were measured by pipetting an aliquot of serum on monitoring panels and putting them in a VetTest chemistry analyzer. A biochemical reaction on the reagent layer led to a change of color which could be detected via spectral analysis.

### 3.10.2. Induction of *Ctnnb1*-Mutated Mouse Liver Tumors

In the main study, generation of liver tumors in male C3H/ He mice (n = 28) was conducted as previously described (Moennikes *et al.*, 2000). Mice were injected a single intraperitoneal dose of DEN (90 µg/ g body weight) at the age of 6 weeks followed by a treatment-free period of 3 weeks. Animals were then fed a diet containing PB (0.05%) for 27 weeks followed by a PB-free diet for at least 1 week.

### 3.10.3. Treatment of Tumor-Bearing Mice with a Single Dose of AAP

After tumor promotion, mice were randomly divided into two groups (10 mice were in the control group, 18 mice in the AAP-treated group) and either given a single intraperitoneal injection of 0.9% saline (w/ v) or of 300 mg/ kg of body weight AAP.

## Methods

Therefore AAP (20 mg/ ml in 0.9% saline) was sonicated for 30-45 min at 50 °C. Sacrifice was between 2 to 45 days after AAP or saline application. The treatment regimen is shown in Figure 6.

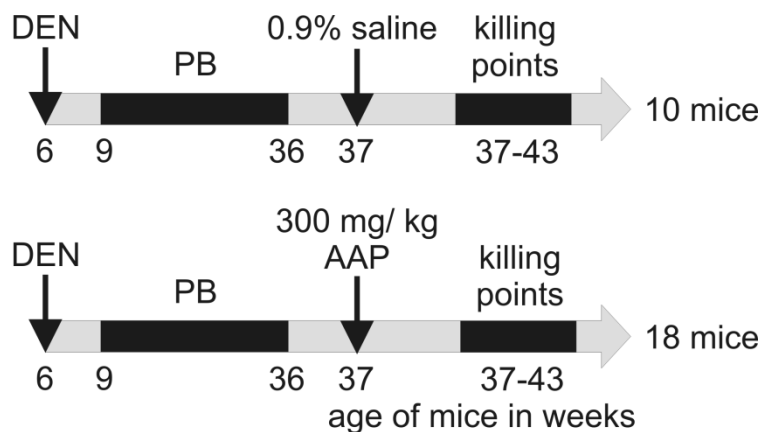


**Figure 6: Treatment regimen of animal experiment II.** After tumor induction with a single intraperitoneal dose of DEN followed by chronic treatment with 0.05% PB, male C3H/ He mice were set on a PB-free diet for 1 week. Mice were injected a single dose of 0.9% saline or 300 mg/ kg of body weight AAP. Sacrifice was 2 to 45 days after treatment. Number of mice in the respective groups is given on the right.

The different time points of sacrifice are shown in Table 7.

Time point of sacrifice [days]	Control group	AAP-treated group
2	7	7
4	-	2
6	-	2
10	-	2
24	-	2
45	3	3

**Table 7: Number of animals killed at different time points after treatment.** Mice in the AAP-treated group were given a single injection of 300 mg/ kg of body weight AAP while mice in the control group received 0.9% saline.

### **3.10.4. Magnetic Resonance Imaging**

A subset of tumor-bearing mice were scanned by non-invasive magnetic resonance imaging (MRI) at 8 days before and several times after (5, 12 and 18) AAP treatment to monitor the number and sizes of detectable tumors (tumors > 1 mm in diameter). MRI was performed by Andreas Schmid at the laboratory of Prof. B. J. Pichler (Laboratory for Preclinical Imaging and Imaging Technology of the Werner Siemens-Foundation, Department of Preclinical Imaging and Radiopharmacy, University of Tuebingen). In brief, animals were anesthetized with an isoflurane/ oxygen mixture and a respiration triggered T2-weighted turbo-spin-echo sequence (TR/ TE 3000/ 205 ms, voxelsize (0.22 mm<sup>3</sup>)) was used for acquisition of MRI data. For further details see also (Schmid *et al.*, 2012).

## **3.11. Immunohistochemistry**

### **3.11.1. Frozen Liver Slices**

Liver sections (10 µm thick) from frozen livers are prepared in a microtome. Cryo slices are fixed in 3% formalin and subsequently stained immunohistochemically.

### **3.11.2. Carnoy Fixation**

Liver tissue is incubated in Carnoy's fixative overnight followed by overnight dehydration in isopropanol and embedment in paraffin.

### **3.11.3. Formalin Fixation**

Tissue is fixed in 4% formalin overnight and thereafter washed for 1 hour with water. Dehydration is done overnight (50-100% isopropanol) before embedment in paraffin.

## Methods

### **3.11.4. Preparation of Paraffin Sections**

After Carnoy (see 3.11.2) or formalin (see 3.11.3) fixation, tissue is embedded in paraffin and liver sections (5  $\mu$ M) are prepared. Before slices can be stained, they are deparaffinized in xylene and rehydrated (100-50% ethanol).

### **3.11.5. G6Pase Staining**

Starting material are cryo sections. The fixation is carried out in glutaraldehyde. Sections are then incubated for 20-30 min in G6Pase incubation buffer. Precipitation of the reaction product is achieved by adding 1% ammonium sulfide followed by a second fixation step and dehydration. For further information see also (Wachstein and Meisel, 1957).

### **3.11.6. HE Staining**

Starting material are cryo sections. Samples are incubated in hemalum for 5 min, fixed and stained in alcoholic eosin for 3 min before dehydration.

### **3.11.7. GS/ CYP/ E-Cadherin/ $\beta$ -Catenin/ BrdU Staining**

Starting material are formalin-fixed cryo sections. Slices are incubated in methanol/ $H_2O_2$  for 15 min to inactivate endogenous peroxidases. Unspecific binding is blocked. Primary antibody is bound overnight at 4 °C in a humid chamber, horseradish peroxidase-conjugated secondary antibody is then added for 1 h at room temperature. Sections are stained with 3-amino-9-ethylcarbazole/  $H_2O_2$  as substrates for 20-30 min.

## Methods

### **3.11.8. GS/ BrdU and GS/ Cx32 Double Staining**

Starting material are formalin-fixed cryo sections. To inactivate endogenous peroxidases, slices are incubated in methanol/ H<sub>2</sub>O<sub>2</sub> for 15 min. Unspecific binding is blocked. Primary antibody is bound overnight at 4 °C in a humid chamber. GS is stained with  $\beta$ -galactosidase-conjugated secondary antibody for 2 h at room temperature followed by incubation with X-Gal staining buffer for 2 h at 37 °C. BrdU or connexin 32 (Cx32) are then stained with horseradish peroxidase (described in 3.11.7).

### **3.11.9. GS/ HNF4 $\alpha$ Double Staining**

Starting material are Carnoy-fixed, paraffin-embedded sections. Unspecific binding is blocked. Primary antibody is bound overnight at 4 °C in a humid chamber. GS is stained as described in 3.11.8. For detection of hepatocyte nuclear factor 4 $\alpha$  (HNF4 $\alpha$ ), biotinylated secondary antibody is added and liver sections are incubated with alkaline phosphatase-conjugated streptavidin for 30 min at room temperature. Fast Red is added as substrate for approximately 40 min.

### **3.11.10. Masson-Goldner Trichrome Staining**

Starting material are Carnoy-fixed, paraffin-embedded sections. The Masson-Goldner trichrome staining kit is applied for the visualization of connective tissue according to the manufacturer's instructions. In brief, staining is achieved by using a combination of three solutions: Ponceau and Fuchsin stain muscle and cytoplasm, Orange G stains erythrocytes and light green SF yellowish stains connective tissue. This results in dark brown cell nuclei, red muscle fibers and cytoplasm, orange erythrocytes and green connective tissue.

## Methods

### **3.11.11. TUNEL Assay**

Starting material are formalin-fixed, paraffin-embedded sections. The *In Situ* Cell Death Detection Kit, POD is used for detection of apoptotic cell death following the manufacturer's protocol for paraffin-embedded tissue sections including pre-treatment with proteinase K and permeabilization solution. Apoptosis-induced cleavage of nuclear DNA is detected by enzymatic incorporation of labeled nucleotides to DNA strand breaks using TdT-mediated dUTP nick end labeling (TUNEL) technique. Individual apoptotic cells are analyzed by light microscopy. DNA strand breaks in positive controls are generated via incubation with benzonase nuclease prior to labeling procedures.

### **3.11.12. $\beta$ -Catenin Staining of Cells**

Cells are fixed on ice with paraformaldehyde (4% w/ v in PBS) for 5 min. Unspecific binding is blocked by use of PBS/ T solution supplemented with 3% BSA for 1 h. Non-phospho, active  $\beta$ -catenin primary antibody is bound overnight at 4 °C in a humid chamber. Cy3-conjugated secondary antibody is then added for 2.5 h at room temperature. Cell nuclei can be counterstained with Hoechst 33258 (see section 3.7.4) and visualized under the fluorescence microscope.

## **3.12. Statistics**

All statistical calculations including mean value, standard deviation and standard error of means are conducted in Excel-files. For the comparison of two groups, the Student's T-test (paired or unpaired) is used. Differences are considered significant when  $p < 0.05$  (indicated by an asterisk (\*)) or a hash (#)).  $P < 0.001$  is indicated by three asterisks (\*\*\*)).



## 4. Results

### 4.1. Ablation of $\beta$ -Catenin in *Ctnnb1*-Mutated Mouse Liver Tumors

The signaling molecule  $\beta$ -catenin plays an important role during rodent and human carcinogenesis. Mutations in the *CTNNB1* gene, leading to aberrant activation of the Wnt/  $\beta$ -catenin signaling pathway, are frequently observed in human liver tumors (De la Coste *et al.*, 1998; Koch *et al.*, 1999; Schmidt *et al.*, 2011). Chemically induced hepatomas in mice very often harbor mutations in *Ctnnb1*, encoding  $\beta$ -catenin (Aydinlik *et al.*, 2001). Yet, the relevance of  $\beta$ -catenin in growth and survival of *Ctnnb1*-mutated liver tumor cells is still not fully understood.

In an experiment performed by Malanchi *et al.* (2008), skin tumors harboring an active Wnt/  $\beta$ -catenin signaling pathway were induced in transgenic mice. Ablation of  $\beta$ -catenin led to complete tumor regression within several weeks indicating that  $\beta$ -catenin is essential for the survival of respective tumor cells. To clarify the role of  $\beta$ -catenin for the maintenance of established *Ctnnb1*-mutated liver tumors in mice, a similar experiment was performed. Transgenic "*Ctnnb1*<sup>loxP/loxP</sup>, TTR-Cre-Tam" mice were generated, harboring a modified *Cre* gene under the control of the hepatocyte-specific TTR promoter. After induction of *Ctnnb1*-mutated liver tumors in transgenic mice, tamoxifen-mediated activation of the *Cre* recombinase resulted in the recognition of loxP sites and subsequent deletion of the *Ctnnb1* gene. The consequences of  $\beta$ -catenin ablation for *Ctnnb1*-mutated liver tumor cells were investigated.

## Results

### 4.1.1. Analysis of Tumor Genotype after KO of *Ctnnb1*

*Ctnnb1*-mutated liver tumors were induced in 51 mice (35 *Ctnnb1* KO mice were positive for the *Cre* gene; 16 *Ctnnb1* WT mice were negative for *Cre*) following an initiation/ promotion protocol as previously described (Moennikes *et al.*, 2000; see also section 3.9.4). At the age of 34 weeks when tumors were established, PB was removed from the diet. One week later, tamoxifen was applied intraperitoneally to all animals for five consecutive days according to the treatment protocol described in (Ganzenberg *et al.*, 2013). Therein, KO of *Ctnnb1* was successful in more than 99% of hepatocytes from transgenic mice of the same strain used in the present experiment. PCR analyses from a subset of GS-positive tumors were performed to check for the presence of *Cre* and the deleted *Ctnnb1* gene in KO mice. Results from two representative tumors from *Ctnnb1* KO and WT mice are shown in Figure 7. *Ctnnb1* KO mice were positive for the *Cre* gene and subsequently for the N-terminally truncated form of *Ctnnb1* as opposed to tumors from WT mice. Non-deleted *Ctnnb1*<sup>loxP/loxP</sup> could still be detected in tumors from both animals groups but with lower amounts in *Ctnnb1* KO mice. The amplified *Ctnnb1*<sup>loxP/loxP</sup> PCR fragment in tumors from KO mice is probably derived from non-recombined DNA of hepatocytes or from other cell types.

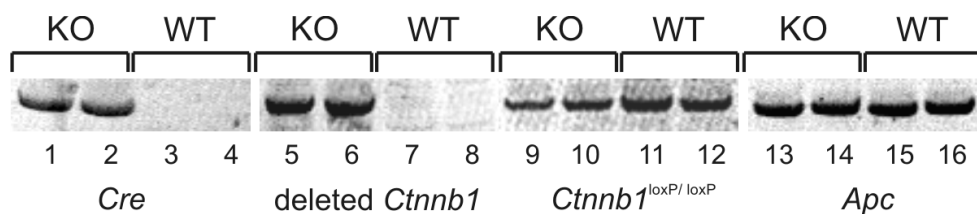


**Figure 7: Genotype of 4 representative tumors from male transgenic *Ctnnb1*<sup>loxP/loxP</sup>, TTR-Cre-Tam WT and KO mice after tamoxifen treatment.** Results from PCR analyses of liver tumors are shown. The *Cre* gene is present in tumors from *Ctnnb1* knockout (KO) mice (lane 1, 2) while *Ctnnb1* wild type (WT) mice are negative for *Cre* (lane 3, 4). Tamoxifen-induced activation of the *Cre*

## Results

recombinase in KO mice results in a truncated *Ctnnb1* gene (lane 5, 6), not observed in mice negative for *Cre* (lane 7, 8). *Ctnnb1*<sup>loxP/loxP</sup> is found in tumors from WT and KO mice (lanes 9-12) with lower amounts in tumors from KO mice, as expected after recombination. An amplified fragment of the *Apc* gene is shown as a reference (lanes 13-16).

### 4.1.2. Analysis of Tumor Phenotype after KO of *Ctnnb1*

Animals were sacrificed between 1 to 7 weeks after tamoxifen treatment. Livers were excised and studied for macroscopically visible tumors and lesions. No obvious differences in the number of detectable tumors between *Ctnnb1* WT and KO animals were observed (data not shown). The mean relative liver weights (liver to body weight ratios) were assessed for *Ctnnb1* KO and WT mice sacrificed at different time points. Values were between 4.93-5.99% and did not significantly differ between different time points of analysis or when comparing livers from *Ctnnb1* WT with KO mice.

GS is a target gene of  $\beta$ -catenin and a model marker for  $\beta$ -catenin activation in murine liver (Loeppen *et al.*, 2002; Cadoret *et al.*, 2002). PCR analyses of GS-positive tumors from *Ctnnb1* WT and KO mice verified the almost 100% concordance between high GS expression and *Ctnnb1* mutations: point mutations in the *Ctnnb1* gene were found in 92.3% of GS-positive tumors (12 out of 13). GS-immunostained liver sections were used to investigate the phenotype of tumors after KO of *Ctnnb1*. Tumors from *Ctnnb1* WT mice displayed unique GS expression (Figure 8A). A different picture emerged when GS-positive tumors from *Ctnnb1* KO mice were studied. Respective tumors exhibited heterogeneous GS expression patterns (Figure 8B). This indicates that the level of *Ctnnb1* KO greatly varied between different tumors. Immunostainings for  $\beta$ -catenin/ BrdU also showed a correspondence between GS expression and membranous  $\beta$ -catenin in respective tumors. GS-

## Results

positive tumors from *Ctnnb1* WT mice displayed high levels of  $\beta$ -catenin (Figure 8C). In contrast, tumors from KO mice with only few GS-positive cells mainly lacked membranous  $\beta$ -catenin (Figure 8D).

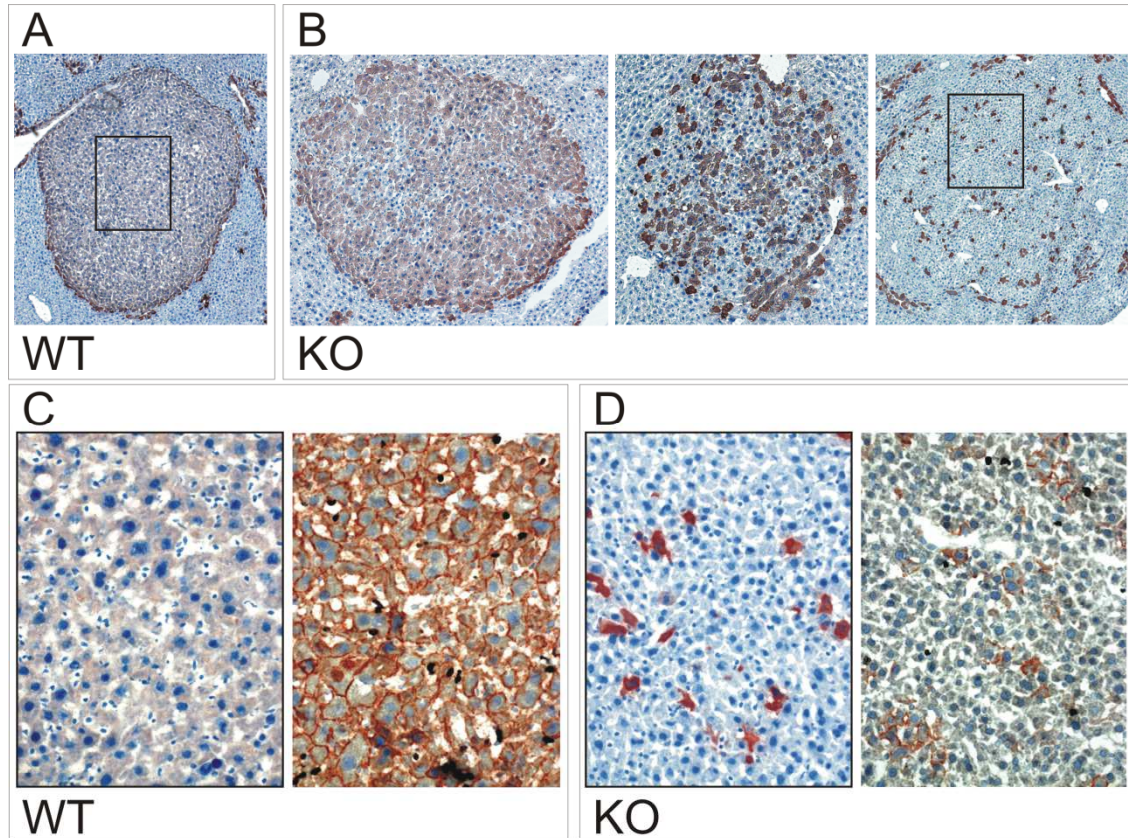


**Figure 8: Phenotype of immunostained liver tumors from *Ctnnb1* WT and KO mice after tamoxifen application. (A)** A representative tumor from a *Ctnnb1* WT animal shows homogeneous expression of glutamine synthetase (GS), a marker for hepatic  $\beta$ -catenin activation. **(B)** Tumors from KO mice, sacrificed at 3 to 7 weeks after  $\beta$ -catenin ablation, exhibit diverse GS-staining patterns. The number of GS-positive tumor cells greatly varies between the three different tumors shown. **(C)** Image detail of tumor marked by black box in **(A)** and stained for GS (left) or  $\beta$ -catenin/ 5-bromodeoxyuridine (BrdU; right). Tumor shows unique GS expression along with membranous  $\beta$ -catenin. **(D)** Image detail of right tumor marked by black box in **(B)** and stained for GS (left) or  $\beta$ -catenin/ BrdU (right). Tumor tissue displays only single cells positive for GS and  $\beta$ -catenin.

To assess whether the level of *Ctnnb1* KO correlated with the time point of analysis or the tumor size, the percentage of GS-positive cells in tumors was estimated. Overall 391 tumors from *Ctnnb1* KO animals were studied (Table 8). One week after

## Results

tamoxifen-induced  $\beta$ -catenin ablation tumors still consisted of ~80% GS-positive cells. At later time points, the number of residual GS-positive cells in examined tumors did not significantly change over time. Great variations were observed within the same groups as indicated by the high standard deviations. Furthermore, no correlation between the tumor size and the level of *Ctnnb1* KO was detected. In contrast, tumors from *Ctnnb1* WT mice consisted of 90-100% GS-positive cells (data not shown).

Time point of analysis	Tumors < 0.5 mm <sup>2</sup> [% of GS-positive cells]	No. of tumors	Tumors $\geq$ 0.5 mm <sup>2</sup> [% of GS-positive cells]	No. of tumors
Week 1	76.5 $\pm$ 25.1	37	84.1 $\pm$ 19.0	32
Week 2	47.1 $\pm$ 32.8	19	20.0 $\pm$ 15.3	11
Week 3	60.7 $\pm$ 25.3	46	66.9 $\pm$ 26.4	46
Week 4	38.0 $\pm$ 28.9	25	50.5 $\pm$ 28.4	20
Week 7	52.1 $\pm$ 31.1	90	53.4 $\pm$ 31.4	65

**Table 8: Percentage of GS-positive cells in tumors from *Ctnnb1* KO mice after  $\beta$ -catenin ablation.** The level of *Ctnnb1* KO in tumors is given by the percentage of GS-positive cells and the mean value is shown for every group. Tumors are stratified into two groups (tumor area < 0.5 mm<sup>2</sup> or  $\geq$  mm<sup>2</sup>). The number of analyzed tumors is depicted for each animal group. Mean  $\pm$  SD are given.

Following the same tamoxifen treatment regimen as previously described (Ganzenberg *et al.*, 2013), KO of *Ctnnb1* was incomplete in livers from transgenic mice in the underlying experiment. The result was the formation of two different tumor subpopulations: one with an intact *Ctnnb1*<sup>loxP/loxP</sup> gene still expressing the GS marker protein and a GS-negative cell population, deleted in *Ctnnb1*. This made it possible to directly compare two cell populations within the same tumor using immunohistochemically stained liver sections.

## Results

### 4.1.3. Importance of $\beta$ -Catenin for the Proliferation of *Cttnb1*-Mutated Tumor Cells

First, the effect of  $\beta$ -catenin ablation on tumor cell proliferation in livers from *Cttnb1* KO mice was studied. Liver sections were immunohistochemically stained for GS and the proliferation marker BrdU and GS-positive and -negative cells were separately analyzed (Figure 9A). The level of *Cttnb1* KO was assessed in each tumor by counting the number of GS-negative cells and tumors were subsequently assigned to two groups (9 tumors to the 25-50% *Cttnb1* KO group, 13 tumors to the > 50% *Cttnb1* KO group). The percentage of BrdU-positive cells within GS-positive and -negative tumor subpopulations was then determined. A significant difference in the proliferative index of GS-positive versus -negative tumor cells was observed (Figure 9B). The GS-positive subpopulation displayed a higher BrdU labeling index than the corresponding GS-negative population. This strongly suggests that  $\beta$ -catenin ablation led to a decrease in cell proliferation. Furthermore, the mean BrdU labeling index of the GS-positive subpopulation in tumors with more than 50% *Cttnb1* KO was lower than that of the GS-positive tumor cells in tumors with only 25-50% *Cttnb1* KO. Mice were killed at 2 to 7 weeks after tamoxifen application and no obvious correlation was found between the time point of tumor analysis and the BrdU labeling index of respective subpopulations.

## Results

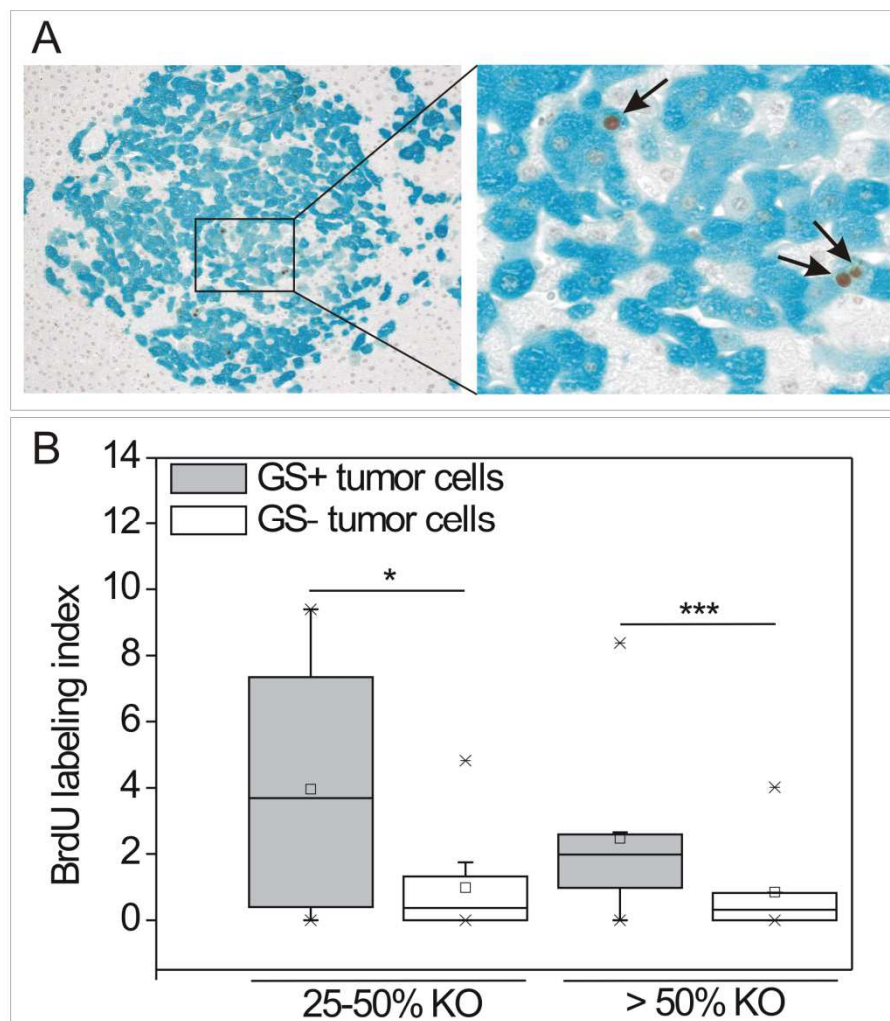


**Figure 9: BrdU labeling index of GS-positive versus -negative tumor cells from *Ctnnb1* KO mice. (A)** Tumor immunostained for GS and the proliferation marker BrdU. The percentage of BrdU-positive cells is determined in the GS-negative and -positive subpopulation. Black arrows indicate the presence of BrdU-positive cells in the GS-positive subpopulation. **(B)** BrdU labeling index of the GS-positive (GS+) and -negative (GS-) tumor cells. A total of 9 tumors, consisting of 25-50% GS-negative cells are assigned to the 25-50% KO group, 13 tumors to the > 50% KO group as they contain more than 50% GS-negative cells. Cells positive for GS show a higher proliferative index than the GS-negative tumor cells. Statistical significances evaluated by paired Student's T-test are indicated by asterisks (\* $p < 0.05$ , \*\*\* $p < 0.001$ ). Box plots show the following values: mean (small center boxes), median (center lines), 25<sup>th</sup> to 75<sup>th</sup> percentile (large boxes), 5<sup>th</sup> and 95<sup>th</sup> percentile (whiskers), outliers (crosses). Livers ( $n = 9$ ) were excised at 2 to 7 weeks after tamoxifen application.

## Results

Former studies demonstrated that the tumor promoter PB selects for the outgrowth of *Ctnnb1*-mutated, GS-positive liver tumors in mice (Aydinlik *et al.*, 2001). Furthermore, clusters of residual  $\beta$ -catenin-positive hepatocytes in livers from *Ctnnb1* KO mice began to grow out in the presence of PB (Braeuning *et al.*, 2010). In the underlying experiment, mice were set on a PB-free diet at least 3 weeks before sacrifice. Despite the absence of PB, tumors from *Ctnnb1* WT mice displayed a high proliferative index as determined by the appearance of BrdU-positive cell nuclei in GS/ BrdU immunostainings (Figure 10).

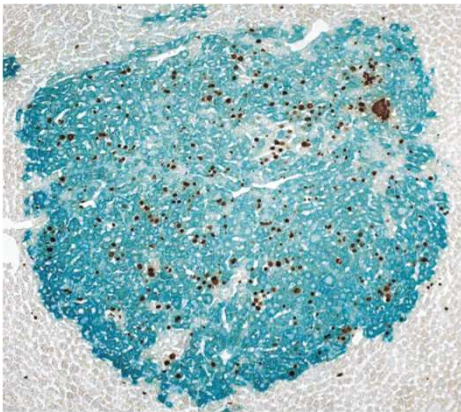


**Figure 10: Liver tumor from a *Ctnnb1* WT animal immunostained for GS/ BrdU.** GS-positive tumor cells show massive BrdU incorporation (brown colored nuclei), an indication for high cell proliferation. Representative tumor image is taken from a *Ctnnb1* WT animal several weeks after mice were set on a phenobarbital (PB) -free diet.

To directly compare the tumor growth in livers from *Ctnnb1* WT with KO mice, the tumor burden over time was determined. The total tumor volume fractions, which are equivalent to the area fractions, were calculated by use of stained liver sections from *Ctnnb1* KO and WT mice sacrificed at 1 and 7 weeks after tamoxifen application (Figure 11). The tumor volume fraction in livers from *Ctnnb1* WT mice was significantly increased after 7 weeks. This is in accordance with the observed high proliferative index of GS-positive tumors from *Ctnnb1* WT mice shown in Figure 10. In contrast, the tumor burden in livers from *Ctnnb1* KO mice did not significantly differ between 1 and 7 weeks.



## Results

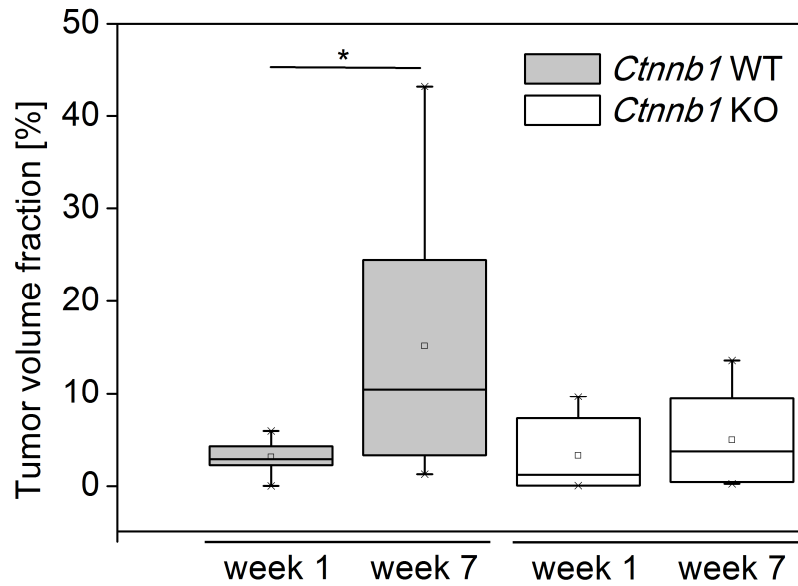


**Figure 11: Time course of tumor volume fraction in livers from *Ctnnb1* WT and KO mice.** A significant increase in tumor burden over time is observed in livers from *Ctnnb1* WT mice while only a slightly higher tumor volume fraction is seen in livers from *Ctnnb1* KO mice after 7 weeks. The unpaired Student's T-test was used for the determination of statistical significance which is indicated by an asterisk (\* $p < 0.05$ ). Group sizes: *Ctnnb1* WT:  $n = 8$  mice per group, *Ctnnb1* KO:  $n = 7$  mice sacrificed at 1 week after tamoxifen application,  $n = 9$  mice sacrificed after 7 weeks.

### 4.1.4. The Role of $\beta$ -Catenin in Cx32-Mediated Cell-Cell Communication

Connexin-mediated gap-junctional intercellular communication (GJIC) is often restricted in tumors and may be a mechanism to trigger tumor cell proliferation (Dermietzel *et al.*, 1987; Chipman *et al.*, 2003). Previous studies showed that *Ctnnb1*-mutated mouse liver tumors, promoted by PB, exhibit reduced levels of the gap junction-forming protein Cx32 (Moennikes *et al.*, 2000; Marx-Stoelting *et al.*, 2008). This might provide respective tumors with a growth advantage. Yet, it remained unclear whether the effect was caused solely by the tumor promoting activity of PB or if  $\beta$ -catenin was implicated. In this study, mice were set on a PB-free diet several weeks before tumor analyses. Subsequently, the levels of Cx32 in membranes of tumor cells could be studied in absence of a potential PB-mediated

## Results

effect. GS/ Cx32-immunostained tumors from *Cttnb1* WT mice were compared with tumors from KO mice. GS-positive tumors from WT mice exhibited reduced membranous Cx32. In contrast, normal liver tissue was positively stained for Cx32 (Figure 12A). Strikingly, Cx32 re-appeared in GS-negative subpopulations of tumors from KO mice after ablation of  $\beta$ -catenin (Figure 12B).

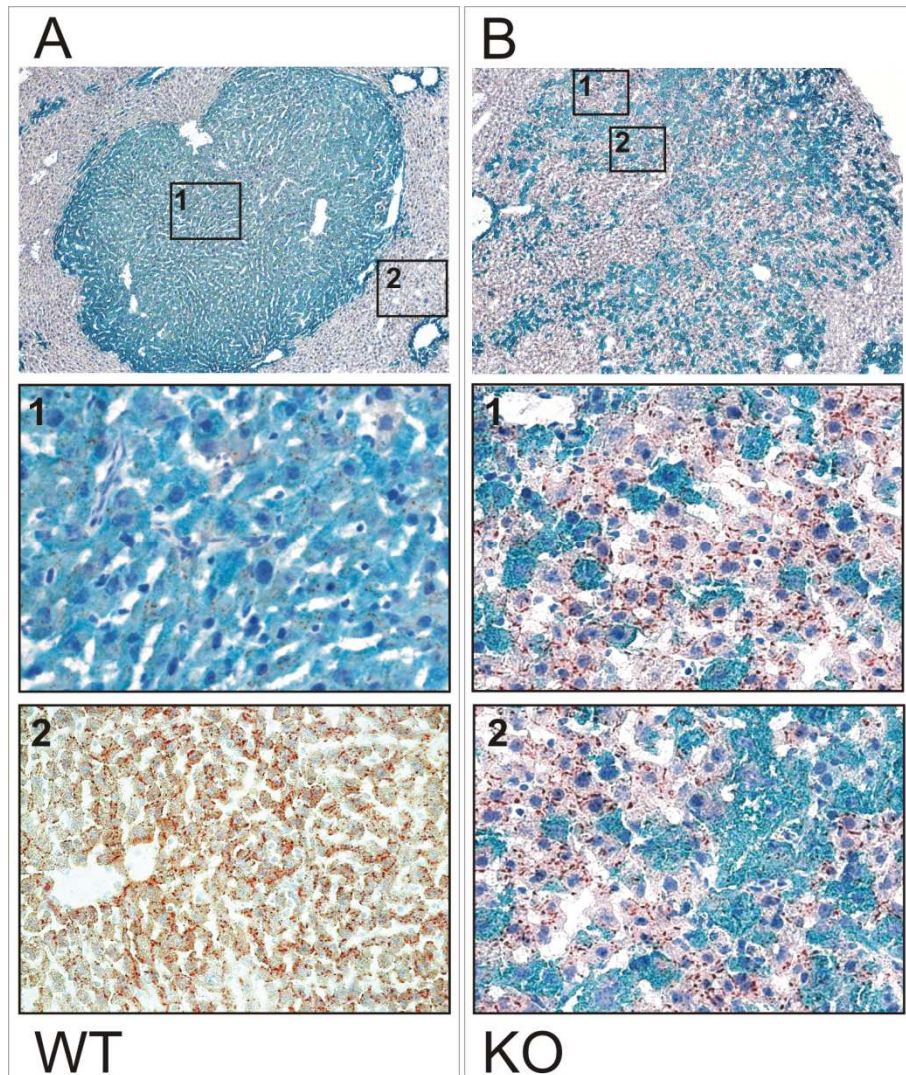


**Figure 12: Cx32 levels in membranes of tumor cells from *Cttnb1* WT and KO mice. (A)** Liver tumor from a *Cttnb1* WT animal immunostained for GS and Connexin 32 (Cx32). Higher magnification shows homogeneous GS expression along with a lack of membranous Cx32 (1). In contrast, normal liver tissue exhibits high Cx32 levels (2) as indicated by the presence of brownish dots. **(B)** Tumor from a *Cttnb1* KO animal consists of GS-positive and -negative subpopulations. Cx32 re-appears at the membranes of GS-negative tumor cells. Image details shown in **(A)** and **(B)** are marked by black

## Results

boxes and referred to as 1 or 2. Representative pictures are depicted from mice killed at 7 weeks after tamoxifen application.

Grading of Cx32 levels in overall 33 tumors from *Ctnnb1* KO mice is shown in Figure 13. GS-positive and -negative subpopulations were separately analyzed in each tumor. Higher Cx32 amounts were found in membranes from GS-negative tumor cells. Respective subpopulations were assigned to classes 3 to 5 with 25 populations assigned to the highest Cx32 grading group. In contrast, GS-positive tumor cells displayed low Cx32 levels (grade 1 to 3).

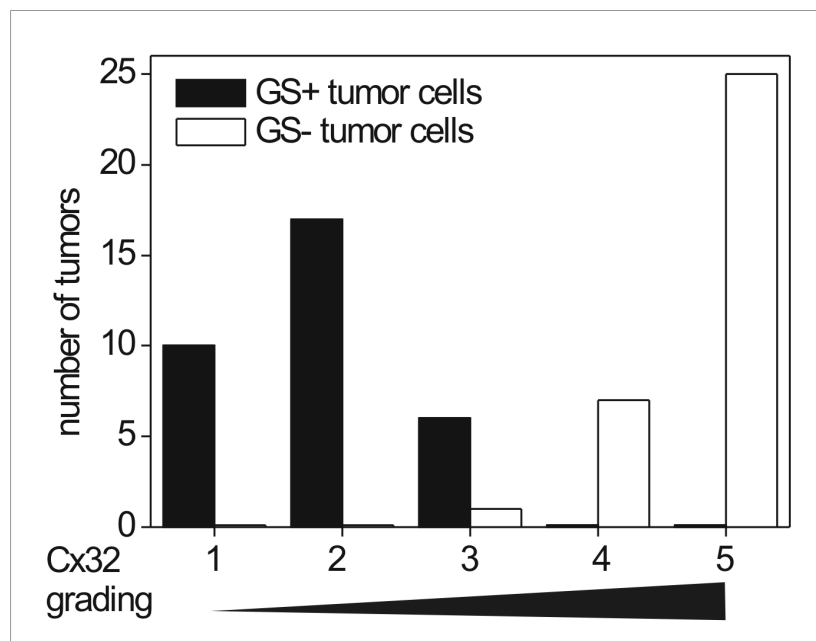


**Figure 13: Cx32 grading of GS-negative and -positive tumor cells from *Ctnnb1* KO mice.** Cx32 levels were assessed in each GS-negative and -positive subpopulation from liver tumors double stained for GS and Cx32. Less membranous Cx32 is present in GS-positive tumor cells as compared to GS-negative cells. A total of 33 tumors were analyzed. Grading classification: grade 1 (low Cx32 levels) to grade 5 (high Cx32 levels).

## Results

### 4.1.5. Effect of $\beta$ -Catenin Ablation on Cell Death in Tumors from *Ctnnb1* KO Mice

The survival of murine skin tumor cells harboring an activated Wnt/  $\beta$ -catenin signaling pathway was shown to depend on the presence of active  $\beta$ -catenin (Malanchi *et al.*, 2008). Thus, the next step was to study whether  $\beta$ -catenin ablation in liver tumors also led to changes in the rate of cell death. At first, images of liver sections from *Ctnnb1* KO mice killed at different time points after tamoxifen-mediated *Ctnnb1* KO were analyzed microscopically. Overall, tumors displayed no overt signs of inflammatory processes like immune cell infiltration, an indication for large-scale cell death. A representative picture of healthy tumor tissue taken from a *Ctnnb1* KO mouse is depicted in Figure 14A in direct comparison with a positive control showing highly necrotic tumor tissue massively infiltrated by immune cells. The latter image is taken from the tumor poisoning experiment described in section 4.3. In addition, the effect of *Ctnnb1* KO on liver tumors was investigated with respect to the appearance of apoptotic tumor cells. Therefore, liver sections from *Ctnnb1* KO and WT mice were stained by TUNEL technology to enable detection of apoptosis at a single cell level. Positive controls of parallel liver sections were prepared by pre-treatment with benzonase before labeling procedures. Tumors from *Ctnnb1* KO mice were largely negative for apoptotic cell nuclei and no apparent differences between TUNEL-stained tumors from *Ctnnb1* KO and WT mice were observed. Figure 14B shows the absence of apoptotic cell nuclei in tumor tissue compared to benzonase-treated positive control. The GS expression pattern of the respective tumor section is shown in Figure 14A. The image was taken from a liver excised at 3 weeks after tamoxifen application.

## Results

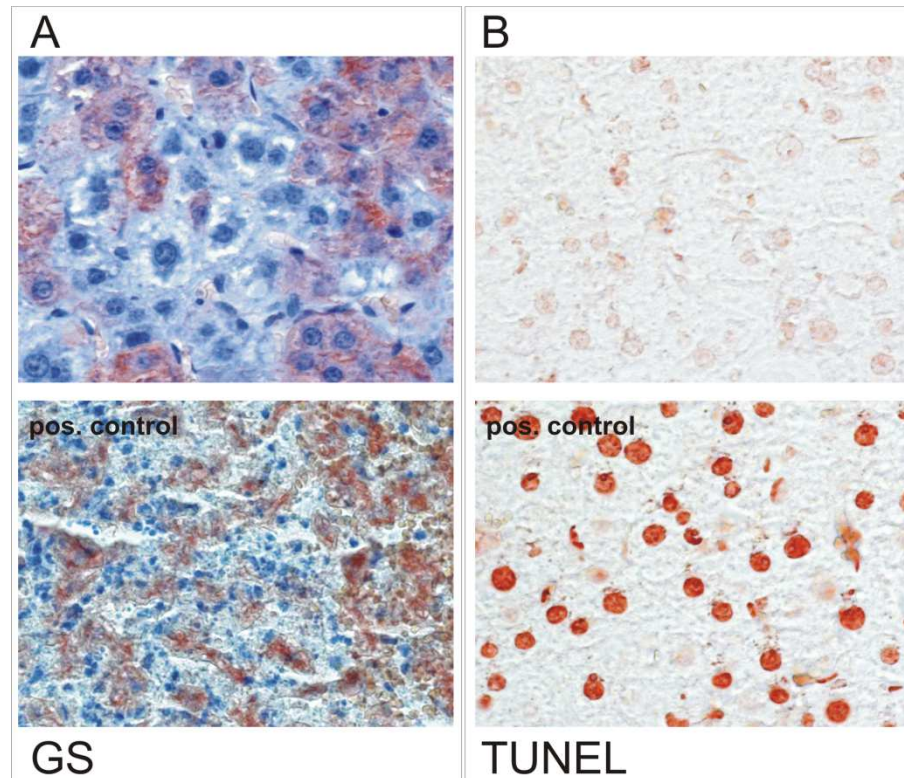


**Figure 14: GS- and TUNEL-immunostained liver tumor tissue after KO of *Ctnnb1*.** (A) Tumor image detail from a *Ctnnb1* KO mouse showing few GS-positive cells after  $\beta$ -catenin ablation. Tissue displays intact cell nuclei without significant signs of inflammation. In contrast, the positive (pos.) control (image is taken from the tumor poisoning experiment described in section 4.3) shows necrotic tumor cell debris still positively stained for GS and the presence of small cell nuclei indicating an infiltration by immune cells. (B) Representative TdT-mediated dUTP nick end labeling (TUNEL) image of tumor tissue from (A) reveals the absence of apoptotic cell nuclei in comparison with a positive control (parallel liver section was pre-treated with benzonase nuclease to induce DNA strand breaks prior to the TUNEL staining protocol). Images are taken from a *Ctnnb1* KO mouse killed at 3 weeks after tamoxifen treatment.

Apoptotic cell death is a rare event in the mouse liver and also difficult to detect (Chabicovsky *et al.*, 2003; Bursch *et al.*, 2004). Thus, a series of *in vitro* experiments was conducted, described in the next chapter, to better understand the role of  $\beta$ -catenin signaling in hepatocyte apoptosis.

## 4.2. Role of Activated $\beta$ -Catenin in Etoposide-Induced Apoptosis in Mouse Hepatoma Cells

There is evidence that activated Wnt/  $\beta$ -catenin signaling in tumor cells plays a role in mediating resistance against chemotherapy-induced apoptosis. Treatment with anticancer drugs in combination with  $\beta$ -catenin inhibition led to enhanced cytotoxicity in different cancer cell lines (Saifo *et al.*, 2010; Ellerkamp *et al.*, 2013; Chen *et al.*, 2001).

*In vitro* experiments in mouse hepatoma cells were performed to further analyze the potential interference of  $\beta$ -catenin with apoptosis induced by the known anticancer drug etoposide. The Wnt/  $\beta$ -catenin signaling pathway was activated in two different 70.4 hepatoma cell clones. 70.4 STF clone 15 cells stably transfected with the STF reporter vector were treated with the proteasome inhibitor bortezomib to prevent  $\beta$ -catenin degradation. Bortezomib strongly enhanced relative luciferase expression as compared to untreated cells (~120 to 310-fold) (Figure 15A). Experiments with Mo clone 50 cells, able to express non-degradable  $\beta$ -catenin<sup>S33Y</sup> under the control of a doxycycline-inducible promoter, were conducted in cooperation with Moritz Horn (see also diploma thesis Moritz Horn, 2010). 70.4 Mo clone 50 cells were transiently transfected with the STF luciferase reporter vector to assess changes in  $\beta$ -catenin-dependent, TCF/ LEF-driven reporter gene expression. The GSK3 $\beta$  inhibitor LiCl led only to a moderate increase in the luciferase reporter signal. In contrast, doxycycline-mediated expression of  $\beta$ -catenin<sup>S33Y</sup> led to ~20-fold enhancement of relative luciferase expression in 70.4 Mo clone 50 cells (Figure 15B). Luciferase activity was normalized to untreated cells. Etoposide had no effect on relative luciferase expression in both 70.4 hepatoma cell clones (data not shown).

## Results

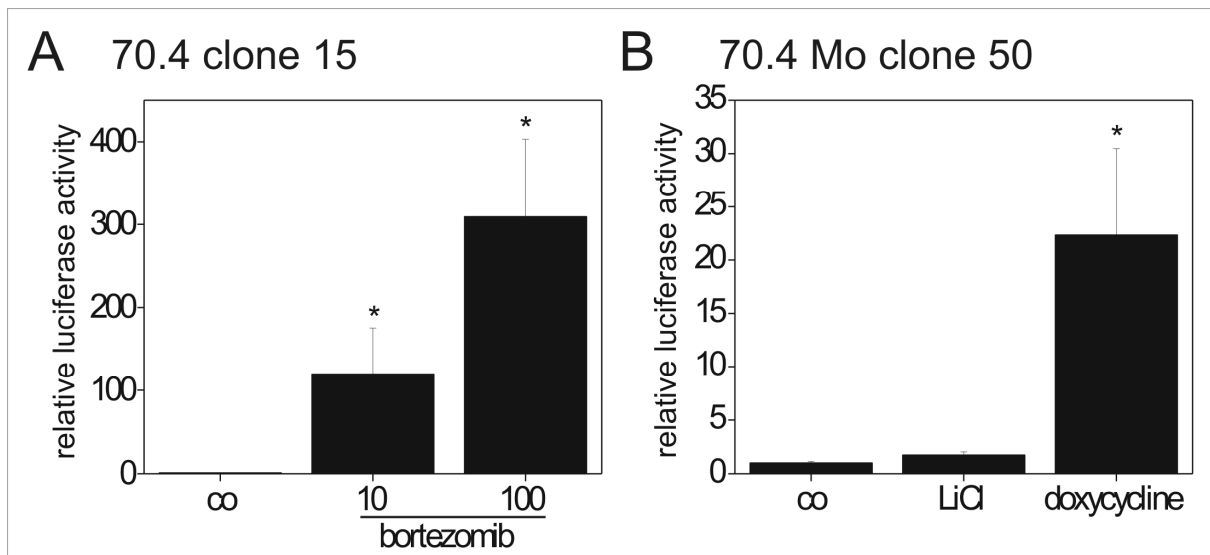


**Figure 15: Activation of  $\beta$ -catenin-dependent TCF/ LEF-driven reporter vector in different mouse hepatoma cells. (A)** 70.4 clone 15 cells stably transfected with a 7x TCF/ LEF-driven luciferase reporter vector (SuperTopflash; STF) were treated with different concentrations of the proteasome inhibitor bortezomib (10, 100 nM) for 24 h and referred to an untreated control (co). Firefly luciferase activity was normalized to cell viability measured by alamar blue assay. Mean +SD (n = 4) are shown. **(B)** 70.4 Mo clone 50 cells were transiently transfected with the STF luciferase reporter vector. Cells were treated with the glycogen synthase kinase 3 $\beta$  inhibitor LiCl (15 mM) for 24 h or with doxycycline (1  $\mu$ g/ ml) to induce the expression of non-degradable  $\beta$ -catenin<sup>S33Y</sup> and referred to an untreated control (co). Firefly luciferase activity was normalized to Renilla. Mean +SD (n = 3) are shown. Statistical significances are indicated by asterisks (\*p < 0.05 versus untreated control).

70.4 clone 15 cells were treated with bortezomib and immunostained for  $\beta$ -catenin (Figure 16). Membranes of both untreated and bortezomib-treated cells showed the presence of  $\beta$ -catenin. Additionally, bortezomib-mediated inhibition of the proteasome led to nuclear accumulation of  $\beta$ -catenin indicative for active Wnt/  $\beta$ -catenin signaling.

## Results

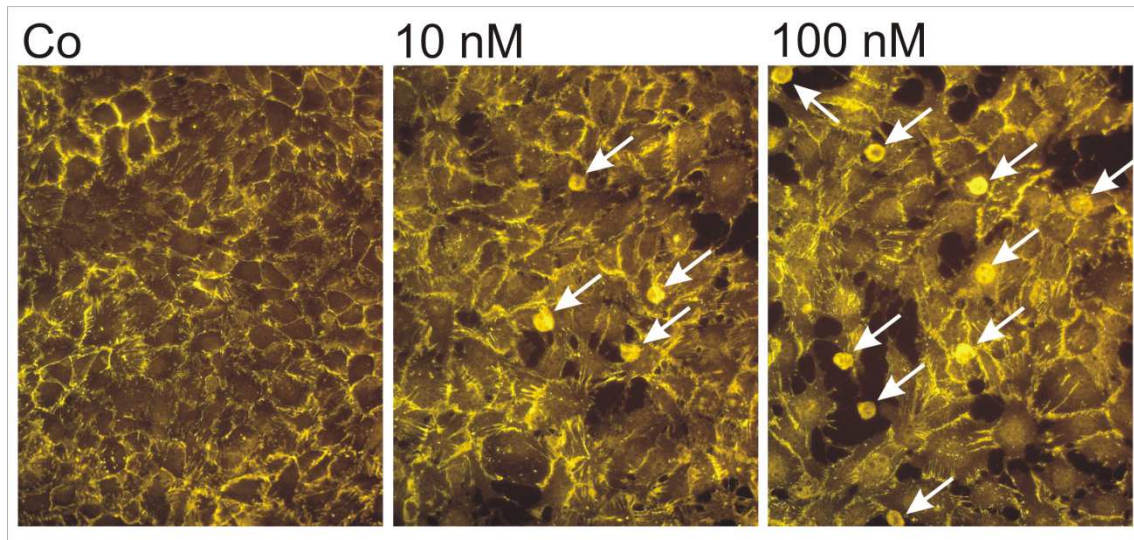


**Figure 16: Immunostaining of 70.4 clone 15 cells after treatment with bortezomib.** Untreated 70.4 clone 15 cells (Co) show the presence of membranous  $\beta$ -catenin. After treatment with the proteasome inhibitor bortezomib (10, 100 nM; 24 h),  $\beta$ -catenin is also found in the nucleus. Respective  $\beta$ -catenin-positive cell nuclei are indicated by white arrows.

To further assess the effect of activated Wnt/  $\beta$ -catenin signaling on etoposide-induced apoptosis, relative caspase 3/ 7 activity was measured (Figure 17). Treatment of 70.4 clone 15 cells with etoposide led to a > 90-fold enhancement of relative caspase 3/ 7 activity (Figure 17A). Bortezomib strongly decreased etoposide-mediated caspase 3/ 7 activation. The proteasome inhibitor alone led only to moderate increases in caspase 3/ 7 activity (~3 to 5-fold, not shown). In accordance with previous findings (diploma thesis Esther Rosenwald, 2008), reduced caspase 3/ 7 activity was seen after combined treatment with etoposide and LiCl compared to cells treated with etoposide alone. Caspase 3/ 7 activity was significantly reduced by a factor of about 25 (Figure 17B). Pre-treatment with doxycycline had no significant effect on etoposide-induced apoptosis in 70.4 Mo clone 50 cells (Figure 17B). Treatment of Mo cells with doxycycline or LiCl alone did not significantly affect caspase 3/ 7 activity (not shown).



## Results

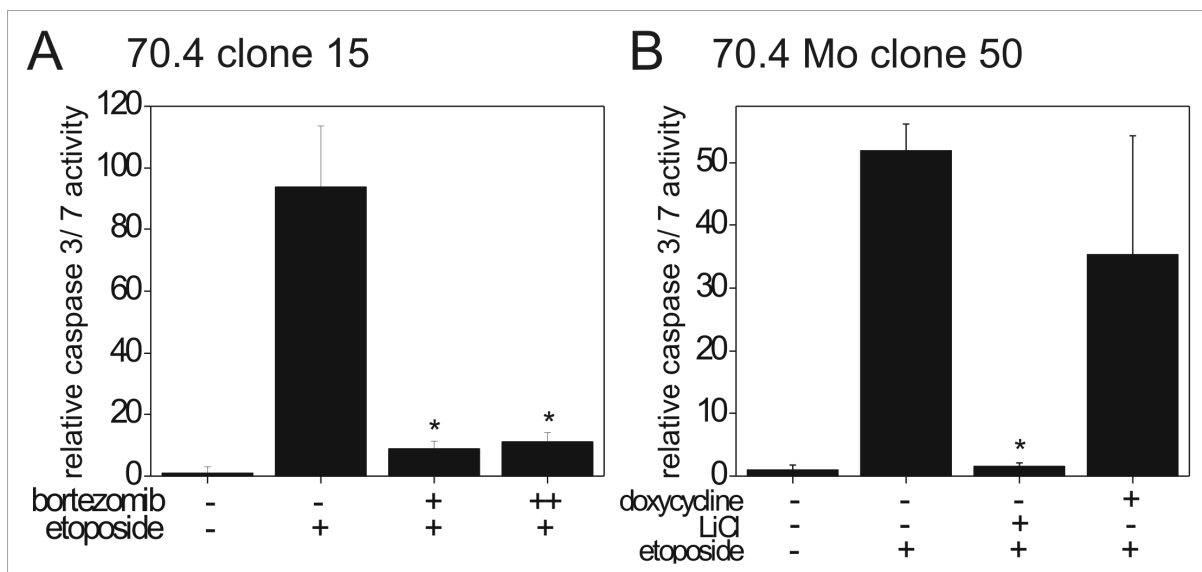


**Figure 17: Etoposide-induced caspase 3/7 activity in presence or absence of activated Wnt/  $\beta$ -catenin signaling. (A)** Combined treatment with bortezomib (+ = 10, ++ = 100 nM) and etoposide (+ = 10  $\mu$ M; 24 h) strongly decreases caspase 3/7 activation in 70.4 clone 15 cells compared to etoposide treatment alone. Mean +SD (n = 3) are shown. Caspase activity was normalized to protein content. **(B)** Activation of caspase 3/7 activity by treatment with etoposide (+ = 10  $\mu$ M; 24 h) is prevented by co-treatment with LiCl (+ = 15 mM) in 70.4 Mo clone 50 cells. Pre-treatment with doxycycline (+ = 1  $\mu$ g/ml; 24 h) to induce the expression of  $\beta$ -catenin<sup>S33Y</sup> does not significantly affect etoposide-induced caspase 3/7 activation. Mean +SD (n = 5) are shown. Statistical significances are indicated by asterisks (\*p < 0.05 versus etoposide treated cells).

Inhibition of the proteasome by bortezomib leads to the accumulation of a broad range of proteins implicated in the regulation of apoptosis (Lue and Wang, 2013; Voorhees *et al.*, 2013). Thus, further analyses were made to clarify the role of  $\beta$ -catenin in bortezomib-mediated prevention of apoptosis. 70.4 STF clone 15 cells were transiently transfected with siRNA against *Cttnb1* 24 h prior to treatment with etoposide alone or in combination with bortezomib. SiRNA transfection led to a ~70% decrease in relative luciferase expression induced by bortezomib as compared to scrambled siRNA control (Figure 18A). Knockdown of *Cttnb1* did not change etoposide-induced caspase activation (Figure 18B). Furthermore, bortezomib-

## Results

mediated decrease of apoptosis was not prevented by siRNA-mediated knockdown of *Ctnnb1*. Similar results were obtained with the proteasome inhibitor MG-132 (not shown).

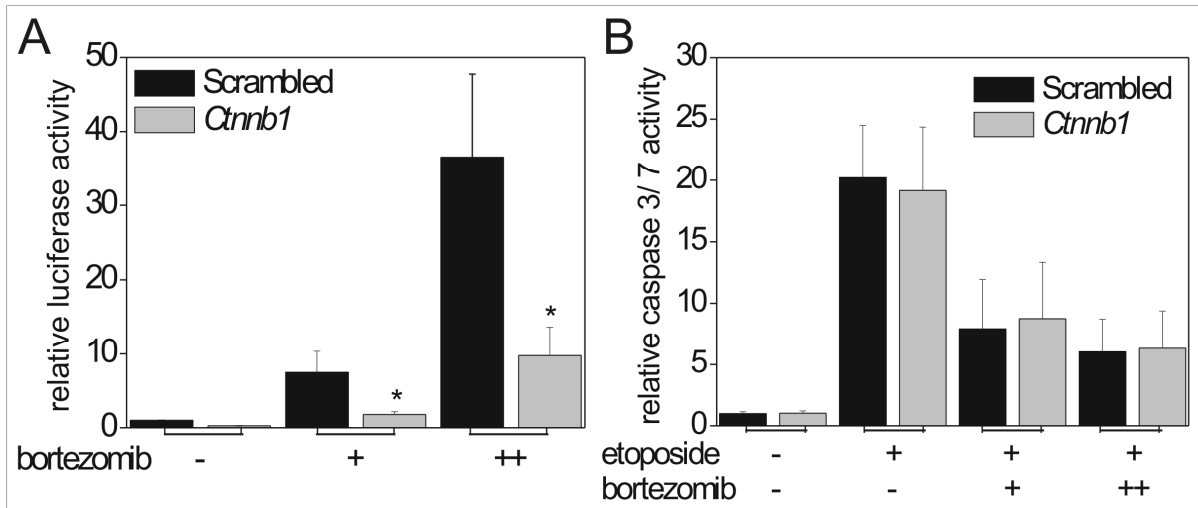


**Figure 18: Role of  $\beta$ -catenin in bortezomib-mediated prevention of apoptosis. (A)** SiRNA transfection against *Ctnnb1* 24 h prior to treatment with bortezomib (+ = 5 nM, ++ = 10 nM; 24 h) significantly decreases relative luciferase activity compared to cells transfected with scrambled siRNA. Mean +SD (n = 3) are shown. Statistical significances are indicated by asterisks (\*p < 0.05 versus cells transfected with scrambled siRNA). **(B)** Activation of caspase 3/ 7 by treatment with etoposide alone (+ = 10  $\mu$ M; 24 h) is not significantly altered by siRNA-mediated knockdown of *Ctnnb1*. Relative caspase activity is decreased by co-treatment with bortezomib (+ = 5 nM, ++ = 10 nM; 24 h), independent of siRNA-mediated *Ctnnb1* knockdown. Mean +SD (n = 3) are shown.

Hoechst staining was performed to assess the presence of apoptotic cell nuclei in 70.4 clone 15 cells (Figure 19). Etoposide treatment decreased the number of adherent cells while the appearance of apoptotic cell nuclei was strongly enhanced as compared to untreated cells or to cells treated with etoposide and bortezomib. Knockdown of *Ctnnb1* by siRNA had no apparent effect in this experiment.

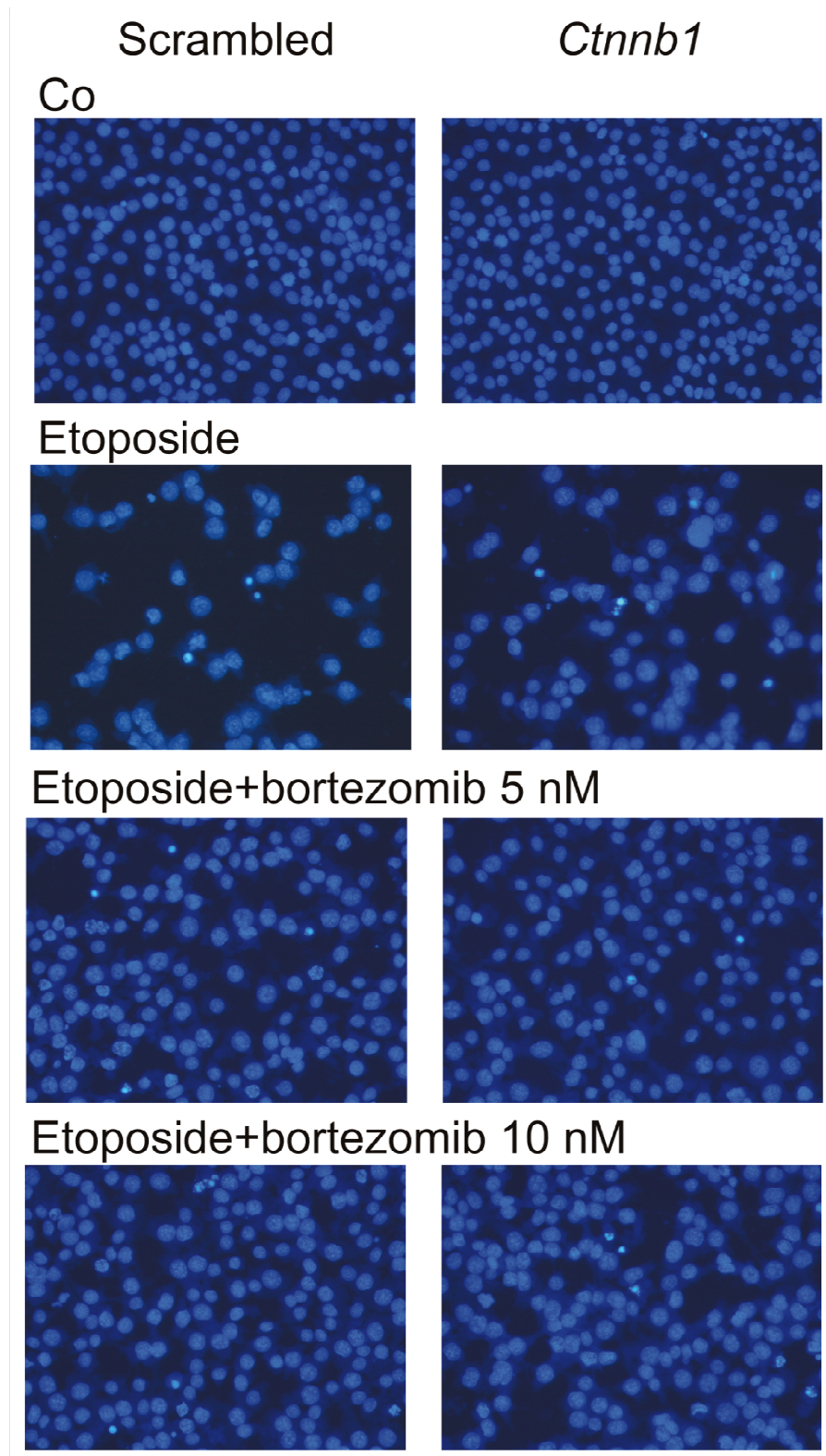


**Figure 19: Hoechst staining for apoptotic cell nuclei in 70.4 clone 15 cells.** Untreated cells (Co) display a confluent cell layer in contrast to cells treated with etoposide (10  $\mu$ M; 24 h). Apoptotic bodies are found after treatment with etoposide. Combined treatment with etoposide and bortezomib (5, 10 nM) increases the number of adherent cells while at the same time the percentage of apoptotic

## Results

cells is decreased. Transfection of siRNA against *Ctnnb1* does not affect the rate of apoptosis when compared to cells transfected with scrambled siRNA.

### **4.3. Selective Poisoning of *Ctnnb1*-Mutated Mouse Liver Tumors by AAP**

New therapeutic strategies concentrate more on the molecular characteristics of cancer cells enabling to exploit tumor-specific changes in signaling and metabolic pathways. Mouse liver tumors harboring an activated form of  $\beta$ -catenin display a characteristic mRNA and protein expression profile (Loeppen *et al.*, 2002, 2005; Stahl *et al.*, 2005). This includes high expression of GS, a marker for hepatic  $\beta$ -catenin activation, and of several enzymes involved in xenobiotic metabolism, especially CYP2E1 and 1A2 (Loeppen *et al.*, 2005). Many drugs are activated via CYP enzymes to toxic metabolites in the liver (Guengerich and Shimada, 1991). Amongst these is AAP (paracetamol) which is metabolized to NAPQI by CYP2E1 and, to a lesser extent, 1A2 (Miner and Kissinger, 1979; Dahlin *et al.*, 1984). At high doses of AAP, NAPQI is no longer detoxified by conjugation with GSH and becomes strongly hepatotoxic.

The idea of the subsequently described experiment was to take advantage of the characteristic enzyme expression profile of *Ctnnb1*-mutated mouse liver tumors with their high levels of AAP-activating CYP enzymes. After tumor initiation with DEN and promotion with PB, tumor-bearing mice were injected a single high dose of AAP. The aim was to selectively poison *Ctnnb1*-mutated, CYP-positive liver tumors.

### 4.3.1. Phenotype of Generated Mouse Liver Tumors

To induce *Ctnnb1*-mutated liver tumors, mice were given a single intraperitoneal DEN injection followed by chronic treatment with PB for 27 weeks as previously described (Moennikes *et al.*, 2000; see also section 3.10.3). When following this treatment protocol, about 80% of tumors harbor activating mutations in *Ctnnb1* (Aydinlik *et al.*, 2001), while a minority of tumors are mutated in the *Ha-ras* or *B-raf* genes leading to constitutive activation of the MAPK pathway. Immunohistochemical analyses of liver sections from tumor-bearing mice were performed. GS-positive tumors showed the expected expression of CYP enzymes 2E1 and 1A2, but were negative for E-cadherin (Figure 20A). Mutation analyses of GS-positive tumors also confirmed the almost 100% concordance between GS expression and mutation in *Ctnnb1*: 11 out of 12 (91.7%) GS-positive tumors were mutated in the *Ctnnb1* gene. In contrast, *Ha-ras* or *B-raf*-mutated tumors displayed an inverse protein expression pattern (see also Hailfinger *et al.*, 2006). They lacked the expression of GS and CYP enzymes, but were positive for E-cadherin, a marker for activated MAPK signaling. Figure 20B shows a representative image of an E-cadherin-positive tumor negative for GS and CYP enzymes.

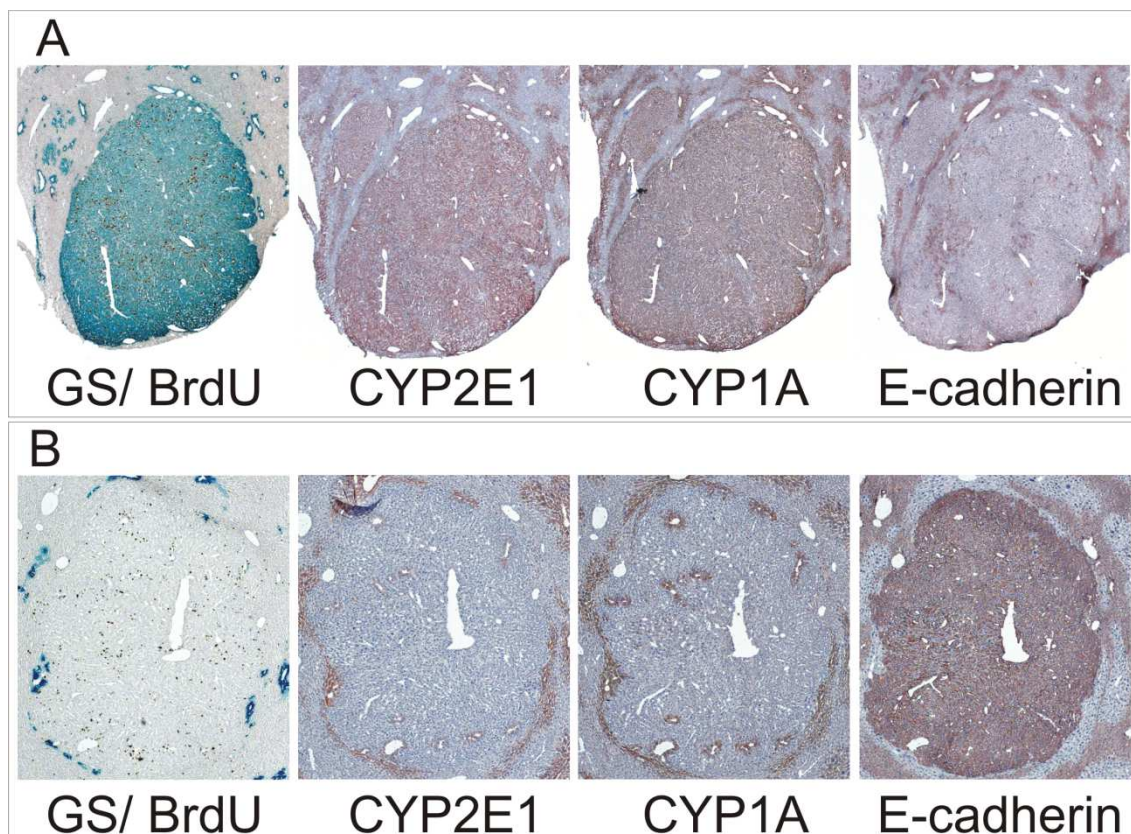


**Figure 20: Immunostainings of *Ctnnb1*-mutated versus *Ha-ras/ B-raf*-mutated mouse liver tumors. (A) *Ctnnb1*-mutated tumor with activated  $\beta$ -catenin is positive for GS and CYP enzymes 2E1 and 1A2, but lacks the expression of E-cadherin. (B) An inverse staining pattern is observed in the E-cadherin-positive tumor harboring an activating mutation in either *Ha-ras* or *B-raf*. The respective tumor is negative for GS and CYP enzymes. Aside from that, both tumors show a high proliferative index as indicated in the GS/ BrdU double stain. Taken from (Singh *et al.*, 2013).**

#### 4.3.2. Hepatotoxicity of AAP in Normal Liver Tissue

An AAP dose finding study was conducted prior to the main experiment. The aim of the study was to find the appropriate AAP dose leading to moderate hepatotoxicity. Therefore, mice of the same strain and age as the ones used in the main study were injected single intraperitoneal doses of 200, 300 or 400 mg/ kg of body weight AAP and killed at 1, 2 or 7 days after treatment. Immunohistochemical analyses of livers were performed and blood levels of liver transaminases (ALT, AST) were measured. Animals in the lowest dosing group showed no signs of intoxication (image not

## Results

shown). In contrast, application of the highest AAP dose caused the death of the animals within one day. Immunostained livers showed large-scale necrosis (Figure 21A). The dose of 300 mg/ kg of body weight AAP killed one animal within 24 hours. The other two mice had slightly increased ALT and AST levels after 2 days (7-fold for ALT, 3-fold for AST). Otherwise, animals behaved normal. Thus, 300 mg/ kg of body weight AAP was chosen for the treatment of mice harboring *Ctnnb1*-mutated liver tumors.

After tumor promotion, mice were injected either a single intraperitoneal dose of 0.9% saline or of 300 mg/ kg of body weight AAP. The earliest time point of analysis was at 2 days after AAP. Necrotic areas were absent from normal liver tissue of tumor-bearing mice treated with 300 mg/ kg of body weight AAP and no striking differences compared to saline-treated mice (-AAP) were observed (Figure 21B, C).

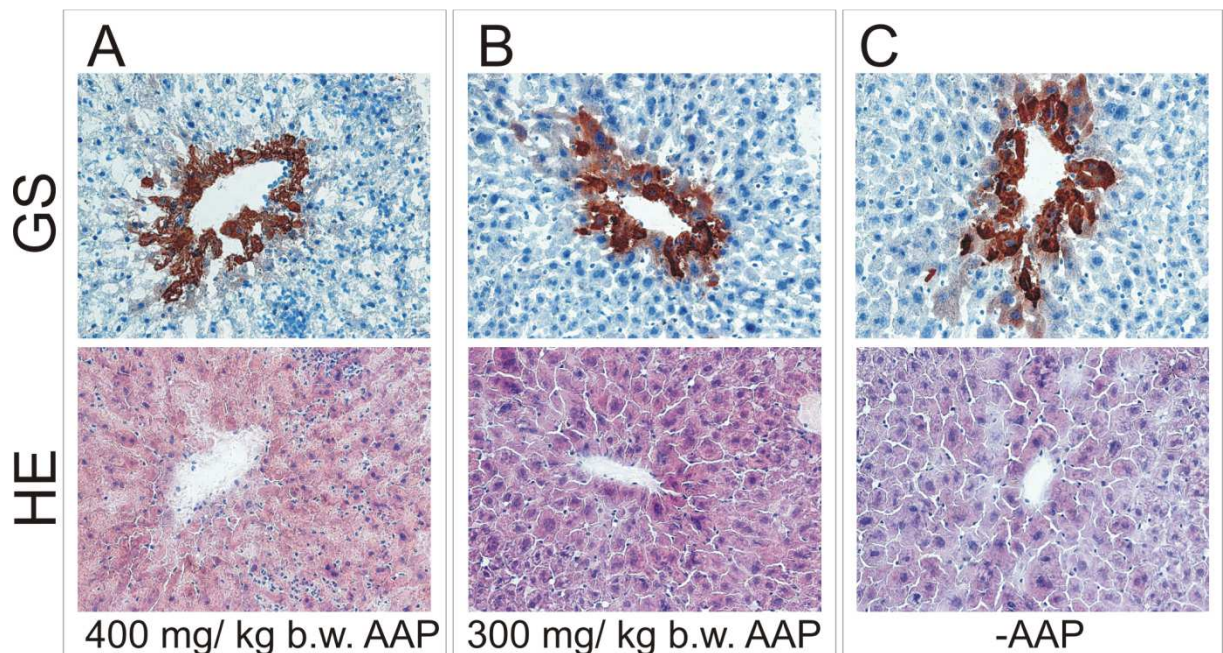


**Figure 21: Immunostained livers after treatment with different doses of AAP.** GS- and hematoxylin/ eosin (HE) -stained central veins of livers from AAP-treated versus saline-treated (-AAP) animals. **(A)** Massive tissue damage along with infiltration by immune cells is observed after application of 400 mg/ kg of body weight (b.w.) AAP. In contrast, normal liver tissues from tumor-

## Results

bearing mice treated with 300 mg/ kg of b.w. AAP (**B**) and from non-AAP-treated animals (**C**) show no signs of toxicity. Livers were excised at 1 to 2 days after treatment. Taken from (Singh *et al.*, 2013).

### 4.3.3. Acute Effects of AAP Treatment on GS-Positive Tumors

To assess acute effects of AAP application on GS-positive tumors, livers from tumor-bearing mice were excised at 2 days after treatment. Differences in the shape and color of tumors between saline-treated (-AAP) and AAP-treated (+AAP) animals were macroscopically visible (Figure 22). Tumors from mice in the control group were hardly visible but could be recognized by their shape. Smaller lesions were reddish colored. As opposed to that, AAP-treated mice harbored bloated tumors which were clearly visible by their white color.

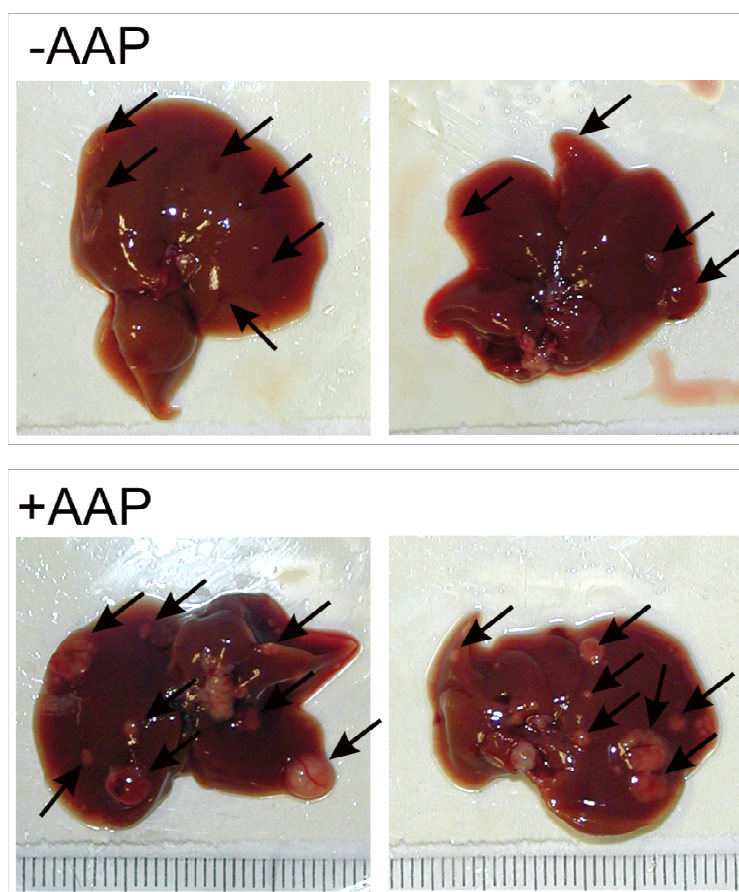


**Figure 22: Representative images of livers from mice after tumor promotion and treatment with saline or AAP.** Livers excised at 2 days after intraperitoneal injection of 0.9% saline (-AAP) or 300 mg/ kg of body weight AAP (+AAP) are shown. Livers from saline-treated animals display barely



## Results

visible lesions and tumors with a glassy or reddish appearance. In contrast, livers from AAP-treated animals harbor mainly white colored, bloated-looking tumors. Tumors are indicated by black arrows.

Histochemically (HE) and enzyme-histochemically (G6Pase) stained liver sections from a non-AAP-treated (-AAP) versus an AAP-treated (+AAP) animal are shown in Figure 23. Tumors from saline-treated animals were barely visible in the HE stain, but were detectable by their reduced G6Pase activity, a general tumor marker in mouse liver. In contrast, tumors from AAP-treated animals were visible as “holes” in respective liver sections, indicative for necrotic tissue. Respective tumors, indicated by black arrows, were also GS-positive (images not shown).

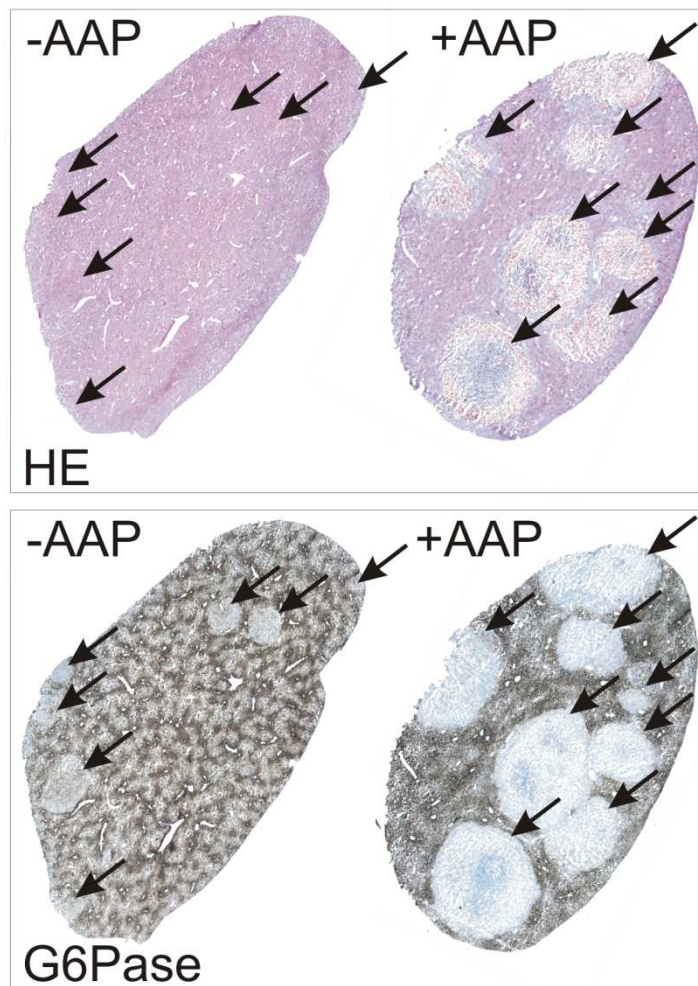


**Figure 23: Immunostaining of liver lobes from AAP-treated and non-AAP-treated mice.** Tumors from saline-treated (-AAP) mice are hardly detectable in the HE stain, but are visualized by their lack

## Results

of glucose-6-phosphatase (G6Pase) activity, a general marker for mouse liver tumors. In contrast, the liver lobe of an AAP-treated (+AAP) animal shows tumors clearly visible as “holes” in the HE and the G6Pase stains. Animals were killed at 2 days after treatment with saline or AAP. Tumors are indicated by black arrows.

A higher magnification of tumors is shown in Figure 24. Tumors from non-AAP-treated (-AAP) mice were clearly negative for G6Pase activity and displayed intact tissue with large tumor cell nuclei. In contrast, GS-positive tumors from AAP-treated (+AAP) mice were highly necrotic and cell debris was infiltrated by immune cells at 2 days after AAP (Figure 24A, B). Despite massive cell death, residual GS protein could still be detected in the damaged tumors via immunostaining. To quantify the degree of necrosis in tumors after AAP treatment, the percentage of necrotic area in each GS-positive tumor was determined. Images of G6Pase-stained liver sections were used to circle tumor areas clearly lacking intact tumor tissue with a pen display. Tumors were stratified into two groups according to their size (tumors  $< 0.5 \text{ mm}^2$  or  $\geq 0.5 \text{ mm}^2$ ). The necrotic area fraction of tumors from mice killed at 2 to 6 days after AAP application compared to saline-treated mice after 2 days is shown in Figure 24C, D. Tumors larger than  $0.5 \text{ mm}^2$  consisted of  $\sim 90\%$  necrotic tissue (Figure 24C). Strikingly, smaller tumors were less affected by AAP treatment and displayed  $\sim 50\%$  necrotic tumor area (Figure 24D).

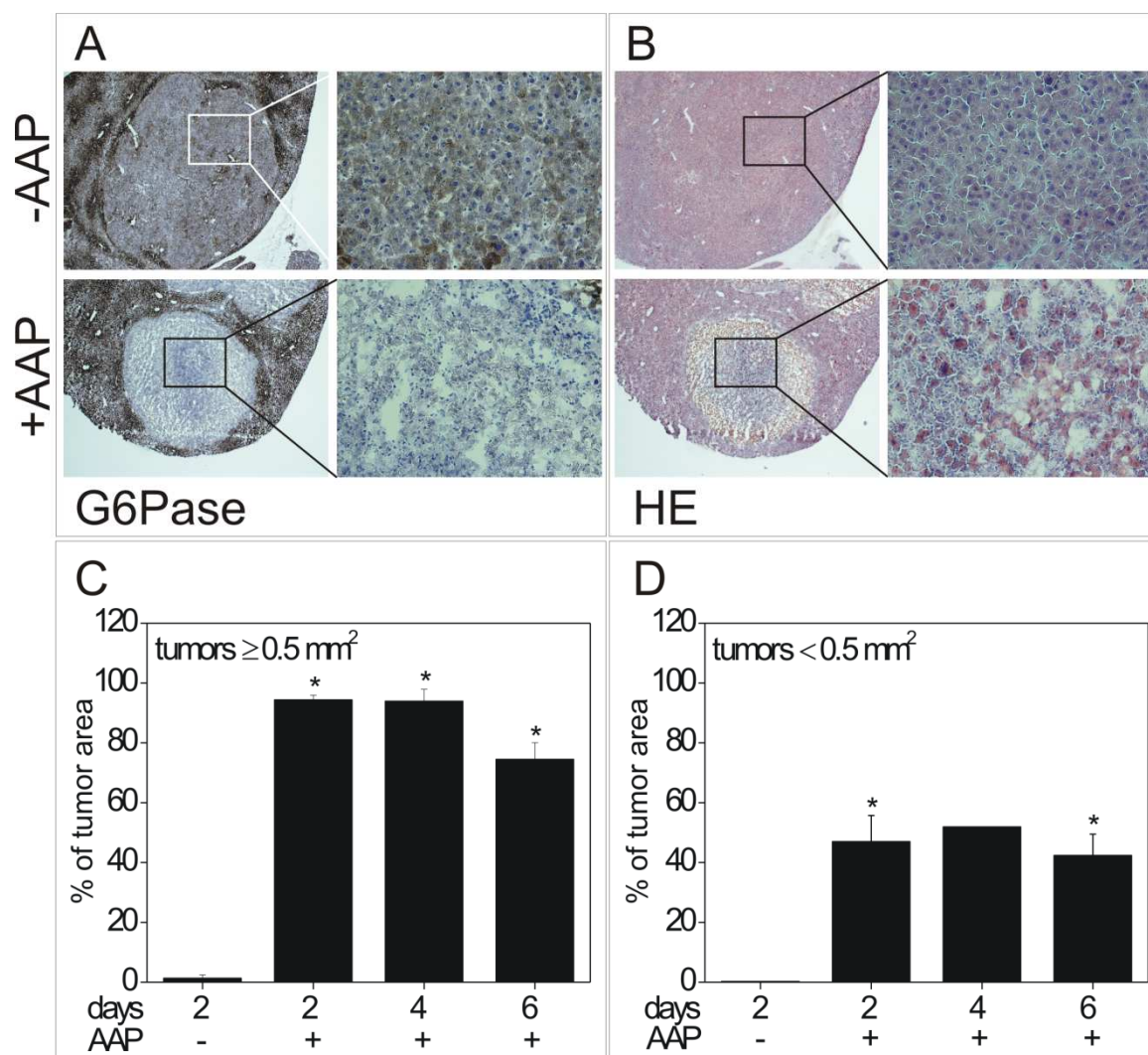


**Figure 24: Acute effects of AAP treatment on GS-positive liver tumors.** Immunostainings for G6Pase (**A**) and HE (**B**) show that livers from saline-treated (-AAP) mice consist of intact tumor tissue, negative for G6Pase. Two days after AAP treatment (+AAP), tumors are highly necrotic. Higher magnification (indicated by boxes) reveals the presence of immune cells (small cell nuclei) and tumor cell debris. Necrotic area fraction of GS-positive tumors  $\geq 0.5 \text{ mm}^2$  (**C**) and of tumors  $< 0.5 \text{ mm}^2$  (**D**) was determined at 2 to 6 days after AAP treatment and compared to the control group after 2 days. Statistical significances are indicated by asterisks (\* $p < 0.05$  versus non-AAP-treated mice after 2 days). Numbers of tumors varied from 2 to 43. Mean +SD are shown. Taken from (Singh *et al.*, 2013).

#### 4.3.4. Resistance of GS-Positive Tumor Cell Populations

Despite the strong effect of AAP, some tumor cell populations were resistant against AAP-induced poisoning. To locate the surviving cells within the tumors, images of

## Results

immunostained liver sections were analyzed. Strikingly, AAP-resistant cells were mainly settled at the border of the tumors from AAP-treated mice (+AAP) (Figure 25). Respective tumor cells were positive for GS and the hepatocyte marker HNF4 $\alpha$  in contrast to necrotic tissue in the tumor center (t) (Figure 25A). Tumors from non-AAP-treated animals (-AAP) consisted of a homogenous cell mass positive for GS and HNF4 $\alpha$  (Figure 25A). Cell nuclei of normal liver tissue (n) were also HNF4 $\alpha$ -positive. Figure 25B shows that the fraction of marginal resistant GS-positive cells was more prominent in smaller tumors. BrdU labeling of cell nuclei revealed a high proliferative index of surviving GS-positive tumor cells and infiltrated immune cells (Figure 25B).

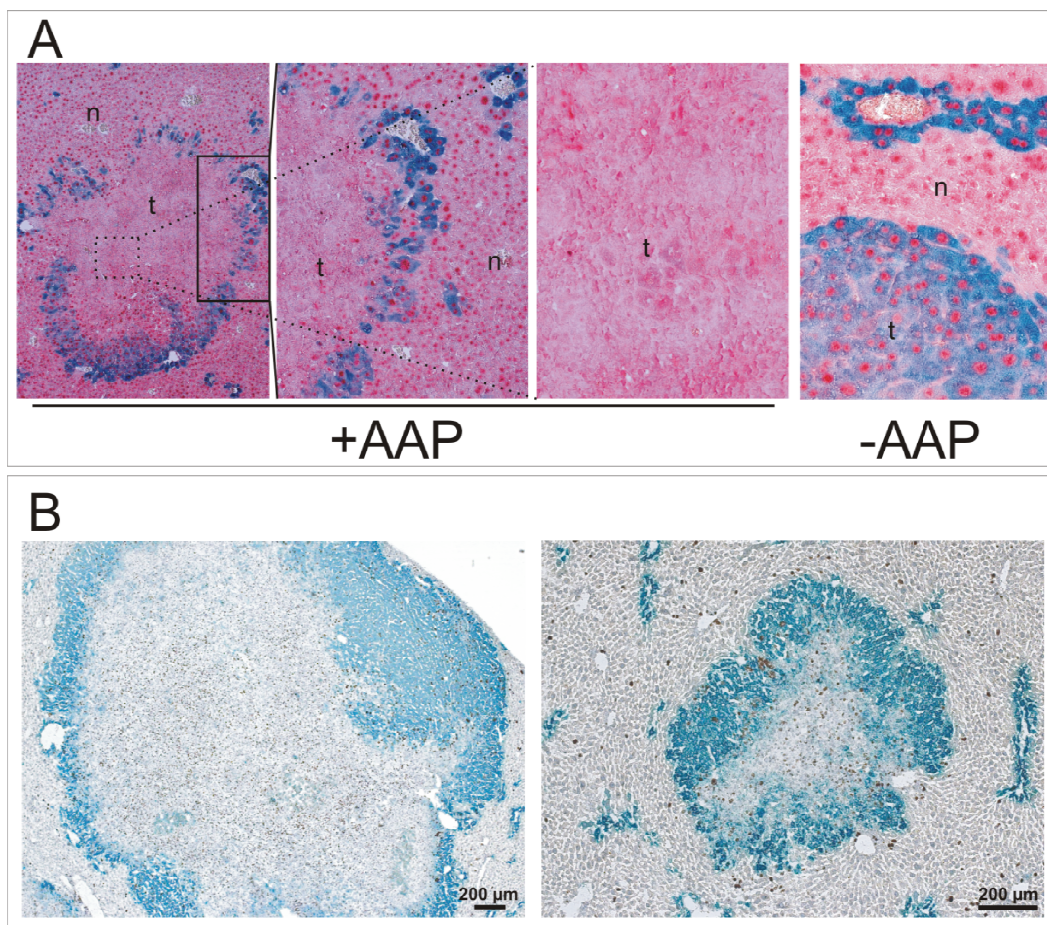


**Figure 25: Resistance of GS-positive tumor cell populations against AAP-induced poisoning.**  
(A) Immunostaining of tumors for hepatocyte nuclear factor (HNF) 4 $\alpha$  and GS from livers of an AAP-

## Results

treated (+AAP) versus a non-AAP-treated (-AAP) animal. Surviving GS-positive tumor cells are located at the outer border of the AAP-poisoned tumor and consist of HNF4 $\alpha$ -positive cell nuclei in contrast to cells located in the tumor center (t). Normal liver tissue (n) and tissue derived from a non-AAP-treated GS-positive tumor (t) are also HNF $\alpha$ -positive. **(B)** Large and small GS-positive tumor at 6 days after AAP treatment. Resistant tumor cells are settled at the edge of the tumors. The percentage of surviving tumor cells seems to be larger in the smaller tumor. Both images show a high number of BrdU-positive cells in the resistant GS-positive cell fraction and the damaged tumor areas. Modified from (Singh *et al.*, 2013).

### 4.3.5. Effects of AAP Treatment on GS-Negative Tumors

The minority of generated tumors was GS-negative and displayed a protein expression pattern indicative for active MAPK signaling (Figure 20B). The respective CYP-negative tumors were not affected by AAP treatment. Immunostained liver lobe sections from an AAP-treated animal harboring two different types of tumors are shown in Figure 26. As expected, the GS-positive tumor referred to as 1, was negative for E-cadherin and destroyed tissue along with inflammatory cells could be observed in the HE stain. Furthermore, the damaged tissue lacked BrdU-positive cell nuclei. In contrast, no signs of toxicity were observed in the GS-negative tumor, positive for E-cadherin, an indication for *Ha-ras* or *B-raf* mutations (labeled as 2). The respective tumor displayed a high proliferative index as determined by the high number of BrdU-positive cells. The tumor consisted of intact cells and no signs of inflammatory processes were detected in the HE stain.

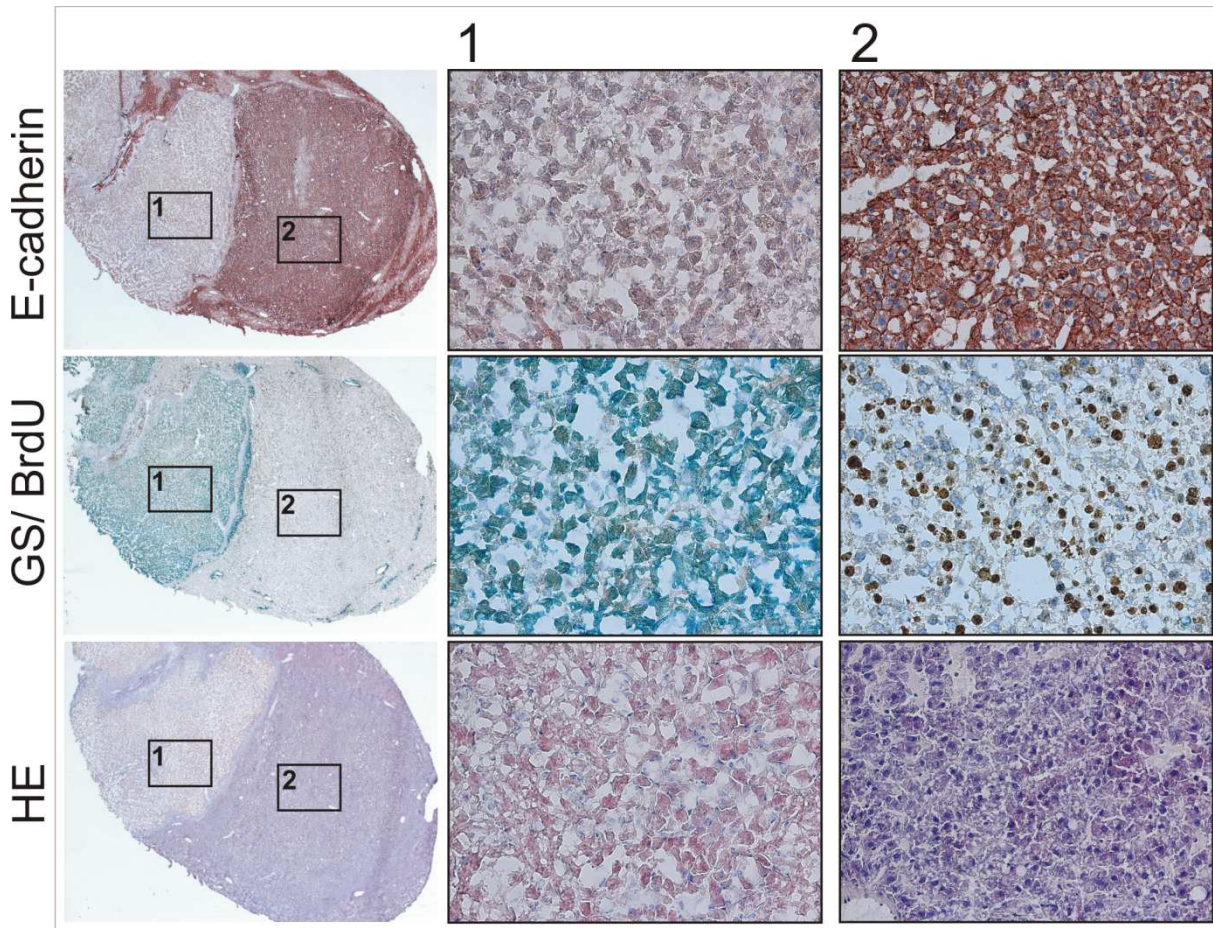


**Figure 26: Effect of AAP treatment on GS-negative tumors.** The GS-positive tumor (1), negative for E-cadherin, consists of cell debris and inflammatory cells as indicated in the HE stain. GS/ BrdU staining reveals the absence of proliferating cells. The E-cadherin-positive tumor (2) is not affected by AAP treatment. HE staining displays intact tumor cell nuclei. The respective tumor also shows a high proliferative index as indicated by the presence of BrdU-positive cells. Image details are marked by black boxes and referred to as 1 or 2. The liver lobe was taken from an animal sacrificed at 4 days after AAP treatment. Modified from (Singh *et al.*, 2013).

#### 4.3.6. Regeneration Processes and Long-Term Effects

A subgroup of AAP-treated mice was killed after 4, 6 or 10 days to monitor regeneration processes of damaged tumor areas. In the following days after AAP application, infiltration of the dead tumor mass by immune cells was observed. Migration started at the border of the poisoned tumors and slowly wandered into the tumor center (Figure 27A). The infiltrated tumor area fraction of GS-positive tumors at

## Results

2 to 6 days after AAP treatment was determined by use of G6Pase-stained liver sections (Figure 27B). Independent of the tumor size, invasion of necrotic tumor tissue significantly increased over time. After 6 days, tumors  $\geq 0.5 \text{ mm}^2$  consisted of ~60% infiltrated area, tumors  $< 0.5 \text{ mm}^2$  displayed ~40% infiltration. At 10 days after AAP, tumors were almost completely infiltrated (images not shown).

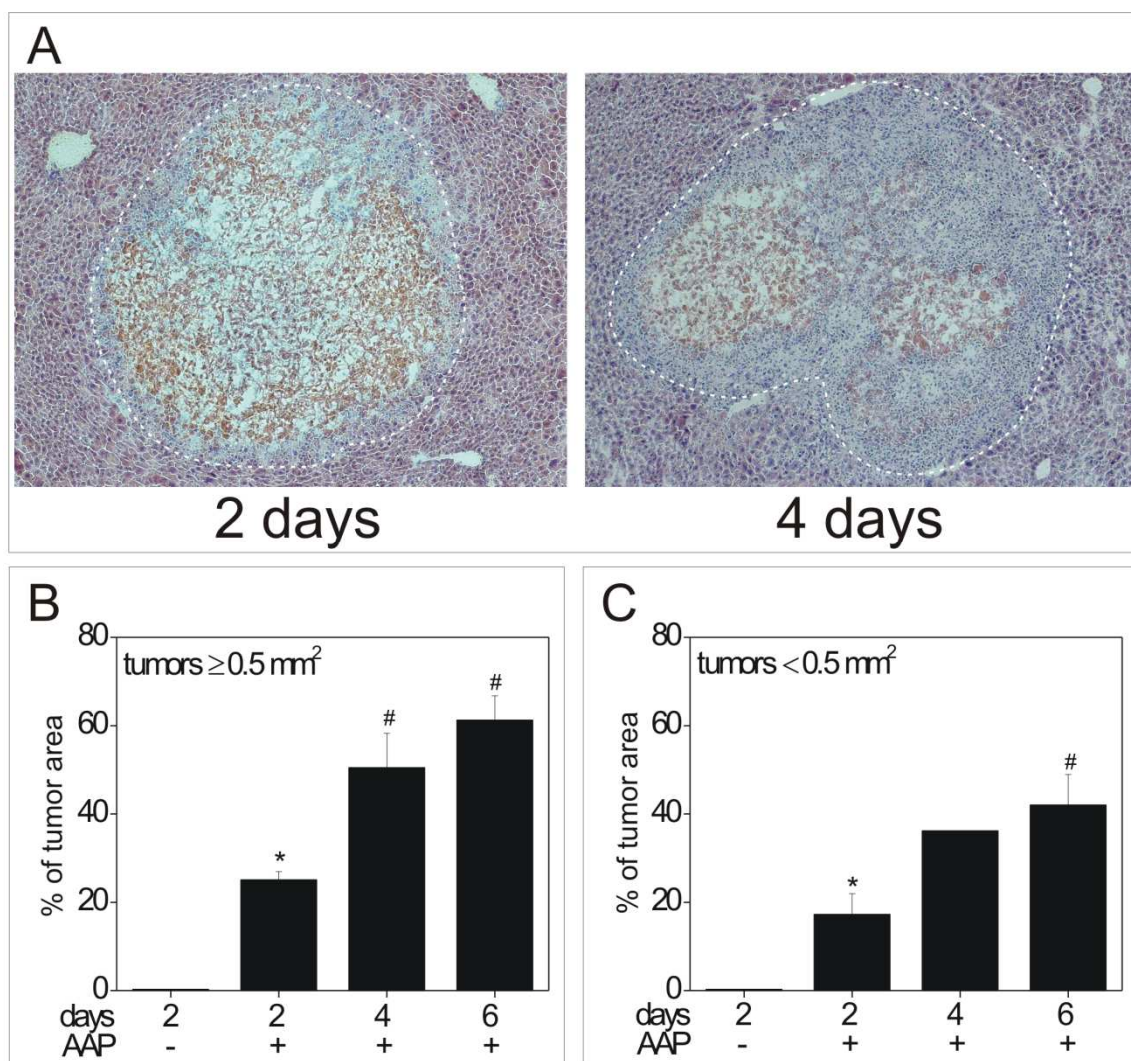


**Figure 27: Infiltration of necrotic tumor tissue after AAP treatment. (A)** HE stains of tumors from animals killed at 2 and 4 days after AAP application are shown. Infiltration by immune cells starts at the tumor border and moves towards the center of the necrotic tumor. Tumors are marked by dotted white line. The infiltrated area fraction of GS-positive tumors  $\geq 0.5 \text{ mm}^2$  **(B)** and of tumors  $< 0.5 \text{ mm}^2$  **(C)** was determined at 2 to 6 days after AAP treatment and compared to the control group after 2 days. Statistical significances are indicated by asterisks or hashes (\* $p < 0.05$  versus non-AAP-treated

## Results

mice after 2 days; #p < 0.05 versus non-AAP-treated and AAP-treated mice after 2 days. Numbers of tumors varied from 2 to 43. Mean +SD are shown. Taken from (Singh *et al.*, 2013).

Analyses of later time points (24 or 45 days after AAP) revealed that the infiltrated necrotic tumor tissue was mainly replaced by normal hepatocytes. Liver lobes consisted of only few GS-positive tumors and isles of GS-positive cells, both of which were proliferating (Figure 28A). Some of the GS-positive cell clusters were also negative for G6Pase, a marker for liver tumors in mice (Figure 28A). This suggests that the respective GS-positive isles were derived from former AAP-poisoned tumors. In some cases, GS-positive tumors also contained fibrotic tissue, visualized in the Masson-Goldner (M/ G) trichrome stain. Figure 28B shows the presence of greenish colored connective tissue in a GS-positive tumor. Unusually, the respective tumor exhibited G6Pase activity and also displayed a remarkable amorphous shape. A high proliferative index was observed in the GS/ BrdU stain. In contrast, livers from non-AAP-treated animals analyzed after 45 days displayed large GS-positive tumors, in part occupying the whole liver lobe (no images shown).



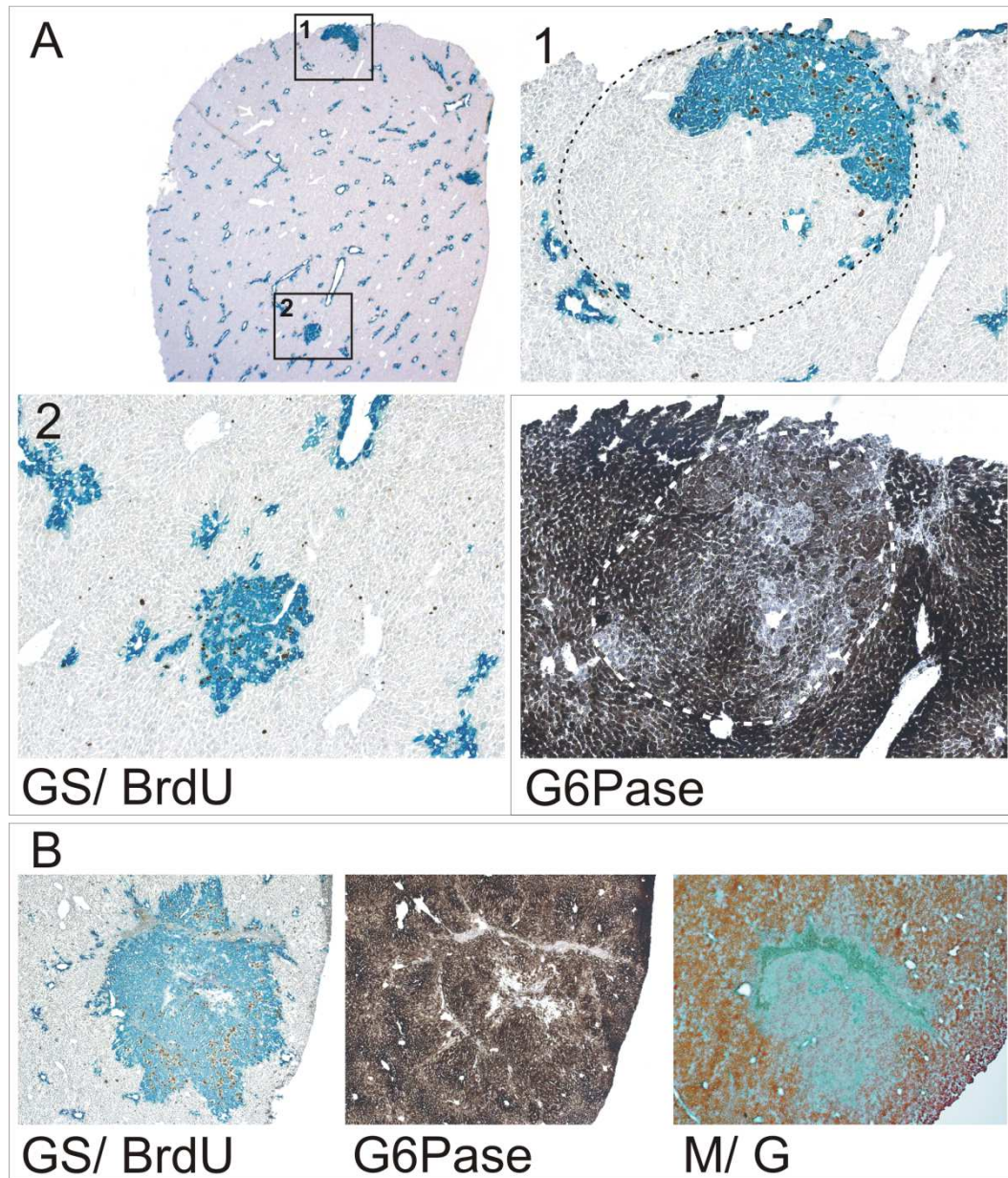


**Figure 28: Long-term effects of AAP treatment on GS-positive liver tumors. (A)** The immunostained liver lobe shows islets of GS-positive cells which probably derive from a previous, AAP-poisoned tumor. Higher magnifications show cell islets that display a high proliferative index as indicated by BrdU-positive cell nuclei. G6Pase staining reveals the shape of a former tumor. Image details are marked by black boxes and referred to as 1 and 2. Liver was excised at 45 days after AAP treatment. **(B)** GS/ BrdU and G6Pase staining show an irregular structured tumor from an animal killed at 24 days after AAP. Fibrotic tissue is visualized by Masson-Goldner (M/ G) trichrome staining. Taken from (Singh *et al.*, 2013).

## Results

The tumor volume fraction, which is equivalent to the area fraction, was determined at 45 days after treatment with either saline or AAP and compared to the control group after 2 days. Non-AAP-treated mice showed an increase in tumor burden from 6.6% to 46.4% after 45 days (Figure 29A). In contrast, the tumor volume fraction from AAP-treated mice was lower than in the saline-treated group after 2 days (2.2%). To assess whether this effect was due to the selective poisoning of GS-positive tumors, the number of GS-positive tumors/ cm<sup>2</sup> was quantified and is shown in Figure 29B. The average amount of GS-positive tumors was only 0.6 in the AAP-treated group after 45 days as opposed to 4.9 in the saline-treated group after 2 days. In accordance with previous findings (Aydinlik *et al.*, 2001), the GS-positive tumor volume fraction accounted for 83.8% in non-AAP-treated mice after 2 days. A strong reduction of GS-positive tumor volume fraction was observed in AAP-treated livers (1.9% in AAP-treated animals after 45 days; Figure 29C).

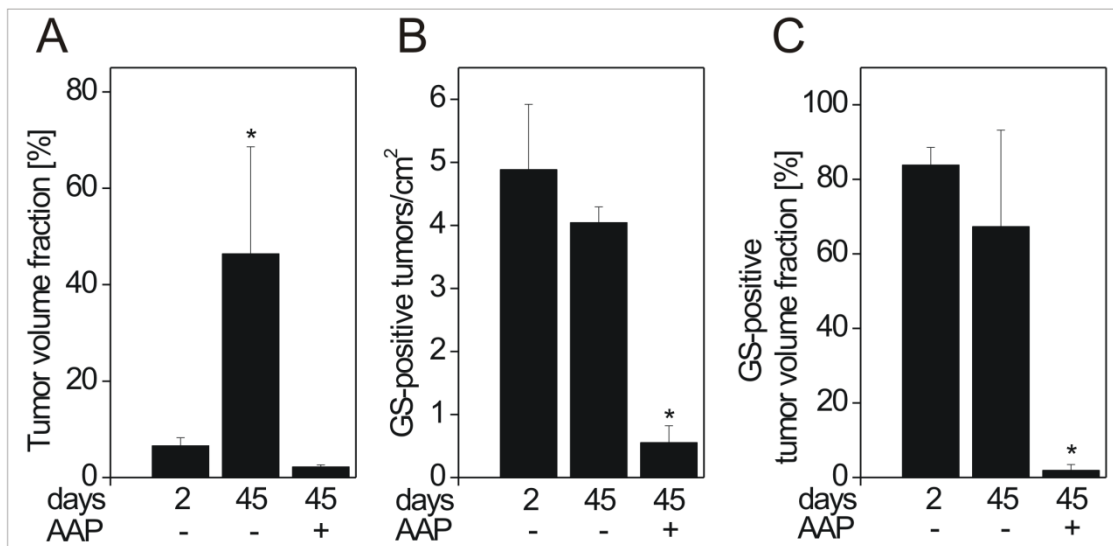


**Figure 29: Assessment of tumor burden over time. (A)** Quantification of tumor volume fraction in livers at 45 days after saline (-) or AAP (+) application compared to saline-treated mice after 2 days. The tumor volume fraction in livers from non-AAP-treated animals is significantly increased after 45 days as opposed to the tumor burden in livers from AAP-treated mice. The number of GS-positive tumors/ cm<sup>2</sup> **(B)** and the GS-positive tumor volume fraction **(C)** is strongly decreased in livers from

## Results

mice at 45 days after AAP treatment. Group sizes: n = 7 mice per group after 2 days, n = 3 mice per group after 45 days. Statistical significances are indicated by asterisks (\*p < 0.05 versus non-AAP-treated mice after 2 days). Mean +SD are shown. Taken from (Singh *et al.*, 2013).

### **4.3.7. Monitoring of Tumor Burden by MRI**

Previous studies showed that MRI is a useful tool to detect liver tumors in mice (Schmid *et al.*, 2012). The non-invasive procedure enables to scan the same animal at different time points. Thus, a subset of animals was monitored by MRI technology at the laboratory of Prof. Pichler by Andreas Schmid in Tuebingen. Animals were anesthetized and measurements were carried out at 8 days before and at 5, 12 and 18 days after AAP treatment. Tumors larger than ~1 mm in diameter could be detected. Series of cross and longitudinal sections were performed. Several tumors, indicated by white circles, were clearly visible in the liver of monitored mice at 8 days before AAP injection (Figure 30). Screening of the same animals at 18 days after AAP revealed that the respective tumors were no longer detectable.

## Results

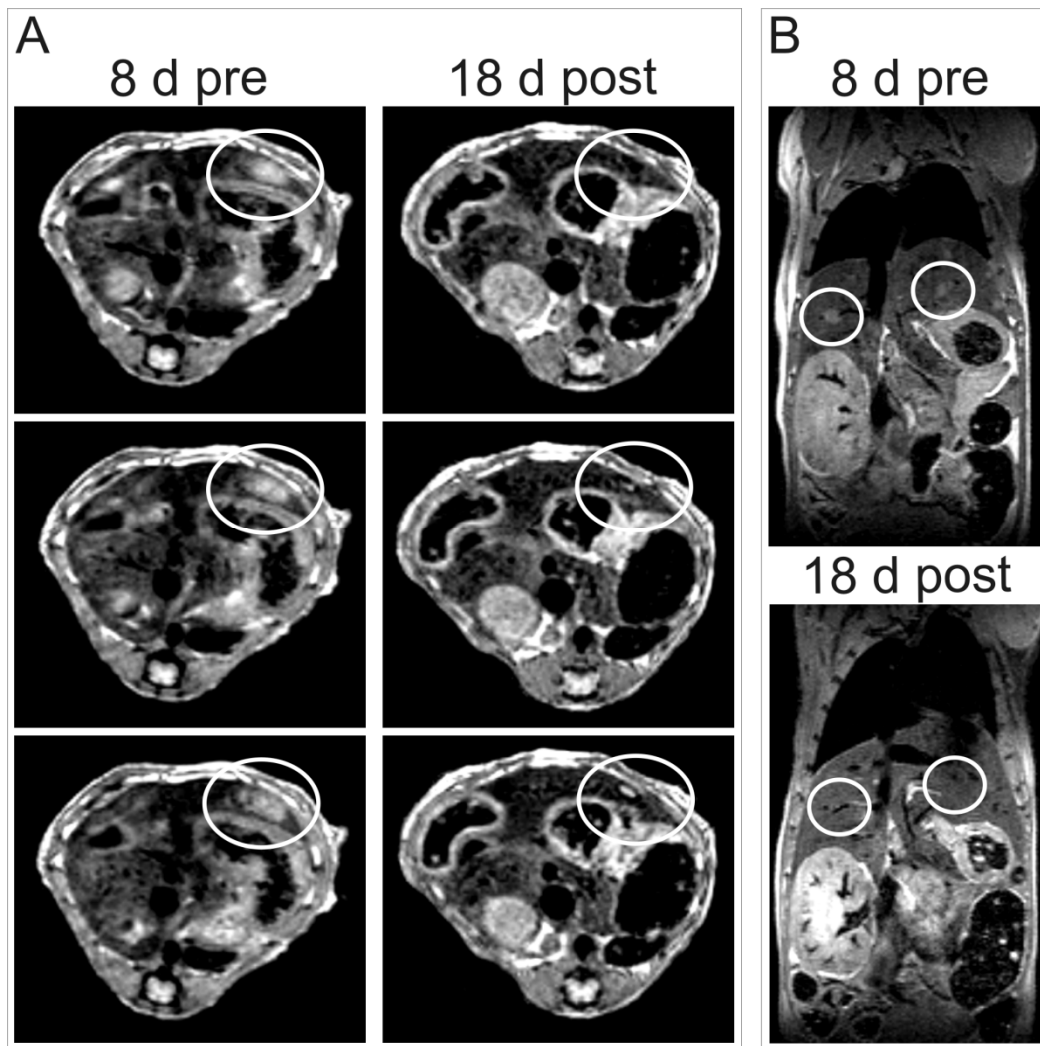


**Figure 30: Monitoring of tumor burden by MRI.** Magnetic resonance imaging (MRI) performed at 8 days before (8 d pre) and 18 days after (18 d post) AAP application is shown. **(A)** Serial cross sections reveal the presence of a large tumor indicated by a white circle in the liver from an animal at 8 days before AAP treatment. At 18 d post AAP the respective tumor is not detectable anymore. **(B)** Liver tumors clearly visible at 8 days before AAP treatment disappear in the MRI image at 18 days after AAP. Longitudinal sections are shown and tumors are marked by white circles. Tumors > 1 mm in diameter are detectable. Serial images were performed and the distances between different imaging levels were 0.22 mm. Taken from (Singh *et al.*, 2013).

Furthermore, the liver tumor volume was assessed at different time points and is shown for two representative mice (Figure 31). In concordance with histological results, the tumor volume steadily decreased after AAP treatment (from 18.3 to 5.6 mm<sup>3</sup> in mouse 1 and from 27.2 to 2.2 mm<sup>3</sup> in mouse 2).

## Results

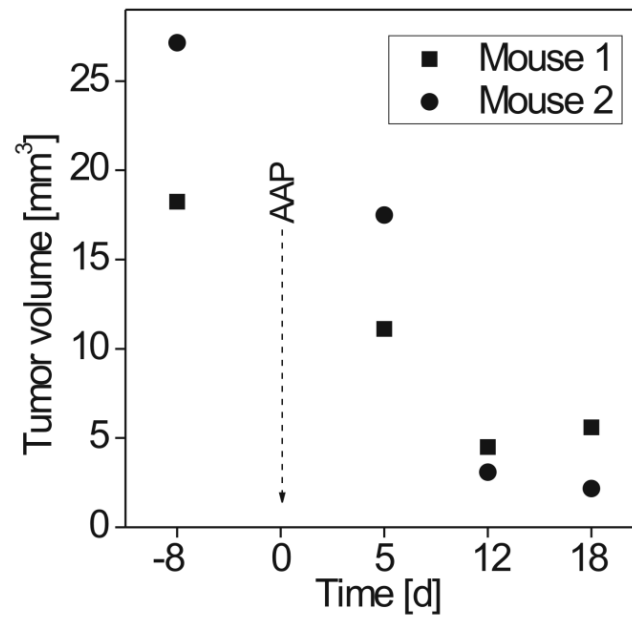


**Figure 31: Time course of tumor burden.** The tumor volume [ $\text{mm}^3$ ] from livers of two representative mice is determined by MRI analysis at 8 days before and at different time points (5, 12, 18 days) after AAP injection. Tumor burden decreases over time in both animals. Taken from (Singh *et al.*, 2013).

## 5. Discussion

The first project in this thesis aimed to get more insights into the role of  $\beta$ -catenin signaling for the growth behavior of *Ctnnb1*-mutated liver tumors in mice. For this purpose, a transgenic mouse strain was used in which a tamoxifen-controllable Cre recombinase led to hepatocyte-specific inactivation of the *Ctnnb1* gene. Mice of this strain were treated with a single injection of DEN followed by promotion with PB. This resulted in the induction of liver tumors of which most had activating mutations in the *Ctnnb1* gene. After hepatocyte-specific deletion of *Ctnnb1* by tamoxifen in mice positive for the *Cre* gene, tumors were characterized. The consequences of  $\beta$ -catenin ablation for the proliferation and survival of liver tumor cells was investigated over time and compared to the tumor growth in mice with an intact *Ctnnb1* gene. To further clarify the role of  $\beta$ -catenin signaling for tumor cell survival, *in vitro* studies were conducted using mouse hepatoma cell lines. In these experiments, the effect of activated Wnt/  $\beta$ -catenin signaling on apoptosis induced by the anticancer drug etoposide was analyzed. Finally, based on the observation that *Ctnnb1*-mutated liver tumors in mice display a characteristic expression profile of drug metabolizing enzymes, a tumor therapy experiment was conducted. AAP was used to selectively target *Ctnnb1*-mutated liver tumor cells highly expressing the CYP enzymes 2E1 and 1A2, which mediate the hepatotoxicity of AAP at high doses.

### 5.1. Ablation of $\beta$ -Catenin in *Ctnnb1*-Mutated Mouse Liver Tumors

It is known that *Ctnnb1*-mutated liver tumors display a distinct mRNA and protein expression profile when compared to normal liver tissue (Stahl *et al.*, 2005; Hailfinger *et al.*, 2006). When considering the possibility that this may have influenced the Cre-mediated knockout of *Ctnnb1* in tumor cells, two aspects have to be considered.

## Discussion

First, the expression of the Cre enzyme was regulated by the promoter of the hepatocyte-specific transthyretin gene. Yet, the expression of this gene is not altered in murine *Ctnnb1*-mutated liver tumors (Stahl *et al.*, 2005). Second, tamoxifen does not directly bind to the estrogen binding sites of the modified Cre recombinase. Instead, it needs metabolic activation. This hydroxylation reaction is mainly catalyzed by CYP enzymes of the families 3A and 2D (Dehal and Kupfer, 1997; Coller *et al.*, 2004), whose mRNA and protein levels also do not differ between normal liver tissue and *Ctnnb1*-mutated liver tumors in mice (Stahl *et al.*, 2005; Hailfinger *et al.*, 2006). Thus, the specific metabolic expression profile of *Ctnnb1*-mutated liver tumor cells should not affect the TTR promoter-mediated Cre expression or the CYP-mediated tamoxifen activation.

Hepatocyte-specific knockout of *Ctnnb1* was accomplished by application of tamoxifen according to the protocol described in Ganzenberg *et al.* (2013). In this study, Cre-mediated deletion of *Ctnnb1* was successful in > 99% of hepatocytes from transgenic mice. In the present experiment, mice of the same strain were used. However, tamoxifen application led to an incomplete knockout. In both the normal tissue and in tumors, a great heterogeneity concerning the degree of *Ctnnb1* knockout was observed. The reason for this phenomenon is unclear. As PB is known to induce the expression of certain xenobiotic enzymes, mice were set on a PB-free diet at least three weeks prior to sacrifice to exclude possible interactions with the metabolism of tamoxifen. Thus, it seems rather unlikely that PB contributed to this unexpected effect. Several studies in rodents show that the expression of hepatic enzymes decreases during age (Stohs *et al.*, 1980; Mori *et al.*, 2007; Lee *et al.*, 2008). Mice in the study from Ganzenberg *et al.* (2013) were considerably younger

## Discussion

than in the present animal study. This fact may have influenced the hepatic activation of tamoxifen subsequently leading to a lower Cre-mediated recombination rate.

The incomplete knockout of *Ctnnb1* resulted in the formation of two different tumor cell subpopulations making it difficult to conduct mRNA or protein analyses of the resected tumor tissue homogenates. Yet, despite unexpected, this mixed genotype enabled to directly compare the growth behavior of two subpopulations within one tumor separately by immunohistochemical stainings.

Several studies suggest that  $\beta$ -catenin positively regulates the proliferation of hepatocytes: enhanced hepatocyte proliferation was observed in transgenic mice after aberrant activation of Wnt/  $\beta$ -catenin signaling (Cadoret *et al.*, 2001; Colnot *et al.*, 2004) while loss of  $\beta$ -catenin resulted in delayed cell proliferation after partial hepatectomy (Tan *et al.*, 2006; Sekine *et al.*, 2007). Consistent with these findings, the present study showed that ablation of  $\beta$ -catenin led to a decrease in the proliferation rate of the GS-negative tumor cell population (Figure 9). Furthermore, the total tumor volume fraction in livers from *Ctnnb1* KO mice showed no significant increase over the six weeks time period (Figure 11), clearly indicating that tamoxifen-mediated knockout of *Ctnnb1* had slowed down the growth of the tumors. However, no signs of tumor cell death processes were found in *Ctnnb1*-mutated liver tumors between three to six weeks after tamoxifen treatment (Figure 14). A different situation is observed in murine skin tumors harboring an activated Wnt/  $\beta$ -catenin signaling pathway (Malanchi *et al.*, 2008). In respective transgenic mice, tumors started to decline three weeks after Cre-mediated knockout of *Ctnnb1* and complete tumor regression was accomplished at six weeks after tamoxifen application. Apparently,  $\beta$ -catenin is essential for the survival of murine skin tumors while it has a different role in liver tumor cells. Malanchi *et al.* (2008) reported that ablation of  $\beta$ -catenin resulted



## Discussion

in the loss of cutaneous cancer stem cells, providing a possible explanation for the observed complete tumor regression in this *in vivo* model.

Contrary to the situation observed in *Ctnnb1* KO mice, monitoring of the tumor burden in livers from *Ctnnb1* WT mice showed an increase over time (Figure 11) along with highly proliferative tumor tissue (Figure 10). The hepatocyte-specific tumor promoter PB is essential for the outgrowth of single *Ctnnb1*-mutated tumor cells in livers from mice (Aydinlik *et al.*, 2001). As PB was absent from the diet for several weeks, one can conclude that the manifested tumors grow independent of PB. One important mechanism of many tumor promoters, including PB, is the inhibition of connexin-mediated GJIC. GJIC is known to be an important process by which growth-inhibiting signals are spread from cell to cell (Yamasaki and Naus, 1996). Thus, restriction of GJIC is a well-known phenomenon observed in tumors to bypass growth inhibition (Chipman *et al.*, 2003). *Ctnnb1*-mutated liver tumors, promoted by PB, exhibit reduced membranous Cx32 levels (Moennikes *et al.*, 2000; Marx-Stoelting *et al.*, 2008) and cell isles, which evaded hepatocyte-specific knockout of *Ctnnb1* in a transgenic mouse model, lacked Cx32 at their membranes (Braeuning *et al.*, 2010). In this context it is interesting that, despite the absence of PB, GS-positive tumors were largely negative for membranous Cx32, but re-appearance of Cx32 was detected in the GS-negative tumor subpopulation after ablation of  $\beta$ -catenin (Figure 12, 13). This observation points towards a connection between reduced membranous Cx32 and active  $\beta$ -catenin signaling. Nonetheless, the mechanism by which  $\beta$ -catenin may regulate Cx32 membranous localization is still unclear and remains to be further elucidated as decreases in mRNA or protein Cx32 levels were not detected in *Ctnnb1*-mutated mouse liver tumors (Marx-Stoelting *et al.*, 2008). Taken together, one can hypothesize that  $\beta$ -catenin ablation led to re-occurring membranous

## Discussion

Cx32 in the tumor cells. Subsequently, they may have received more growth-restraining signals resulting in a decrease in tumor cell proliferation. This hypothesis is supported by the observation that the mean proliferative index of the GS-positive subpopulation was lower when the cells were surrounded by more GS-negative cells (Figure 9). In an environment where more cells are Cx32-positive, the growth of GS-positive tumor cells could be better controlled. Subsequently, the fraction of GS-positive tumor cells should more rapidly increase in tumors initially consisting of only 25-50% *Cttnb1* KO cells than in tumors with more than 50% *Cttnb1* KO cells (see Figure 32).

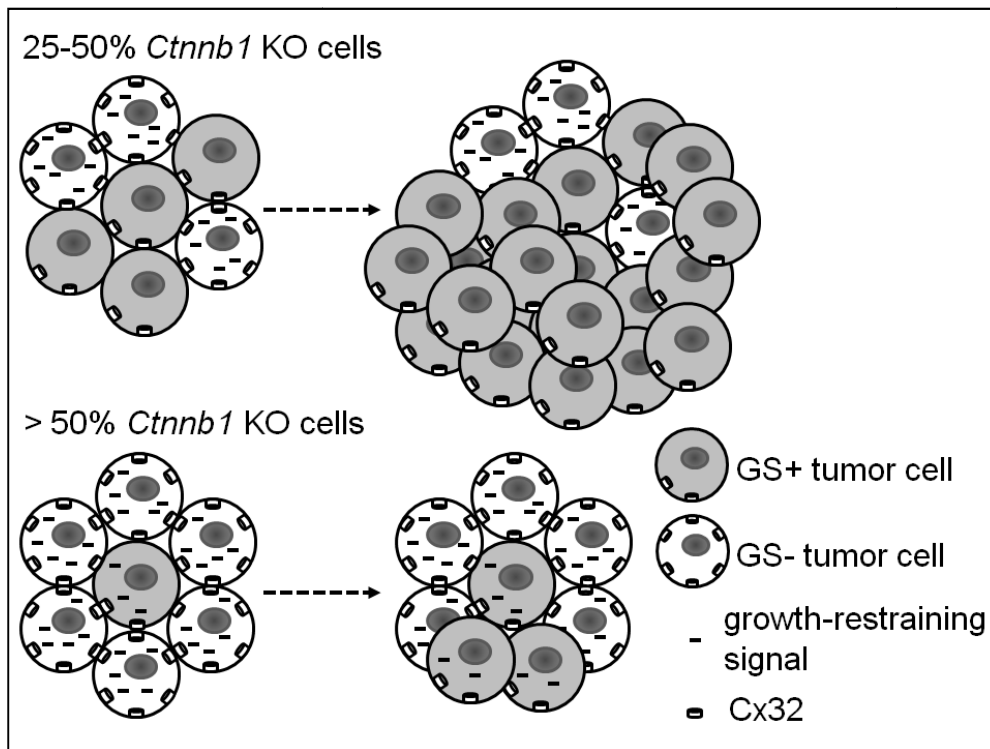


**Figure 32: Growth behavior of GS-positive cells in tumors with 25-50% *Cttnb1* KO cells and in tumors with > 50% *Cttnb1* KO cells.**

In summary, this study underlines the important role of  $\beta$ -catenin in the control of murine liver tumor growth and provides a possible mechanism by which cell proliferation may be regulated in this system. This knowledge is of relevance for the development of potential new therapeutic drugs targeting the de-regulated Wnt/  $\beta$ -

## Discussion

catenin signaling pathway in hepatocellular malignancies, especially in the case of HCC often showing therapy resistance.

### **5.2. Role of $\beta$ -Catenin in Etoposide-Induced Apoptosis in Mouse Hepatoma Cells**

TUNEL-stained liver sections showed the absence of apoptotic cell nuclei in tumor tissue after knockout of *Ctnnb1* (Figure 14). However, these results have to be interpreted with caution as the rate of apoptosis in the mouse liver is generally very low (Chabicovsky *et al.*, 2003; Bursch *et al.*, 2004) and the TUNEL labeling technique has its limitations concerning the specificity and sensitivity of apoptosis detection (Labat-Moleur *et al.*, 1998). Therefore, *in vitro* studies in mouse hepatoma cells were conducted to clarify the role of  $\beta$ -catenin in the regulation of hepatocyte apoptosis. The following experiments were performed in 70.4 mouse hepatoma cells, generated in our laboratory. Those cells carry wild type *Ctnnb1* but are homozygous for p53 mutations that are located in the DNA-binding domain restraining the function of p53 as a transcription factor. Nevertheless, apoptosis can be induced in 70.4 cells suggesting that transcriptionally active p53 is not required for the induction of apoptosis in this cell line (Unger *et al.*, 1998). This is consistent with the activation of effector caspase activity after etoposide treatment observed in this experiment (Figure 17). Several studies showed that activation of the Wnt/  $\beta$ -catenin signaling pathway induces resistance towards chemotherapeutic agents in various cell lines (Chen *et al.*, 2001; Yeung *et al.*, 2010; Vangipuram *et al.*, 2012). Similar effects were also observed in human hepatoma cells (Noda *et al.*, 2009). In contrast, the *in vitro* experiments conducted in the present work strongly point toward a minor role of  $\beta$ -catenin in the prevention of chemotherapy-induced apoptosis in mouse hepatoma

## Discussion

cells, suggesting that the function of  $\beta$ -catenin in the regulation of apoptosis is cell type- and species-specific: while the inhibition of GSK3 $\beta$  by LiCl strongly decreased etoposide-induced caspase activation, the doxycyclin-mediated expression of non-degradable  $\beta$ -catenin<sup>S33Y</sup> had no significant influence on caspase 3/ 7 activity (Figure 17). Etoposide induces double-strand breaks via inhibition of topoisomerase II, resulting in cell cycle arrest that should be followed by an activation of the intrinsic apoptotic pathway (Karpinich *et al.*, 2002). GSK3 $\beta$  can have pro- and antiapoptotic functions: it is able to inhibit the extrinsic apoptotic pathway, but on the other hand to promote the intrinsic one (Beurel and Jope, 2006). Thus, inhibition of GSK3 $\beta$  could have prevented etoposide-mediated activation of the intrinsic apoptotic pathway. In addition, inhibition of the proteasome strongly activated the Wnt/  $\beta$ -catenin signaling pathway and also prevented etoposide-induced apoptosis. Yet, knockdown of *Ctnnb1* did not change the experimental outcome (Figure 18, 19). It cannot be ruled out that the incomplete siRNA-mediated knockdown of *Ctnnb1* allowed moderate Wnt/  $\beta$ -catenin signaling that still might have influenced apoptotic processes in the examined cell line. However, the more likely explanation lies in the fact that bortezomib-mediated inhibition of the proteasome prevents the degradation of many other proteins involved in apoptotic processes. In terms of its role in cancer therapy, bortezomib is assumed to induce apoptosis and to sensitize cancer cells to chemotherapeutic agents (Vorhees *et al.*, 2003; Crawford *et al.*, 2011). Thereby, one mode of action is mediated through the NF $\kappa$ B (nuclear factor  $\kappa$ B)/ I $\kappa$ B (inhibitor of nuclear factor  $\kappa$ B) system. Accumulation of I $\kappa$ B, the most important inhibitor of NF $\kappa$ B, results in the prevention of NF $\kappa$ B activation (Vorhees *et al.*, 2003). However, the function of NF $\kappa$ B signaling is controversial as it may act as a pro- and antiapoptotic factor, depending on the cell type or the type of inducer (Van Antwerp *et al.*, 1998;

## Discussion

Grimm *et al.*, 1996). Indeed, Watanabe and colleagues (2000) found evidence that the inhibition of NF $\kappa$ B signaling by proteasome inhibitors could have provoked the prevention of etoposide-induced apoptosis in human leukemia cells. This mechanism might potentially also play a role in the 70.4 mouse hepatoma cells used in this study (Figure 33).

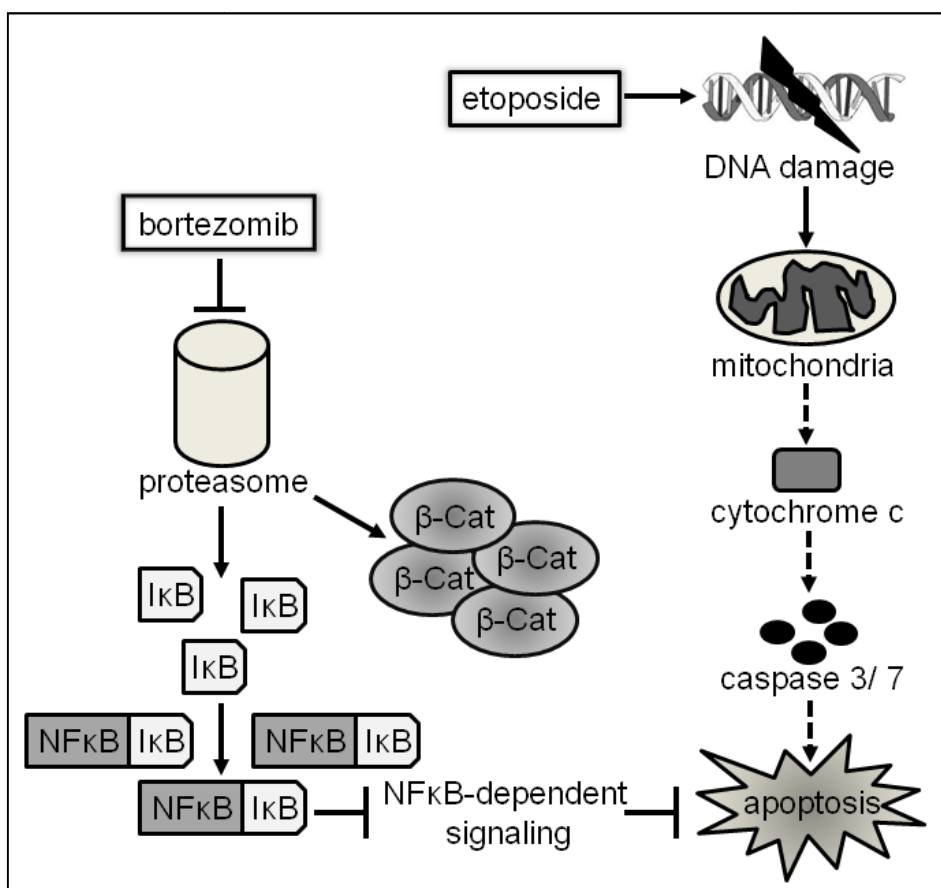


**Figure 33: Possible mechanism of bortezomib-mediated prevention of etoposide-induced apoptosis in 70.4 mouse hepatoma cells.**

Bortezomib is currently used in the therapy of several cancers (Goy *et al.*, 2005; Field-Smith *et al.*, 2006; Horton *et al.*, 2007). The present results might be of relevance when considering that it is mainly used in the combination with other chemotherapeutic drugs (Crawford *et al.*, 2011). Yet, it must be kept in mind that the treatment outcome probably strongly depends on the cell type and on the anticancer agent bortezomib is combined with.

## Discussion

The present *in vitro* analyses demonstrated that the inhibition of etoposide-mediated apoptosis most likely was caused by  $\beta$ -catenin-independent mechanisms. These results support the *in vivo* observation that  $\beta$ -catenin plays a minor role in the regulation of mouse hepatocyte apoptosis.

### **5.3. Selective Poisoning of *Cttnb1*-Mutated Mouse Liver Tumors by AAP**

The basis for the underlying tumor therapy experiment was the specific enzyme expression profile of *Cttnb1*-mutated mouse liver tumors. These tumors highly express the CYP enzymes 2E1 and 1A2 compared to normal liver tissue, whereas *Cttnb1* wild type tumors exhibit decreased expression of respective enzymes (Loeppen *et al.*, 2005). This is in line with the observed high levels of CYP2E1 and 1A2 in immunohistochemically stained liver tumors of the present experiment (Figure 20A). In contrast, E-cadherin-positive tumors, mutated in either *Ha-ras* or *B-raf*, did not express these enzymes (Figure 20B). The pivotal role of the CYP enzymes 2E1 and 1A2 in mediating the hepatotoxicity of AAP has been demonstrated before (Raucy *et al.*, 1989; Lee *et al.*, 1996; Gonzalez, 2007). The present study supports these observations as the applied dose of 300 mg/ kg of body weight AAP selectively poisoned CYP-positive tumors (Figure 24, 29), while CYP-negative tumors, mutated in either *Ha-ras* or *B-raf*, were not affected by AAP treatment (Figure 26). In addition, HE-stained liver sections showed no indication for AAP-mediated hepatotoxicity in the normal liver tissue of tumor-bearing mice (Figure 21).

Consistent with previous studies from our group (Schmid *et al.*, 2012), non-invasive MRI analyses proved to be a useful technique for tumor imaging. In the underlying study, it was used to detect and quantitatively analyze the tumor burden of animals

## Discussion

before and after treatment with AAP (Figure 30, 31) and the results gained by MRI were in accordance with histological observations. However, there are limitations of this technique as the detection limit is ~1 mm of tumor diameter and therefore the total liver tumor volume cannot be determined by this method (Schmid *et al.*, 2012). Nevertheless, MRI might be a useful tool to monitor the effect of an antitumor agent *in vivo*. Furthermore, this technique allows the recording of several measurement parameters such as the tissue-specific relaxation time or the movement of water molecules. This could provide additional information with respect to possible tissue alterations after drug application, e.g. detection of necrosis. Unfortunately however, due to technical problems during the MRI analyses of animals, these parameters could not be utilized for further evaluation in the present experiment and therefore should be the subject of future investigations.

Smaller tumors were less affected by AAP treatment with only about 50% of the tumor area being necrotic (Figure 24D). Independent of the tumor size, residual AAP-resistant cells were mainly localized at the outer border of the poisoned tumors (Figure 25). There are several characteristic properties of tumors that may have contributed to this site-specific effect.

Clearly the most striking difference between the AAP-resistant and the non-AAP-resistant tumor population is the fact that the surviving tumor cells are in direct contact to neighboring normal liver cells. There is a complex interplay of tumors with their microenvironment, which plays a role in conferring tumor cells resistant to cytotoxins and protects them from cell death via different mechanisms (Castells *et al.*, 2012). Thus, communication between adjacent normal hepatocytes and tumor cells may have somehow decreased their susceptibility against AAP treatment. On the other hand, it is reported that GJIC can propagate cell death (Udawatte and Ripps,

## Discussion

2005; Krutovskikh *et al.*, 2002) thereby possibly facilitating the expansion of the necrotic area in the inner tumor tissue. Yet, the results from the first *in vivo* experiment as well as from other studies (Moennikes *et al.*, 2000; Marx-Stoelting *et al.*, 2008) showed that Cx32-mediated GJIC is restricted in *Ctnnb1*-mutated mouse liver tumors and hence it is unlikely that this mechanism contributed significantly to the observed effect.

Nevertheless, heterogeneity within tumors influences the susceptibility of tumor cells to drug treatment (Tredan *et al.*, 2007). Larger tumors often consist of a necrotic core and of a shell of proliferating tumor cells. This is mainly caused by local differences in tumor vascularization resulting in a better supply with nutrients and oxygen in the peripheral tumor regions (Sutherland, 1986; Cui and Friedman, 2001). Thus, cells located in the inner tumor area could be more susceptible to toxic agents, like high doses of AAP. As smaller tumors lack large areas of necrotic tissue, this would also explain the weaker AAP-mediated toxic effect on those tumors.

Savransky *et al.* (2009) showed that mice exposed to recurrent hypoxia exhibit significantly increased AAP-induced hepatotoxicity while on the other hand hyperbaric oxygen reduced early AAP-induced liver injury (Salhanick *et al.*, 2006). Although it is difficult to directly compare the experimental setup in the above-mentioned studies with the conditions in *Ctnnb1*-mutated liver tumors, a combination of hypoxic conditions and AAP-mediated cytotoxic stress may have led to synergistic effects in the central tumor areas. One possible factor involved in this process may be the transcription factor HIF1 $\alpha$  (hypoxia-inducible factor 1 $\alpha$ ). HIF1 $\alpha$  mediates the cellular response to hypoxia and was also shown to promote AAP-induced hepatocellular death (Ke and Costa, 2006; Sparkenbaugh *et al.*, 2011).



## Discussion

Immunohistochemical stainings of CYP enzymes 2E1 and 1A2 gave no hints for local variations concerning their expression in the *Cttnb1*-mutated tumor tissue (Figure 20A). Thus, the resistance of peripheral tumor cells against AAP-induced toxicity does not seem to be caused by differences in the toxification process of AAP. In contrast, studies from Schmidt *et al.* (2011) showed less intensive immunostainings for CYP2E1 in human HB cells that were located at the outer tumor border directly contacting the stroma. *Cttnb1*-mutated liver tumors in mice exhibit high expression of several GST enzymes (Stahl *et al.*, 2005; Giera *et al.*, 2010) and the conjugation of the reactive intermediate NAPQI with GSH is catalyzed by those enzymes (Mitchell *et al.*, 1973). Yet, the GSH concentration is the limiting factor concerning AAP-mediated hepatotoxicity. Possible local differences concerning the levels of GSH within tumors could have affected the response of tumor cells against high dose AAP application. Further analyses are required to clarify the role of GSH in the site-specific susceptibility of tumor cells against AAP-induced poisoning.

The modulation of GSH levels as a strategy to sensitize tumor cells against chemotherapeutic agents is the topic of current research in oncology (Traverso *et al.*, 2013). To overcome the resistance of some surviving tumor cells, combined treatment with AAP and a cytostatic drug could be an option. In fact, cisplatin is commonly used for the treatment of HB (von Schweinitz, 2012) and it is inactivated by GSH (Meijer *et al.*, 1990; Hamilton *et al.*, 1985). Combination of AAP with cisplatin could be a strategy to deplete GSH by AAP which thereby sensitizes tumor cells against cisplatin. Indeed, a synergistic effect of cisplatin and AAP treatment was observed in several liver cancer cell lines *in vitro*, but there was no correlation with the CYP2E1 status in the respective tumor cells (Neuwelt *et al.*, 2009).

## Discussion

Human HCCs often harbor mutations in *CTNNB1* (Giles *et al.*, 2003), but in contrast to *Ctnnb1*-mutated mouse liver tumors they generally exhibit low levels of CYP enzymes (Xu *et al.*, 2001; Okabe *et al.*, 2001). Furthermore, CYP2E1 expression is decreased in HCC tissue (Ho *et al.*, 2004; Man *et al.*, 2004) and its gene expression was not altered in *CTNNB1*-mutated HCCs (Stahl *et al.*, 2005). A different situation is observed in human HBs, which are frequently mutated in *CTNNB1* (Lopez-Terrada *et al.*, 2009; Koch *et al.*, 1999). Studies from Schmidt *et al.* (2011) showed that HBs can express CYP2E1, although there were great variations between tumors from different patients concerning the CYP2E1 expression levels and some HBs did not exhibit positive CYP2E1 immunostaining at all.

The dose of 300 mg/ kg of body weight AAP was chosen for the treatment of tumor-bearing mice as it caused moderate hepatotoxicity in mice from the AAP dose finding study. It led to the selective poisoning of *Ctnnb1*-mutated, CYP-positive liver tumors while the normal liver tissue did not exhibit signs of centrilobular necrosis, the region where toxic effects of AAP are first observed (Figure 21). In humans, the recommended poisoning intervention dose is 150 mg/ kg of body weight AAP (Tenenbein, 2004; Jackson *et al.*, 1984), considerably lower as the applied dose in the present experiment. However, the metabolic turnover rate in rodents is quite fast due to a high liver-to-body weight ratio (Kleiber, 1975). Thus, this enables rodents to detoxify AAP much faster than adults. The same is true for young children who also have higher relative liver weights. Therefore, a higher AAP intervention dose is proposed for young children, accounting for 200-250 mg/ kg body weight (Tenenbein, 2004; Bond, 2004; Sia and Chan, 2006), a dose much closer to the dose used in the current animal study.

## Discussion

Treatment of HB with AAP may be suitable for some patients, considering the following aspects: overdosing of AAP is known to cause severe injury of the normal liver tissue that can lead to fatal liver failure. In addition, there are interindividual genomic variations that may affect the susceptibility towards high doses of AAP and thus may complicate the treatment regimen. In addition, studies from Schmidt *et al.* (2011) showed that the expression of the CYP2E1 enzyme in human *CTNNB1*-mutated HBs is more heterogeneous than in mouse liver tumors. Taken together, treatment of patients with AAP could rather be an alternative therapeutic option for patients with re-occurring chemotherapy-resistant HB, but only if the tumor is CYP2E1-positive. To date, there is only one publication available concerning the use of AAP in human HB therapy. Kobrinsky and colleagues (2005) successfully treated a patient suffering from chemotherapy-resistant HB with AAP. However, the treatment regimen strongly differed from the present experimental setup. It included repeated doses of AAP that were substantially higher as the applied dose in this animal study and they were followed by N-acetylcysteine rescue. Furthermore, no information was provided concerning the mutational status of the treated HB tumor or its CYP2E1 expression profile.

This study showed that the selective poisoning of murine *Ctnnb1*-mutated liver tumors with a single dose of 300 mg/ kg of body weight AAP is possible in this experimental system. However, despite the strong impact of AAP, some tumor cells displayed resistance against AAP-induced poisoning. Those cells have to be characterized more closely to find a possible explanation for the observed effect. Yet, this treatment approach could be potentially applied to tumor patients suffering from therapy-resistant, CYP-positive HBs.

## 6. Summary

In mice, liver tumors with activating mutations in *Ctnnb1*, encoding  $\beta$ -catenin, can be chemically induced by a single injection of the liver carcinogen N-nitrosodiethylamine (DEN) followed by chronic treatment with the tumor promoter phenobarbital (PB). This *in vivo* tumor model was used to study the role of  $\beta$ -catenin in hepatocarcinogenesis more closely and to clarify whether the characteristic metabolic profile of *Ctnnb1*-mutated mouse liver tumors can be exploited for therapeutic purposes.

Ablation of  $\beta$ -catenin in established *Ctnnb1*-mutated liver tumors from transgenic mice demonstrated that  $\beta$ -catenin plays an essential role in the regulation of murine liver tumor cell proliferation. Knockout of *Ctnnb1* resulted in a decrease in their proliferative index while at the same time the gap junction-forming protein connexin 32 (Cx32) re-appeared at the outer membranes of the tumor cells. It thus can be hypothesized that reduction of membranous Cx32 may promote tumor cell proliferation by isolating the cells from growth-restraining signals coming from neighboring normal cells. Immunohistochemical analyses gave no indications for apoptosis in tumor cells deprived of  $\beta$ -catenin and detection of changes in tumor burden over time revealed an arrest in tumor growth in livers from mice with a conditional knockout of *Ctnnb1*.

By use of *in vitro* experiments with mouse hepatoma cells it could be demonstrated that the activation of  $\beta$ -catenin signaling did not prevent apoptosis induced by treatment with the anticancer drug etoposide. These results confirmed the *in vivo* observation that  $\beta$ -catenin plays a minor role in apoptotic processes of mouse hepatocytes.

## Summary

Treatment of tumor-bearing mice with a single application of 300 mg/ kg of body weight acetaminophen (AAP) resulted in the selective poisoning of *Ctnnb1*-mutated liver tumor cells highly expressing the metabolic enzymes cytochrome P450 (CYP) 2E1 and 1A2, which mediate the hepatotoxicity of AAP at high doses. Quantification of the necrotic tumor area in immunohistochemically stained liver sections revealed that larger tumors consisted of ~90% necrotic tissue at 2 days after AAP treatment. Although the AAP-resistant tumor cells, mainly settled at the border of the damaged tumors, re-started to proliferate in the following days, histological and magnetic resonance imaging (MRI) analyses of later time points demonstrated an enduring reduction of the tumor burden in livers from AAP-treated mice.

## 7. Zusammenfassung

Lebertumoren mit aktivierenden Mutationen im *Ctnnb1*-Gen, welches für das Protein  $\beta$ -Catenin codiert, können in Mäusen durch eine Einzeldosis des Leberkanzerogens Diethylnitrosamin (DEN), gefolgt von einer chronischen Behandlung mit dem Tumorpromoter Phenobarbital (PB), chemisch induziert werden. Dieses *in vivo*-Tumormodell wurde herangezogen, um die Bedeutung von  $\beta$ -Catenin für die Hepatokanzerogenese genauer zu untersuchen und aufzuklären, ob das charakteristische metabolische Profil von *Ctnnb1*-mutierten Mauslebertumoren für therapeutische Zwecke genutzt werden kann.

Die Abschaltung von  $\beta$ -Catenin in bereits manifesten *Ctnnb1*-mutierten Lebertumoren von transgenen Mäusen zeigte, dass  $\beta$ -Catenin maßgeblich an der Regulation der Proliferation von murinen Lebertumorzellen beteiligt ist. Die  $\beta$ -Catenin-Abschaltung führte zu einem Rückgang ihrer Proliferationsrate, während gleichzeitig wieder mehr *gap junction*-formendes Connexin 32 (Cx32) an der Membran der Tumorzellen auftrat. Dies deutet darauf hin, dass die Reduktion von membranständigem Cx32 die Zellproliferation vorantreibt, indem die Tumorzellen gegenüber wachstumshemmenden Signalen von benachbarten normalen Zellen isoliert werden. Immunhistochemische Untersuchungen ergaben keine Hinweise auf Apoptose in den  $\beta$ -Catenin-abgeschalteten Tumorzellen und die Erfassung von Veränderungen der Tumorlast über die Zeit veranschaulichte, dass das Tumorwachstum in den Lebern der Mäuse mit konditionellem *Ctnnb1* knockout aufgehalten wurde.

Mittels *in vitro*-Versuchen in Maushepatomzelllinien konnte gezeigt werden, dass die Aktivierung des  $\beta$ -Catenin-Signalwegs die durch das Krebsmedikament Etoposid ausgelöste Apoptose nicht verhindern konnte. Diese Ergebnisse bestätigten die *in*

## Zusammenfassung

*vivo*-Beobachtungen, dass  $\beta$ -Catenin eine untergeordnete Rolle bei apoptotischen Vorgängen in Maushepatozyten spielt.

Die Behandlung von tumortragenden Mäusen mit einer Einzeldosis von 300 mg/ kg Körpergewicht Acetaminophen (AAP) führte zu einer gezielten Vergiftung von *Ctnnb1*-mutierten Lebertumorzellen, die eine hohe Expressionsrate der metabolischen Cytochrom P450 (CYP)-Enzyme 2E1 und 1A2 aufweisen, welche die Hepatotoxizität von AAP bei hohen Dosen vermitteln. Die Quantifizierung der nekrotischen Tumorfläche in immunhistochemisch gefärbten Leberschnitten belegte, dass die größeren Tumore 2 Tage nach AAP-Behandlung zu ~90% nekrotisch waren. Obwohl die vorwiegend am Rande der Tumoren angesiedelten, AAP-resistenten Tumorzellen im Laufe der Zeit wieder proliferierten, konnte über histologische und kernspintomographische (MRT) Untersuchungen zu späteren Zeitpunkten gezeigt werden, dass es in den Lebern der AAP-behandelten Tiere zu einem dauerhaften Rückgang der Tumorlast kam.

## 8. Literature

- Aydinlik H, Nguyen TD, Moennikes O, Buchmann A, Schwarz M (2001) Selective pressure during tumor promotion by phenobarbital leads to clonal outgrowth of beta-catenin-mutated mouse liver tumors. *Oncogene* 20:7812-7816
- Barrett JC and Wiseman RW (1987) Cellular and molecular mechanisms of multistep carcinogenesis: relevance to carcinogen risk assessment. *Environ Health Perspect* 76:65-70
- Bauer-Hofmann R, Klimek F, Buchmann A, Mueller O, Bannasch P, Schwarz M (1992) Role of mutations at codon 61 of the c-Ha-ras gene during diethylnitrosamine-induced hepatocarcinogenesis in C3H/He mice. *Mol Carcinog* 6:60-67
- Behari J (2010) The Wnt/ $\beta$ -catenin signaling pathway in liver biology and disease. *Expert Rev Gastroenterol Hepatol* 4:745-756
- Benhamouche S, Decaens T, Godard C, Chambrey R, Rickman DS, Moinard C, Vasseur-Cognet M, Kuo CJ, Kahn A, Perret C, Colnot S (2006) Apc tumor suppressor gene is the "zonation-keeper" of mouse liver. *Dev Cell* 10:759-770
- Beurel E and Jope RS (2006) The paradoxical pro- and anti-apoptotic actions of GSK3 in the intrinsic and extrinsic apoptosis signaling pathways. *Prog Neurobiol* 79:173-189
- Bond GR (2004) Reduced toxicity of acetaminophen in children: it's the liver. *J Toxicol Clin Toxicol* 42:149-152
- Bosch FX, Ribes J, Diaz M, Cleries R (2004) Primary liver cancer: worldwide incidence and trends. *Gastroenterology* 127:5-16
- Braeuning A, Ittrich C, Kohle C, Buchmann A, Schwarz M (2007a) Zonal gene expression in mouse liver resembles expression patterns of Ha-ras and beta-catenin mutated hepatomas. *Drug Metab Dispos* 35:503-507
- Braeuning A, Menzel M, Kleinschnitz EM, Harada N, Tamai Y, Kohle C, Buchmann A, Schwarz M (2007b) Serum components and activated Ha-ras antagonize expression of perivenous marker genes stimulated by beta-catenin signaling in mouse hepatocytes. *Febs J* 274:4766-4777
- Braeuning A, Singh Y, Rignall B, Buchmann A, Hammad S, Othman A, von Recklinghausen I, Godoy P, Hoehme S, Drasdo D, Hengstler JG, Schwarz M (2010) Phenotype and growth behavior of residual beta-catenin-positive hepatocytes in livers of beta-catenin-deficient mice. *Histochem Cell Biol* 134:469-481
- Bursch W, Grasl-Kraupp B, Wastl U, Hufnagl K, Chabicovsky M, Taper H, Schulte-Hermann R (2004) Role of apoptosis for mouse liver growth regulation and tumor promotion: comparative analysis of mice with high (C3H/He) and low (C57Bl/6J) cancer susceptibility. *Toxicol Lett* 149:25-35
- Cadoret A, Ovejero C, Saadi-Kheddouci S, Souil E, Fabre M, Romagnolo B, Kahn A, Perret C (2001) Hepatomegaly in transgenic mice expressing an oncogenic form of beta-catenin. *Cancer Res* 61:3245-3249
- Cadoret A, Ovejero C, Terris B, Souil E, Levy L, Lamers WH, Kitajewski J, Kahn A, Perret C (2002) New targets of beta-catenin signaling in the liver are involved in the glutamine metabolism. *Oncogene* 21:8293-8301
- Castells M, Thibault B, Delord JP, Couderc B (2012) Implication of tumor microenvironment in chemoresistance: tumor-associated stromal cells protect tumor cells from cell death. *Int J Mol Sci* 13:9545-9571



## Literature

- Chabircovsky M, Wastl U, Taper H, Grasl-Kraupp B, Schulte-Hermann R, Bursch W (2003) Induction of apoptosis in mouse liver adenoma and carcinoma in vivo by transforming growth factor-beta1. *J Cancer Res Clin Oncol* 129:536-542
- Chen S, Guttridge DC, You Z, Zhang Z, Fribley A, Mayo MW, Kitajewski J, Wang CY (2001) Wnt-1 signaling inhibits apoptosis by activating beta-catenin/T cell factor-mediated transcription. *J Cell Biol* 157:429-440
- Chipman JK, Mally A, Edwards GO (2003) Disruption of gap junctions in toxicity and carcinogenicity. *Toxicol Sci* 71:146-153
- Coller JK, Krebsfaenger N, Klein K, Wolbold R, Nuessler A, Neuhaus P, Zanger UM, Eichelbaum M, Muerdter TE (2004) Large interindividual variability in the in vitro formation of tamoxifen metabolites related to the development of genotoxicity. *Br J Clin Pharmacol* 57:105-111
- Colnot S, Decaens T, Niwa-Kawakita M, Godard C, Hamard G, Kahn A, Giovannini M, Perret C (2004) Liver-targeted disruption of Apc in mice activates beta-catenin signaling and leads to hepatocellular carcinomas. *Proc Natl Acad Sci USA* 101:17216-17221
- Crawford LJ, Walker B, Irvine AE (2011) Proteasome inhibitors in cancer therapy. *J Cell Commun Signal* 5:101-110
- Croce CM (2008) Oncogenes and cancer. *N Engl J Med* 358:502-511
- Cui S and Friedman A (2001) Analysis of a mathematical model of the growth of necrotic tumors. *Journal of Math Anal Appl* 255:636-677
- Cummings AJ, King ML, Martin BK (1967) A kinetic study of drug elimination: the excretion of paracetamol and its metabolites in man. *Br J Pharmacol Chemother* 29:150-157
- Dahlin DC, Miwa GT, Lu AY, Nelson SD (1984) N-acetyl-p-benzoquinone imine: a cytochrome P-450-mediated oxidation product of acetaminophen. *Proc Natl Acad Sci USA* 81:1327-1331
- Darbari A, Sabin KM, Shapiro CN, Schwarz KB (2003) Epidemiology of primary hepatic malignancies in U.S. children. *Hepatology* 38:560-566
- de La Coste A, Romagnolo B, Billuart P, Renard CA, Buendia MA, Soubrane O, Fabre M, Chelly J, Beldjord C, Kahn A, Perret C (1998) Somatic mutations of the beta-catenin gene are frequent in mouse and human hepatocellular carcinomas. *Proc Natl Acad Sci USA* 95:8847-8851
- Dehal SS and Kupfer D (1997) CYP2D6 catalyzes tamoxifen 4-hydroxylation in human liver. *Cancer Res* 57:3402-3406
- Dermietzel R, Yancey SB, Traub O, Willecke K, Revel JP (1987) Major loss of the 28-kD protein of gap junction in proliferating hepatocytes. *J Cell Biol* 105:1925-1934
- Dixon MF, Nimmo J, Prescott LF (1971) Experimental paracetamol-induced hepatic necrosis: a histopathological study. *J Pathol* 103:225-229
- Dong H, Haining RL, Thummel KE, Rettie AE, Nelson SD (2000) Involvement of human cytochrome P450 2D6 in the bioactivation of acetaminophen. *Drug Metab Dispos* 28:1397-1400
- Ellerkamp V, Lieber J, Nagel C, Wenz J, S. W. Warmann SW, Fuchs J, Armeanu-Ebinger S (2013) Pharmacological inhibition of beta-catenin in hepatoblastoma cells. *Pediatr Surg Int* 29:141-149
- Field-Smith A, Morgan GJ, Davies FE (2006) Bortezomib (Velcade™) in the treatment of multiple myeloma. *Ther Clin Risk Manag* 2:271-279
- Foulds L (1954) The experimental study of tumor progression: a review. *Cancer Res* 14:327-339

## Literature

- Ganzenberg K, Singh Y, Braeuning A (2013) The time point of  $\beta$ -catenin knockout in hepatocytes determines their response to xenobiotic activation of the constitutive androstane receptor. *Toxicology* 308:113-121
- Gaujoux S, Hantel C, Launay P, Bonnet S, Perlemoine K, Lefevre L, Guillaud-Bataille M, Beuschlein F, Tissier F, Bertherat J, Rizk-Rabin M, Ragazzon B (2013) Silencing mutated  $\beta$ -catenin inhibits cell proliferation and stimulates apoptosis in the adrenocortical cancer cell line H295R. *PLoS One* 8:e55743
- Gebhardt R (1992) Metabolic zonation of the liver: regulation and implications for liver function. *Pharmacol Ther* 53:275-354
- Gebhardt R and Mecke D (1983) Heterogeneous distribution of glutamine synthetase among rat liver parenchymal cells in situ and in primary culture. *Embo J* 2:567-570
- Giera S, Braeuning A, Kohle C, Bursch W, Metzger U, Buchmann A, Schwarz M (2010) Wnt/beta-catenin signaling activates and determines hepatic zonal expression of glutathione S-transferases in mouse liver. *Toxicol Sci* 115:22-33
- Giles RH, van Es JH, Clevers H (2003) Caught up in a Wnt storm: Wnt signaling in cancer. *Biochim Biophys Acta* 1653:1-24
- Gonzalez FJ (2007) The 2006 Bernard B. Brodie Award Lecture. Cyp2e1. *Drug Metab Dispos* 35:1-8
- Goy A, Younes A, McLaughlin P, Pro B, Romaguera JE, Hagemester F, Fayad L, Dang NH, Samaniego F, Wang M, Broglio K, Samuels B, Gilles F, Sarris AH, Hart S, Trehu E, Schenkein D, Cabanillas F, Rodriguez AM (2005) Phase II study of proteasome inhibitor bortezomib in relapsed or refractory B-cell non-Hodgkin's lymphoma. *J Clin Oncol* 23:667-675
- Grimm S, Bauer MK, Baeuerle PA, Schulze-Osthoff K (1996) Bcl-2 down-regulates the activity of transcription factor NF-kappaB induced upon apoptosis. *J Cell Biol* 134:13-23
- Guengerich FP and Shimada T (1991) Oxidation of toxic and carcinogenic chemicals by human cytochrome P-450 enzymes. *Chem Res Toxicol* 4:391-407
- Hailfinger S, Jaworski M, Braeuning A, Buchmann A, Schwarz M (2006) Zonal gene expression in murine liver: lessons from tumors. *Hepatology* 43:407-414
- Hamilton TC, Winker MA, Louie KG, Batist G, Behrens BC, Tsuruo T, Grotzinger KR, McKoy WM, Young RC, Ozols RF (1985) Augmentation of adriamycin, melphalan, and cisplatin cytotoxicity in drug-resistant and -sensitive human ovarian carcinoma cell lines by buthionine sulfoximine mediated glutathione depletion. *Biochem Pharmacol* 34:2583-2586
- He TC, Sparks AB, Rago C, Hermeking H, Zawel L, da Costa LT, Morin PJ, Vogelstein B, Kinzler KW (1998) Identification of c-MYC as a target of the APC pathway. *Science* 281:1509-1512
- Hinson JA, Roberts DW, James LP (2010) Mechanisms of acetaminophen-induced liver necrosis. *Handb Exp Pharmacol* 196:369-405
- Ho JC, Cheung ST, Leung KL, Ng IO, Fan ST (2004) Decreased expression of cytochrome P450 2E1 is associated with poor prognosis of hepatocellular carcinoma. *Int J Cancer* 111:494-500
- Horn M (2010) Generation of a stably transfected mouse hepatoma cell line with inducible expression of activated  $\beta$ -catenin<sup>S33Y</sup>. Diploma thesis in biochemistry
- Horton TM, Pati D, Plon SE, Thompson PA, Bomgaars LR, Adamson PC, Ingle AM, Wright J, Brockman AH, Paton M, Blaney SM (2007) A phase 1 study of the proteasome inhibitor bortezomib in pediatric patients with refractory leukemia: a Children's Oncology Group study. *Clin Cancer Res* 13:1516-1522

## Literature

- Huelsken J, Vogel R, Erdmann B, Cotsarelis G, Birchmeier W (2001) beta-Catenin controls hair follicle morphogenesis and stem cell differentiation in the skin. *Cell* 105:533-545
- Jackson CH, MacDonald NC, Cornett JW (1984) Acetaminophen: a practical pharmacologic overview. *Can Med Assoc J* 131:25-32
- Jaworski M, Buchmann A, Bauer P, Riess O, Schwarz M (2005) B-raf and Ha-ras mutations in chemically induced mouse liver tumors. *Oncogene* 24:1290-1295
- Jungermann K (1995) Zonation of metabolism and gene expression in liver. *Histochem Cell Biol* 103:81-91
- Jungermann K and Katz N (1982) Functional hepatocellular heterogeneity. *Hepatology* 2:385-395
- Jungermann K and Katz N (1989) Functional specialization of different hepatocyte populations. *Physiol Rev* 69:708-764
- Jungermann K and Sasse D (1978) Heterogeneity of liver parenchymal cells. *Trends Biochem Sci* 3:198-202
- Karpnich NO, Tafani M, Schneider T, Russo MA, Farber JL (2002) The course of etoposide-induced apoptosis in Jurkat cells lacking p53 and Bax. *J Cell Physiol* 208:55-63
- Ke Q and Costa M (2006) Hypoxia-inducible factor-1 (HIF-1). *Mol Pharmacol* 70:1469-1480
- Klaus A and Birchmeier W (2008) Wnt signalling and its impact on development and cancer. *Nat Rev Cancer* 8:387-398
- Kleiber M (1975) Metabolic turnover rate: a physiological meaning of the metabolic rate per unit body weight. *J Theor Biol* 53:199-204
- Kobrinsky NL, Sjolander DE, Goldenberg JA, Ortmeier TC (2005) Successful treatment of doxorubicin and cisplatin resistant hepatoblastoma in a child with Beckwith-Wiedemann syndrome with high dose acetaminophen and N-acetylcysteine rescue. *Pediatr Blood Cancer* 45:222-225
- Koch A, Denkhau D, Albrecht S, Leuschner I, von Schweinitz D, Pietsch T (1999) Childhood hepatoblastomas frequently carry a mutated degradation targeting box of the beta-catenin gene. *Cancer Res* 59:269-273
- Kress S, Koenig J, Schweizer J, Loehrke H, Bauer-Hofmann R, Schwarz M (1992) p53 mutations are absent from carcinogen-induced mouse liver tumors but occur in cell lines established from these tumors. *Mol Carcinog* 6:148-158
- Krutovskikh VA, Piccoli C, Yamasaki H (2002) Gap junction intercellular communication propagates cell death in cancerous cells. *Oncogene* 21:1989-1999
- Labat-Moleur F, Guillermet C, Lorimier P, Robert C, Lantuejoul S, Brambilla E, Negoescu A (1998) TUNEL apoptotic cell detection in tissue sections: critical evaluation and improvement. *J Histochem Cytochem* 46:327-334
- Lee SS, Buters JT, Pineau T, Fernandez-Salguero P, Gonzalez FJ (1996) Role of CYP2E1 in the hepatotoxicity of acetaminophen. *J Biol Chem* 271:12063-12067
- Lee JS, Ward WO, Wolf DC, Allen JW, Mills C, DeVito MJ, Corton JC (2008) Coordinated changes in xenobiotic metabolizing enzyme gene expression in aging male rats. *Toxicol Sci* 106:263-283
- Leenders MW, Nijkamp MW, Borel Rinkes IH (2008) Mouse models in liver cancer research: a review of current literature. *World J Gastroenterol* 14:6915-6923
- Levine AJ (1993) The tumor suppressor genes. *Annu Rev Biochem* 62:623-651

## Literature

- Loeppen S, Schneider D, Gaunitz F, Gebhardt R, Kurek R, Buchmann A, Schwarz M (2002) Overexpression of glutamine synthetase is associated with beta-catenin mutations in mouse liver tumors during promotion of hepatocarcinogenesis by phenobarbital. *Cancer Res* 62:5685-5688
- Loeppen S, Koehle C, Buchmann A, Schwarz M (2005) A beta-catenin-dependent pathway regulates expression of cytochrome P450 isoforms in mouse liver tumors. *Carcinogenesis* 26:239-248
- Logan CY and Nusse R (2004) The Wnt signaling pathway in development and disease. *Annu Rev Cell Dev Biol* 20:781-810
- Lopez-Terrada D, Gunaratne PH, Adesina AM, Pulliam J, Hoang DM, Nguyen Y, Mistretta T, Margolin J, Finegold MJ (2009) Histologic subtypes of hepatoblastoma are characterized by differential canonical Wnt and Notch pathway activation in DLK+ precursors. *Hum Pathol* 40:783-794
- Lue S and Wang J (2013) The resistance mechanisms of proteasome inhibitor bortezomib. *Biomark Res* 1:13
- MacDonald BT, Tamai K, He X (2009) Wnt/beta-catenin signaling: components, mechanisms, and diseases. *Dev Cell* 17:9-26
- Malanchi I, Peinado H, Kassen D, Hussenet T, Metzger D, Chambon P, Huber M, Hohl D, Cano A, Birchmeier W, Huelsken J (2008) Cutaneous cancer stem cell maintenance is dependent on beta-catenin signalling. *Nature* 452:650-653
- Man XB, Tang L, Qiu XH, Yang LQ, Cao HF, Wu MC, Wang HY (2004) Expression of cytochrome P450E1 gene in hepatocellular carcinoma. *World J Gastroenterol* 10:1565-1568
- Maronpot RR, Fox T, Malarkey DE, Goldsworthy TL (1995) Mutations in the ras proto-oncogene: clues to etiology and molecular pathogenesis of mouse liver tumors. *Toxicology* 101:125-156
- Marquardt H and Schäfer SG (2003) *Lehrbuch der Toxikologie*. Wissenschaftliche Verlagsges.
- Marx-Stoelting P, Mahr J, Knorpp T, Schreiber S, Templin MF, Ott T, Buchmann A, Schwarz M (2008) Tumor promotion in liver of mice with a conditional Cx26 knockout. *Toxicol Sci* 103:260-267
- Meijer C, Mulder NH, Hospers GA, Uges DR, de Vries EG (1990) The role of glutathione in resistance to cisplatin in a human small cell lung cancer cell line. *Br J Cancer* 62:72-77
- Miner DJ and Kissinger PT (1979) Evidence for the involvement of N-acetyl-quinoneimine in acetaminophen metabolism. *Biochem Pharmacol* 28:3285-3290
- Mitchell JR, Jollow DJ, Potter WZ, Gillette JR, Brodie BB (1973) Acetaminophen-induced hepatic necrosis. IV. Protective role of glutathione. *J Pharmacol Exp Ther* 187:211-217
- Moennikes O, Buchmann A, Romualdi A, Ott T, Werringloer J, Willecke K, Schwarz M (2000) Lack of phenobarbital-mediated promotion of hepatocarcinogenesis in connexin32-null mice. *Cancer Res* 60:5087-5091
- Mori K, Blackshear PE, Lobenhofer EK, Parker JS, Orzech DP, Roycroft JH, Walker KL, Johnson KA, Marsh TA, Irwin RD, Boorman GA (2007) Hepatic transcript levels for genes coding for enzymes associated with xenobiotic metabolism are altered with age. *Toxicol Pathol* 35:242-251
- Morin PJ (1999) Beta-catenin signaling and cancer. *Bioessays* 21:1021-1030
- Neuwelt AJ, Wu YJ, Knap N, Losin M, Neuwelt EA, Pagel MA, Warmann S, Fuchs J, Czauderna P, Wozniak M (2009) Using acetaminophen's toxicity mechanism

## Literature

- to enhance cisplatin efficacy in hepatocarcinoma and hepatoblastoma cell lines. *Neoplasia* 11:1003-1011
- Noda T, Nagano H, Takemasa I, Yoshioka S, Murakami M, Wada H, Kobayashi S, Marubashi S, Takeda Y, Dono K, Umeshita K, Matsuura N, Matsubara K, Doki Y, Mori M, Monden M (2009) Activation of Wnt/beta-catenin signalling pathway induces chemoresistance to interferon-alpha/5-fluorouracil combination therapy for hepatocellular carcinoma. *Br J Cancer* 100:1647-1658
- Nowell PC (1986) Mechanisms of tumor progression. *Cancer Res* 46:2203-2207
- Nusse R and Varmus HE (1982) Many tumors induced by the mouse mammary tumor virus contain a provirus integrated in the same region of the host genome. *Cell* 31:99-109
- Okabe H, Satoh S, Kato T, Kitahara O, Yanagawa R, Yamaoka Y, Tsunoda T, Furukawa Y, Nakamura Y (2001) Genome-wide analysis of gene expression in human hepatocellular carcinomas using cDNA microarray: identification of genes involved in viral carcinogenesis and tumor progression. *Cancer Res* 61:2129-2137
- Oliveira PA, Colaço A, Chaves R, Guedes-Pinto H, De-La-Cruz P LF, Lopes C (2007) Chemical carcinogenesis. *An Acad Bras Cienc* 79:593-616
- Orford K, Orford CC, Byers SW (1999) Exogenous expression of beta-catenin regulates contact inhibition, anchorage-independent growth, anoikis, and radiation-induced cell cycle arrest. *J Cell Biol* 146:855-868
- Parkin DM, Bray F, Ferlay J, Pisani P (2002) Global cancer statistics, 2002. *CA Cancer J Clin* 55:74-108
- Polakis P (1999) The oncogenic activation of beta-catenin. *Curr Opin Genet Dev* 9:15-21
- Polakis P (2000) Wnt signaling and cancer. *Genes Dev* 14:1837-1851
- Pritchard J, Brown J, Shafford E, Perilongo G, Brock P, Dicks-Mireaux C, Keeling J, Phillips A, Vos A, Plaschkes J (2000) Cisplatin, doxorubicin, and delayed surgery for childhood hepatoblastoma: a successful approach--results of the first prospective study of the International Society of Pediatric Oncology. *J Clin Oncol* 18:3819-3828
- Rappaport AM, Borowy ZJ, Loughheed WM, Lotto WN (1954) Subdivision of hexagonal liver lobules into a structural and functional unit; role in hepatic physiology and pathology. *Anat Rec* 119:11-33
- Raucy JL, Lasker JM, Lieber CS, Black M (1989) Acetaminophen activation by human liver cytochromes P450IIE1 and P450IA2. *Arch Biochem Biophys* 271:270-283
- Reynolds M, Douglass EC, Finegold M, Cantor A, Glicksman A (1992) Chemotherapy can convert unresectable hepatoblastoma. *J Pediatr Surg* 27:1080-1084
- Rosenwald E (2008) The influence of the Wnt/  $\beta$ -Catenin signaling pathway on cytostatica-induced apoptosis in mouse hepatoma cells. Diploma thesis in biochemistry
- Saifo MS, Rempinski DR Jr, Rustum YM, Azrak RG (2010) Targeting the oncogenic protein beta-catenin to enhance chemotherapy outcome against solid human cancers. *Mol Cancer* 9:310
- Salhanick SD, Belikoff B, Orlow D, Holt D, Reenstra W, Buras JA (2006) Hyperbaric oxygen reduces acetaminophen toxicity and increases HIF-1alpha expression. *Acad Emerg Med* 13:707-714

## Literature

- Savransky V, Reinke C, Jun J, Bevans-Fonti S, Nanayakkara A, Li J, Myers AC, Torbenson MS, Polotsky VY (2009) Chronic intermittent hypoxia and acetaminophen induce synergistic liver injury in mice. *Exp Physiol* 94:228-239
- Schmid A, Rignall B, Pichler BJ, Schwarz M (2012) Quantitative analysis of the growth kinetics of chemically induced mouse liver tumors by magnetic resonance imaging. *Toxicol Sci* 126:52-59
- Schmidt A, Braeuning A, Ruck P, Seitz G, Armeanu-Ebinger S, Fuchs J, Warmann SW, Schwarz M (2011) Differential expression of glutamine synthetase and cytochrome P450 isoforms in human hepatoblastoma. *Toxicology* 281:7-14
- Sekine S, Lan BY, Bedolli M, Feng S, Hebrok M (2006) Liver-specific loss of beta-catenin blocks glutamine synthesis pathway activity and cytochrome p450 expression in mice. *Hepatology* 43:817-825
- Sekine S, Gutiérrez PJ, Lan BY, Feng S, Hebrok M (2007) Liver-specific loss of beta-catenin results in delayed hepatocyte proliferation after partial hepatectomy. *Hepatology* 45:361-388
- Shang XZ, Zhu H, Lin K, Tu Z, Chen J, Nelson DR, Liu C (2004) Stabilized beta-catenin promotes hepatocyte proliferation and inhibits TNFalpha-induced apoptosis. *Lab Invest* 84:332-341
- Sharma RP and Chopra VL (1976) Effect of the Wingless (wg1) mutation on wing and haltere development in *Drosophila melanogaster*. *Dev Biol* 48:461-465
- Shen DW, Lu YG, Chin KV, Pastan I, Gottesman MM (1991) Human hepatocellular carcinoma cell lines exhibit multidrug resistance unrelated to MRD1 gene expression. *J Cell Sci* 98:317-322
- Shtutman M, Zhurinsky J, Simcha I, Albanese C, D'Amico M, Pestell R, Ben-Ze'ev A (1999) The cyclin D1 gene is a target of the beta-catenin/LEF-1 pathway. *Proc Natl Acad Sci USA* 96:5522-5527
- Sia JYS and Chan YC (2006) Case report: paracetamol poisoning in a 2-year-old child-from international overview to the role of the Hong Kong Poison Information Centre. *Hong Kong J Emerg Med* 13:225-231
- Singh Y, Braeuning A, Schmid A, Pichler BJ, Schwarz M (2013) Selective poisoning of Ctnnb1-mutated hepatoma cells in mouse liver tumors by a single application of acetaminophen. *Arch Toxicol* [Epub ahead of print]
- Slaga TJ (1983) Cellular and molecular mechanisms of tumour promotion. *Cancer Surv* 2:595-612
- Sparkenbaugh EM, Saini Y, Greenwood KK, LaPres JJ, Luyendyk JP, Copple BL, Maddox JF, Ganey PE, Roth RA (2011) The role of hypoxia-inducible factor-1 $\alpha$  in acetaminophen hepatotoxicity. *J Pharmacol Exp Ther* 338:492-502
- Stahl S, Ittrich C, Marx-Stoelting P, Kohle C, Altug-Teber O, Riess O, Bonin M, Jobst J, Kaiser S, Buchmann A, Schwarz M (2005) Genotype-phenotype relationships in hepatocellular tumors from mice and man. *Hepatology* 42:353-361
- Stein TJ, Jochem A, Holmes KE, Sandgren EP (2011) Effect of mutant  $\beta$ -catenin on liver growth homeostasis and hepatocarcinogenesis in transgenic mice. *Liver Int* 31:303-312
- Stohs SJ, Al-Turk WA, Hassing JM (1980) Altered drug metabolism in hepatic and extrahepatic tissues in mice. *Age* 3:88-92
- Sutherland RM (1986) Importance of critical metabolites and cellular interactions in the biology of microregions of tumors. *Cancer* 58:1668-1680
- Taieb J, Barbare JC, Rougier P (2006) Medical treatments for hepatocellular carcinoma (HCC): what's next? *Ann Oncol* 10:308-314

## Literature

- Takahashi-Yanaga F and Sasaguri T (2007) The Wnt/beta-catenin signaling pathway as a target in drug discovery. *J Pharmacol Sci* 104:293-302
- Tan X, Behari J, Cieply B, Michalopoulos GK, Monga SP (2006) Conditional deletion of beta-catenin reveals its role in liver growth and regeneration. *Gastroenterology* 131:1561-1572
- Tannour-Louet M, Porteu A, Vaulont S, Kahn A, Vasseur-Cognet M (2002) A tamoxifen-inducible chimeric Cre recombinase specifically effective in the fetal and adult mouse liver. *Hepatology* 35:1072-1081
- Tenenbein M (2004) Acetaminophen: the 150 mg/kg myth. *J Toxicol Clin Toxicol* 42:145-148
- Thomas MB and Zhu AX (2005) Hepatocellular carcinoma: the need for progress. *J Clin Oncol* 23:2892-2899
- Thummel KE, Lee CA, Kunze KL, Nelson SD, Slattery JT (1993) Oxidation of acetaminophen to *N*-acetyl-*p*-aminobenzoquinone imine by human CYP3A4. *Biochem Pharmacol* 45:1563-1569
- Traverso N, Ricciarelli R, Nitti M, Marengo B, Furfaro AL, Pronzato MA, Marinari UM, Domenicotti C (2013) Role of glutathione in cancer progression and chemoresistance. *Oxid Med Cell Longev* 2013:972913
- Trédan O, Galmarini CM, Patel K, Tannock IF (2007) Drug resistance and the solid tumor microenvironment. *J Natl Cancer Inst* 99:1441-1454
- Udawatte C and Ripps H (2005) The spread of apoptosis through gap-junctional channels in BHK cells transfected with Cx32. *Apoptosis* 10:1019-1029
- Unger C, Buchmann A, Buenemann CL, Kress S, Schwarz M (1998) Wild-type function of the p53 tumor suppressor protein is not required for apoptosis of mouse hepatoma cells. *Cell Death Differ* 5:87-95
- Van Antwerp DJ, Martin SJ, Verma IM, Green DR (1998) Inhibition of TNF-induced apoptosis by NF-kappa B. *Trends Cell Biol* 8:107-111
- Vangipuram SD, Buck SA, Lyman WD (2012) Wnt pathway activity confers chemoresistance to cancer stem-like cells in a neuroblastoma cell line. *Tumour Biol* 33:2173-2183
- von Schweinitz D, Byrd DJ, Hecker H, Weinel P, Bode U, Burger D, Erttmann R, Harms D, Mildenerger H (1997) Efficiency and toxicity of ifosfamide, cisplatin and doxorubicin in the treatment of childhood hepatoblastoma. *Eur J Cancer* 33:1243-1249
- von Schweinitz D (2012) Hepatoblastoma: recent developments in research and treatment. *Semin Pediatr Surg* 21:21-30
- Voorhees PM, Dees EC, O'Neil B, Orlowski RZ (2003) The proteasome as a target for cancer therapy. *Clin Cancer Res* 9:6316-6325
- Wachstein M and Meisel E (1957) Histochemistry of hepatic phosphatases of a physiologic pH; with special reference to the demonstration of bile canaliculi. *Am J Clin Pathol* 27:13-23
- Warmann S, Hunger M, Teichmann B, Flemming P, Gratz KF, Fuchs J (2002) The role of the MDR1 gene in the development of multidrug resistance in human hepatoblastoma: clinical course and in vivo model. *Cancer* 95:1795-1801
- Watanabe K, Kubota M, Hamahata K, Lin Y, Usami I (2000) Prevention of etoposide-induced apoptosis by proteasome inhibitors in a human leukemic cell line but not in fresh acute leukemia blasts. A differential role of NF-kappa B activation. *Biochem Pharmacol* 60:823-830
- Weinberg RA (1991) Tumor suppressor genes. *Science* 254:1138-1146

## Literature

- Weinstein IB, Gattoni-Celli S, Kirschmeier P, Lambert M, Hsiao W, Backer J, Jeffrey A (1984) Multistage carcinogenesis involves multiple genes and multiple mechanisms. *J Cell Physiol Suppl* 3:127-137
- Whittaker S, Marais R, Zhu AX (2010) The role of signaling pathways in the development and treatment of hepatocellular carcinoma. *Oncogene* 29:4989-5005
- Xu XR, Huang J, Xu ZG, Qian BZ, Zhu ZD, Yan Q, Cai T, Zhang X, Xiao HS, Qu J, Liu F, Huang QH, Cheng ZH, Li NG, Du JJ, Hu W, Shen KT, Lu G, Fu G, Zhong M, Xu SH, Gu WY, Huang W, Zhao XT, Hu GX, Gu JR, Chen Z, Han ZG (2001) Insight into hepatocellular carcinogenesis at transcriptome level by comparing gene expression profiles of hepatocellular carcinoma with those of corresponding noncancerous liver. *Proc Natl Acad Sci USA* 98:15089-15094
- Yamasaki H and Naus CC (1996) Role of connexin genes in growth control. *Carcinogenesis* 17:1199-1213
- Yeung J, Esposito MT, Gandillet A, Zeisig BB, Griessinger E, Bonnet D, So CW (2010)  $\beta$ -Catenin mediates the establishment and drug resistance of MLL leukemic stem cells. *Cancer Cell* 18:606-618
- Yoshino M, Okazaki N, Yoshida T, Kanda Y, Miki M, Oda H, Sasagawa Y, Hayashi S, Hashimoto N (1989) A phase II study of etoposide in patients with hepatocellular carcinoma by the Tokyo Liver Cancer Chemotherapy Study Group. *Jpn J Clin Oncol* 19:120-122
- Zeller E, Mock K, Horn M, Colnot S, Schwarz M, Braeuning A (2012) Dual-specificity phosphatases are targets of the Wnt/ $\beta$ -catenin pathway and candidate mediators of  $\beta$ -catenin/Ras signaling interactions. *Biol Chem* 393:1183-1191
- Zhang T, Otevrel T, Gao Z, Gao Z, Ehrlich SM, Fields JZ, Boman BM (2001) Evidence that APC regulates survivin expression: a possible mechanism contributing to the stem cell origin of colon cancer. *Cancer Res* 61:8664-8667



## 9. Curriculum Vitae

### Personal Information

Name	Yasmin Singh
Nationality	German
Date of birth	December 2, 1982
Place of birth	Ulm, Germany

### Education

June 19, 2002	Albert-Schweitzer-Gymnasium, Laichingen, Germany Graduation: general qualification for university entrance (allgemeine Hochschulreife)
10/ 2002 - 09/ 2003	Study of Pharmacy, Eberhard-Karls-Universität Tübingen
10/ 2003 - 09/ 2008	Study of Biochemistry, Eberhard-Karls-Universität Tübingen Major subjects: toxicology and pharmaceutical chemistry Diploma thesis: "Vorhersage fruchtschädigender Wirkungen durch genetische Reportersysteme in humanen sacrococcygealen Teratomzellen"
September 26, 2008	Diploma in Biochemistry
03/ 2009 - 07/ 2013	Ph. D. Studies, Institute of Experimental and Clinical Pharmacology and Toxicology, Department of Toxicology, Eberhard-Karls-Universität Tübingen Dissertation thesis: „Role of $\beta$ -Catenin Signaling for the Growth and Selective Poisoning of <i>Ctnnb1</i> -Mutated Mouse Liver Tumors"